

DISS. ETH No. 22494

# Probing $G\alpha_{i1}$ activation at single amino acid resolution

A thesis submitted to attain the degree of  
Doctor of Sciences of ETH ZÜRICH  
(Dr. sc. ETH Zürich)

presented by

**DAWEI SUN**

M.Sc. (Chemistry), Korea Advanced Institute of Science and Technology, Republic of Korea

born on 31.08.1980

citizen of P.R.China

accepted on the recommendation of  
Prof. Gebhard Schertler, examiner  
Dr. Dmitry Veprintsev, scientific supervisor  
Prof. Gerhard Wider, co-examiner  
Prof. Stephan Grzesiek, co-examiner

2015

# Contents

<b>Abbreviations</b> .....	iv
<b>Summary</b> .....	vi
<b>Zusammenfassung</b> .....	vii
<b>Publications</b> .....	ix
<b>Chapter 1 Introduction</b> .....	1
1.1 The heterotrimeric G protein cycle .....	1
1.2 General overview of GPCRs .....	2
1.3 Heterotrimeric G protein subunits .....	3
1.4 Heterotrimeric G protein structure .....	4
1.6 GPCR-G complex state .....	6
1.7 Hypothesized mechanism of receptor-mediated G protein activation.....	8
<b>Chapter 2 Materials and methods</b> .....	11
2.1 Expression and purification of recombinant WT $G\alpha_{i1}$ .....	11
2.2 Preparation of native $G\beta\gamma_t$ subunit .....	11
2.3 Preparation of native rhodopsin .....	12
2.4 Expression of constitutively active rhodopsin at bioreactor scale .....	12
2.5 Purification of RhoM257Y- $G_i$ and RhoM257Y- $G_i$ complex .....	12
2.6 CD measurement.....	13
2.7 Mass spectroscopy .....	13
2.8 Analysis of nucleotide content of WT $G\alpha_{i1}$ by perchloric acid .....	13
2.9 G protein activation assay .....	13
2.10 CPM fluorescence assisted thermostability assay .....	14
2.11 Analysis of rhodopsin-G protein complex by FSEC .....	14
2.12 HTP alanine mutagenesis scanning.....	15
2.13 HTP culture and purification of $G\alpha_{i1}$ alanine mutants.....	15
2.14 Native gel electrophoresis-based thermostability assay (NPAGE-TS) .....	15
2.15 HTP measurement of $G\alpha_{i1}$ alanine mutants' effect on receptor-bound state.....	16
2.16 HTP differential scanning fluorimetry to measure thermostability.....	17
2.17 Analysis of heterotrimer formation by FSEC .....	17
2.18 Modelling of Rhodopsin- $G_i$ complex .....	17
2.19 Sequence alignment of $G\alpha_{i1}$ subunits .....	18
<b>Chapter 3 Results</b> .....	21
3.1 Characterization of recombinant WT $G\alpha_{i1}$ .....	21

3.1.1 Expression and purification of recombinant WT $G\alpha_{i1}$ .....	21
3.1.2 Biophysical Characterization of recombinant WT $G\alpha_{i1}$ .....	21
3.1.3 Analysis of the GDP content in recombinant WT $G\alpha_{i1}$ .....	22
3.1.4 Verification of the functional activity of recombinant WT $G\alpha_{i1}$ .....	23
3.2 Characterization of recombinant WT $G\alpha_{i1}$ in receptor-bound state .....	24
3.2.1 Characterization of the coupling affinity between $G_i$ and rhodopsin.....	24
3.2.2 Characterization of the thermostability of the rhodopsin- $G_i$ complex.....	25
3.2.3 Characterization of the activity of rhodopsin- $G_i$ complex.....	27
3.2.4 Preparation of rhodopsin- $G_i$ complex in large scale .....	28
3.3 HTP alanine mutagenesis scanning of $G\alpha_{i1}$ .....	29
3.3.1 Mutagenesis strategy and workflow .....	30
3.3.2 Primer design by AAScan.....	30
3.3.3 MutantChecker: sequencing results analysis .....	33
3.3.4 PCR cloning primer design software .....	34
3.3.5 Optimization of PCR conditions and HTP Ala mutagenesis workflow.....	36
3.4 Probing $G\alpha_{i1}$ activation at single amino acid resolution .....	38
3.4.1 Development of HTP purification .....	38
3.4.2 Thermal shift analysis of WT $G\alpha_{i1}$ .....	39
3.4.3 Characterization of thermostability of $G\alpha_{i1}$ alanine mutants in the nucleotide-bound state .....	41
3.4.4 Characterization of Rho*- $G_i$ (WT) complex by native gel electrophoresis .....	42
3.4.5 Development of NPAGE assay in HTP format .....	44
3.4.6 Characterization of effects of alanine substitutions in $G\alpha_{i1}$ on receptor-bound state by HTP NPAGE assay .....	45
3.4.7 Characterization of inefficiently coupling alanine mutants in heterotrimer formation .....	46
<b>Chapter 4 Discussion .....</b>	<b>47</b>
4.1 Interpretation of alanine scanning mutagenesis of $G\alpha_{i1}$ .....	47
4.2 Definition and description of stabilization clusters.....	48
4.3 Critical role of N- and C-terminus of $G\alpha_{i1}$ in receptor-mediated response .....	49
4.4 Receptor coupling rearranges stabilization cluster I in the GTPase domain.....	51
4.5 Y320 in cluster I as the signal transduction hub.....	53
4.8 Perturbation of the inter-domain interface facilitates domain separation and GDP release .....	57
4.9 Differences between GDP and GTP states.....	58
<b>Chapter 5 Conclusion and perspectives .....</b>	<b>61</b>

## Acknowledgments

I would like to take this chance to thank all the persons who have been involved to successfully complete this project.

First of all, I would like to show greatest appreciation to my mentor and supervisor, Dr. Dmitry Veprintsev for his support, help, encouragement and guidance in all these years. He not only provided the outstanding research environment, but also taught me how to foster the scientific mind and how to be a good scientist.

I want to express my sincere gratitude to Prof. Gebhard Schertler for his continuous support and invaluable advice for my project. His insightful suggestions and wisdom have helped me a lot in my research.

I am very thankful to Prof. Gerhard Wider and Prof. Stephan Grzesiek for their support and time as a co-examiner.

Also, I would like to acknowledge all my lab members (Dr. Xavier Deupi, Dr. Shoji Maeda, Dr. Chayne Piscitelli, Dr. Gregor Cicchetti, Franziska Heydenreich, Sandro Mendieta, Daniel Mayer, Dr. Jaussi Rolf, Dr. Dalibor Milić, Dr. Valerie Panneels, Antonietta Gasperina, and Ulla Sutter). It has been a great time to work with all of you.

My research also benefits a lot from the effective cooperation with Tilman Flock and Dr. M. Madan Babu from MRC-LMB. Without their involvement and inputs, this project could not have been completed smoothly.

I would like to thank all the members of my family, my parents and my wife's parents for their affections, encouragement and support. Lastly, I want to show my heartfelt thanks to my families for taking care of my two lovely daughters in these years, allowing me to more focus on my research. Thanks for their endless love, understanding and patience and always being with me to face the ups and downs of life.

## Abbreviations

AC:	Adenylyl cyclase
Ala:	Alanine
AtGPA1:	G $\alpha$ protein from <i>Arabidopsis thaliana</i>
cAMP:	3',5'-cyclic adenylyl monophosphate
ConA:	Concanavalin A
Conc.:	Concentration
CPM:	N-[4-(7-diethylamino-4-methyl-3-coumarinyl) phenyl]maleimide
Da:	Dalton
DDM:	$\beta$ -dodecyl-D-n-maltoside
DEER:	Double electron resonance
DSF:	Differential scanning fluorimetry
DTT:	Dithiothreitol
<i>E.coli</i> :	<i>Escherichia coli</i>
EDTA:	Ethylenediaminetetraacetic acid
EL:	Extracellular loops
em:	Emission
ex:	Excitation
FSEC:	Fluorescence-detection size-exclusion chromatography
FSEC-TS:	Fluorescence-detection size-exclusion chromatography-based thermostability assay
GAP:	GTPase activating protein
GDI:	Guanine nucleotide dissociation inhibitor
GDP:	Guanosine diphosphate
GEF:	Guanine nucleotide exchange factor
GF:	Gel-filtration
G $_i$ :	G $\alpha_{i1}\beta\gamma_i$ heterotrimer
GPCRs:	G protein-coupled receptors
GRK:	G protein-coupled receptor kinase
G $_t$ :	Transducin
GTP:	Guanosine-5'-triphosphate
GTP $\gamma$ S:	Guanosine 5'-O-[gamma-thio]triphosphate
G $\alpha$ :	G protein alpha subunit
G $\alpha$ -GDP:	GDP-bound G $\alpha$ state
G $\alpha$ -GTP $\gamma$ S:	GTP $\gamma$ S-bound G $\alpha$ state
G $\alpha_{i1}$ (Ala):	G $\alpha_{i1}$ alanine mutants
G $\alpha_{i1}$ (Ala)-GDP:	G $\alpha_{i1}$ alanine mutant in GDP-bound state
G $\alpha_{i1}$ (Ala)-GTP $\gamma$ S:	G $\alpha_{i1}$ alanine mutant in GTP $\gamma$ S-bound state
G $\alpha_{i1}$ (WT)-GDP:	Wild-type G $\alpha_{i1}$ in GDP-bound state
G $\alpha_{i1}$ (WT)-GTP $\gamma$ S:	Wild-type G $\alpha_{i1}$ in GTP $\gamma$ S-bound state
G $\alpha_{i1}$ :	Human G protein alpha-subunit
G $\beta\gamma$ :	G protein beta/gamma heterodimer
Hepes:	N-(2-hydroxyethyl)-piperazine-N'-2-ethanesulfonic acid
His-tag:	Histidine tag
HLT:	Lipoyl domain tag
h:	Hour
HTP:	High-throughput

IL:	Intracellular loops
IMAC:	Metal ion affinity chromatography
IPTG:	Isopropyl- $\beta$ -D-thiogalactopyranoside
LC-MS:	Liquid chromatography–mass spectrometry
LMNG:	Lauryl-maltose neopentyl glycol
MS:	Mass spectroscopy
MW:	Molecular weight
NPAGE:	Native polyacrylamide gel electrophoresis
NPAGE-TS:	Native polyacrylamide gel electrophoresis-based thermostability assay
NaPi:	Sodium phosphate buffer
NM:	Not measurable
PCR:	Polymerase chain reaction
PDB:	Protein data bank
PLC $\beta$ :	Phospholipase C $\beta$
POPC:	1-palmitoyl-2-oleoyl-sn-glycerol-3-phosphatidylcholine
RFU:	Relative fluorescence units
RGS:	Regulator of G protein signaling
Rho*-G <sub>i</sub> (Ala):	Activated native rhodopsin-G <sub>i</sub> (G $\alpha_{i1}$ alanine mutant/G $\beta\gamma_t$ ) tetrameric complex
Rho*-G <sub>i</sub> (WT):	Activated native rhodopsin-G <sub>i</sub> (wild-type G $\alpha_{i1}$ /G $\beta\gamma_t$ ) tetrameric complex
Rho:	Rhodopsin
RMSD:	Root-mean-square deviation
ROS:	Rod outer segment
s:	Second
SD:	Standard deviation
SDS-PAGE:	Sodium dodecyl sulfate-polyacrylamide gel electrophoresis
SEC:	Size exclusion chromatography
Std.:	Standard
<i>T</i> <sub>50</sub> :	Dissociation temperature
TEV:	Tobacco Etch Virus
<i>T</i> <sub>m</sub> (Ala)	<i>T</i> <sub>m</sub> of G $\alpha_{i1}$ alanine mutant
TM:	Transmembrane helices
<i>T</i> <sub>m</sub> :	Melting temperature
Tris:	Tris(hydroxymethyl)aminomethane
Trp:	Tryptophan
w/:	with
wo/:	without
WT:	Wild-type

## Summary

G protein-coupled receptors (GPCRs) play an important role in many physiological processes such as vision, olfaction and response to hormones, neurotransmitters and chemokines [1]. The binding of an extracellular ligand to a GPCR results in the recruitment and activation of heterotrimeric G proteins by catalyzing GDP/GTP exchange in the  $G\alpha$  subunit of the G protein. This leads to conformational changes and subsequent dissociation of the  $G\alpha$  subunit from the  $G\beta\gamma$  subunits. Both  $G\alpha$  and  $G\beta\gamma$  may interact with effectors and thereby initiate different intracellular signaling cascades. Even though a wide range of biochemical, biophysical, mutagenesis and computational methods have been applied to understand the mechanism of G protein activation, until now it is still not well-known how GPCRs propagate the signal through the distal C-terminal region of  $G\alpha$  to cause allosteric release of GDP.

In this thesis, by applying alanine scanning mutagenesis and high-throughput (HTP) measurements of the effects of alanine substitution on the stability of  $G\alpha_{i1}$  alone and stability of the complex, I generated a comprehensive map of the residues stabilizing the  $G\alpha_{i1}$  subunit in nucleotide-bound as well as receptor-bound states at single amino acid resolution. Mapping the data on the structure of the  $G\alpha_{i1}$  protein and on a model of receptor- $G_i$  complex have allowed me to identify stabilization clusters I and II in the GTPase and cluster III in the helical domain. Many alanine substitutions in cluster I had opposite effects on the stability of the GDP-bound state of  $G\alpha_{i1}$  and the rhodopsin- $G\alpha_{i1}$  complex, suggesting that it undergoes large conformational changes upon complex formation. Most substitutions in clusters II and III destabilized both the nucleotide- and receptor-bound states, suggesting their role as structural scaffolds of both GTPase and helical domains. Cluster I consists of helices  $\alpha 1$  and  $\alpha 5$  which are packed against strands  $\beta 1-3$  when nucleotide is bound. In the receptor-bound state, the interactions between  $\alpha 5$  and  $\alpha 1/\beta 1-3$  are weakened and compensated by new interactions between  $\alpha 5$  and strands  $\beta 4-6$ . The most prominent examples of residues involved in this rearrangement are Y320, which is crucial for the stabilization of the receptor-bound state, and F336, important for the stability of the GDP- and GTP-bound states. G protein activation is mediated via destabilization of helix  $\alpha 1$ , caused by rearrangement of cluster I. This leads to the perturbation and weakening of the inter-domain interface, dissociation of the helical domain from the GTPase domain and release of GDP.

The exhaustive coverage and single amino acid resolution of my mutagenesis analysis, combined with the stability measurements obtained for both  $G\alpha_{i1}$  and the Rho\*- $G_i$  complex, and, most importantly, comparison of the energetics of the GDP-, receptor- and GTP $\gamma$ S-bound states allowed me to obtain the most detailed data set on the process of G protein activation currently available. My results show that the interactions involved in the stabilization of the receptor-bound conformation of  $G\alpha_{i1}$  are broader and more complex than previously suggested.

## Zusammenfassung

G-protein gekoppelte Rezeptoren (GPCRs) spielen eine wichtige Rolle in vielen physiologischen Prozessen wie Sehvermögen und Geruchssinn, sowie in der Reaktion auf Hormone, Neurotransmitter und Chemokine. Bindung eines extrazellulären Liganden an einen GPCR führt zur Rekrutierung und Aktivierung heterotrimerer G-proteine via GDP/GTP Austausch in der  $G\alpha$ -Untereinheit des G-proteins. Dies führt zu konformationellen Änderungen und darauffolgender Dissoziation der  $G\alpha$ - von den  $G\beta\gamma$ -Untereinheiten. Sowohl  $G\alpha$  als auch  $G\beta\gamma$  können mit Effektoren interagieren und dadurch verschiedene intrazelluläre Signalkaskaden initiieren. Obwohl viele verschiedene biochemische, biophysikalische, mutagenesebasierte und computergestützte Methoden auf das Problem angewendet wurden, bleibt der detaillierte Mechanismus der G-Protein-Aktivierung weiterhin ungeklärt. Bis jetzt ist es nicht bekannt wie GPCRs das Signal über die distale C-terminale Region weiterleiten und die allosterische Freisetzung von GDP katalysieren.

In dieser Doktorarbeit habe ich mittels Alanin-Mutagenese-Scan und Hochdurchsatzmessungen des Effekts von Alanin-Substitutionen auf die Stabilität von  $G\alpha_{i1}$  und Rhodopsin-  $G\alpha_{i1}$ -Proteinkomplex eine umfassende Karte stabilisierender Positionen innerhalb der  $G\alpha_{i1}$ -Untereinheit in ihren nukleotid- und rezeptorgebundenen Formen mit der Auflösung jeder einzelnen Aminosäure generiert. Die Übertragung der Daten auf die Struktur von  $G\alpha_{i1}$  und auf ein Modell des Rhodopsin-  $G\alpha_{i1}$ -Komplexes hat es mir ermöglicht die Stabilisationscluster I und II in der GTPase- und Stabilisationscluster III in der helicalen Domäne zu identifizieren. Viele Aminosäuresubstitutionen durch Alanin im Cluster I hatten gegensätzliche Effekte auf die Stabilität des GDP-gebundenen  $G\alpha_{i1}$  und die des Rhodopsin-  $G\alpha_{i1}$ -Komplexes was darauf hindeutet, dass sich die Konformation im Cluster I stark ändert, wenn sich der Komplex bildet. Die meisten Substitutionen in den Clustern II und III haben sowohl die GDP-gebundene Form des  $G\alpha_{i1}$  als auch den Rhodopsin-  $G\alpha_{i1}$ -Komplex destabilisiert, was darauf hinweist, dass sie das strukturelle Gerüst der GTPase- und der helicalen Domäne bilden. Cluster I besteht aus Helix  $\alpha 1$  und  $\alpha 5$ , die im nukleotidgebundenen Zustand mit den  $\beta$ -Faltblättern 1-3 interagieren. Wenn Rezeptor gebunden wird, werden die Interaktionen zwischen  $\alpha 5$  und  $\alpha 1/\beta 1-3$  geschwächt, was durch neue Interaktionen zwischen  $\alpha 5$  und  $\beta 4-6$  kompensiert wird. Die markantesten Beispiele von Aminosäuren, die in diese strukturelle Neuordnung involviert sind, sind das für die Stabilisierung des rezeptorgebundenen Zustands kritische Y320 und F336, das wichtig für die Stabilität der GDP- und GTP-gebundenen Zustände ist. G Proteinaktivierung wird über die Destabilisierung von Helix  $\alpha 1$  herbeigeführt, die durch die Neuordnung des Clusters I zustande kommt. Dies führt zur Störung der Interaktionen und Schwächung an der Schnittstelle zwischen den beiden Domänen was zur Dissoziation der helicalen- von der GTPase-Domäne und Freisetzung des GDP führt.



Die vollständige Abdeckung der gesamten Aminosäuresequenz durch meine Mutagenesestudie, kombiniert mit den Stabilitätsmessungen von  $G\alpha_{i1}$  und Rhodopsin-  $G\alpha_{i1}$ , aber vor allem der Vergleich der Energetik der GDP-, Rezeptor- und  $GTP\gamma S$ -gebundenen Zustände hat es mir erlaubt den aktuell detailliertesten Datensatz zur G-Protein-Aktivierung zu generieren. Meine Resultate zeigen, dass die Interaktionen, die an der Stabilisierung der rezeptorgebundenen Konformation von  $G\alpha_{i1}$  beteiligt sind umfassender und komplizierter sind als bisher angenommen.

## Publications:

- *Dawei Sun*, Andrea Prota, Dmitry B Veprintsev (**In Preparation**)  
Studies of a highly conserved valine provide insights into the mechanism of G protein activation.
- *Dawei Sun*, Tilman Flock, Xavier Deupi, Shoji Maeda, Sandro Mendieta, Daniel Mayer, Roger Dawson, Gebhard Schertler, M. Madan Babu, Dmitry Veprintsev (**Under peer-review in Nature**)  
Probing G $\alpha_{i1}$  protein activation at single amino acid resolution.
- Tilman Flock, *Dawei Sun*, Charles Ravarani, A. Venkatakrishnan, Melis Kayikci, Chris Tate, Dmitry Veprintsev, M. Madan Babu (**Under peer-review in Nature**)  
Mechanism of a universal allosteric activation mechanism in G proteins decouples allostery from GPCR interaction specificity.
- Shoji Maeda, *Dawei Sun*, Ankita Singhal, Marcello Foggetta, Joerg Standfuss, Michael Hennig, Roger J.P. Dawson, Dmitry Veprintsev, Gebhard Schertler. “Crystallization scale preparation of a stable GPCR signaling complex between constitutively active rhodopsin and G-protein”, *PLOS ONE*, 9(6): e98714 (2014).
- *Dawei Sun*, Martin Ostermaier, Franziska Heydenreich, Daniel Mayer, Joerg Standfuss, Rolf Jaussi and Dmitry B. Veprintsev. “AlaScan–automatic primer design for scanning mutagenesis”, *PLOS ONE*, 10(8): e78878 (2013).

## Patent:

- Mutants stabilizing the active state of the G protein and screening methodology (European Patent, **in progress**)  
*Dawei Sun*, Gebhard Schertler, Dmitry Veprintsev

# Chapter 1 Introduction

## 1.1 The heterotrimeric G protein cycle

Heterotrimeric G proteins constitute one of the most important components in the signal transduction pathway mediated by GPCRs. Heterotrimeric G proteins are composed by  $\alpha$ ,  $\beta$  and  $\gamma$  subunits, among which the  $G\alpha$  subunit possesses the catalytic GTPase activity, while the  $\beta$  and  $\gamma$  subunits act as an obligate heterodimer without intrinsic catalytic activity. In the canonical G protein cycle, the heterotrimeric G proteins serve as the molecular switches that connect transmembrane receptors with downstream effectors (Fig. 1.1). When the receptor is activated by extracellular stimuli, it changes its conformation and functions as a guanine nucleotide exchange factor (GEF) exchanging the GDP in the nucleotide-binding pocket of G proteins for GTP. The activated GTP-bound G proteins quickly dissociate into an active GTP-bound  $G\alpha$  ( $G\alpha$ -GTP) state and the  $\beta\gamma$  heterodimer. The  $G\alpha$ -GTP state further modulates downstream targets such as adenylyl cyclase (AC), phospholipase C $\beta$  (PLC $\beta$ ) and the small GTPase Rho [2]. The dissociated  $\beta\gamma$  heterodimer also regulates its own downstream effectors, including mitogen-activated protein kinases, phosphoinositide 3 kinases, K<sup>+</sup>-selective ion channels and the voltage-gated calcium channel [2]. The downstream signaling is terminated when the  $G\alpha$  subunit hydrolyzes the bound GTP to GDP. The GTP hydrolysis is accelerated by the regulator of G protein signaling (RGS), GTPase activating protein (GAP) [2]. The  $G\alpha$  subunit is converted to the inactive GDP-bound state and can re-associate with  $G\beta\gamma$  heterodimer to form the inactive heterotrimeric complex and may couple with the activated receptor again.

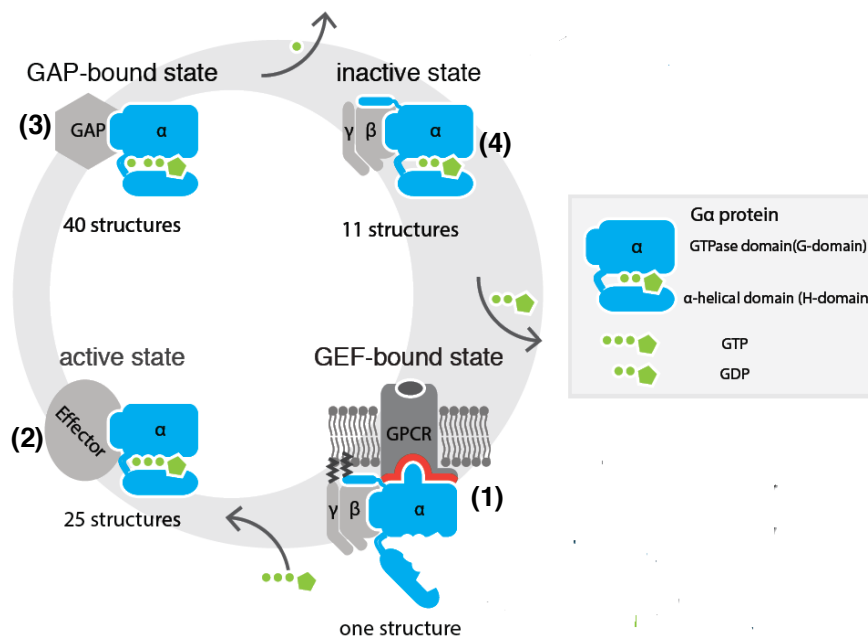


**Fig. 1.1. Heterotrimeric G protein cycle states.** The signaling cycle of G proteins involves (1) release of GDP upon binding with GPCRs (GEF), (2) binding of GTP and recruiting of downstream signaling effectors in the GTP bound form, and (3) hydrolysis of GTP promoted by GAP, leading to (4) the inactive GDP-bound state.

## 1.2 General overview of GPCRs

GPCRs form one of the largest protein families in humans with approximately 800 members. They respond to a wide range of extracellular ligands, such as photons, odorants, inorganic ions, lipids, catecholamine, neurotransmitters and large glycoprotein hormones, and convey these signals to the different intracellular responses by activation of heterotrimeric G proteins [3]. GPCRs are also involved in many diseases, such as neurological disorders, several forms of cancer, osteoporosis and inflammatory diseases. Therefore, today, GPCRs are the targets of ~30% of pharmaceuticals on the market [4].

Based on the phylogenetic analysis, GPCRs can be classified into five main families: the rhodopsin family (701 members), the adhesion family (24 members), the frizzled/taste family (24 members), the glutamate family (15 members) and the secretin family (15 members) [5]. Among the five families, the rhodopsin family is the largest, most diverse and best-studied one, forming four main groups with 13 sub-branches [5].

All the GPCRs adopt a similar seven-transmembrane (TM)  $\alpha$ -helical topology connected by three intracellular loops (IL) and three extracellular loops (EL), as well as an extracellular N-terminus and an intracellular C-terminus (Fig. 1.2) [3, 6]. The 7TM architecture of GPCRs has been qualitatively confirmed by the emergence of many GPCRs crystal structures, such as rhodopsin,  $\beta_1$  and  $\beta_2$  adrenergic receptors,  $A_{2A}$  adenosine, CXCR4 chemokine, D3 dopamine, H1 histamine, neurotensin 1, M2 and M3 muscarinic receptors [7]. As the first determined GPCR structure [8], the crystal structure of rhodopsin provides a first glimpse into the architecture of GPCRs and serves as a model for rhodopsin family GPCRs. The observed N-S-x-x-N-P-x-x-Y motif within TM7, the DRY motif between TM3 and IL2, and the XBBXXB (B: basic amino acid) motif in IL3 in the rhodopsin structure are shown to be highly conserved in members of the rhodopsin-like GPCR family [6, 9]. Additionally, the C-terminus of rhodopsin contains an eighth  $\alpha$ -helix and palmitoylated cysteine residues which are common features shared by other GPCRs [6, 9]. However, rhodopsin is unique and distinguished from non-opsin receptors by a covalently bound inverse agonist, 11-*cis*-retinal, which leads to the inherent stability of rhodopsin. Another unique feature of rhodopsin is its abundance in retina, accounting for 95% of the total protein in the rod outer segment (ROS) membrane. Thus, both features allow the preparation of large amounts of pure native rhodopsin from bovine retinas. This is also one of the reasons why rhodopsin is chosen in this project to study receptor-mediated G protein activation.

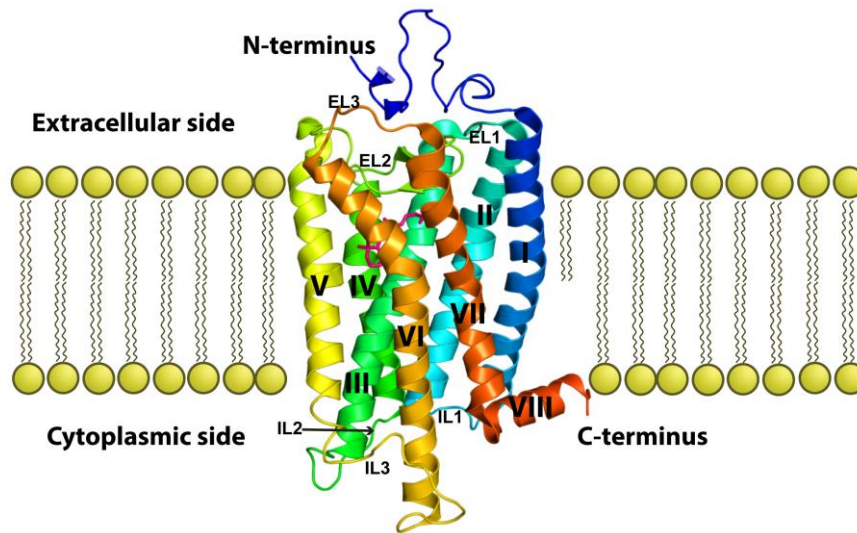


**Fig. 1.2. General architecture of 7TM receptors.** The crystal structure of ground-state rhodopsin bound with its natural ligand 11-*cis*-retinal (PDB 1U19). The opsin molecule is shown with a rainbow coloring scheme. The transmembrane helices are numbered with roman numerals. The bound 11-*cis*-retinal is shown in pink. All the GPCRs adopt a similar seven transmembrane  $\alpha$ -helical topology connected by three intracellular loops (IL 1-3) and three extracellular loops (EL 1-3).

### 1.3 Heterotrimeric G protein subunits

So far, 21  $G\alpha$  subunits encoded by 16 genes, 6  $G\beta$  subunits encoded by 5 genes and 12  $G\gamma$  subunits encoded by 12 genes have been identified in mammals [10]. Classically, the G proteins can be divided into four main classes based on the sequence similarity in the  $G\alpha$  subunit:  $G\alpha_s$  ( $G\alpha_s$ ,  $G\alpha_{olf}$ ),  $G\alpha_{i/o}$  ( $G\alpha_{i1}$ ,  $G\alpha_{i2}$ ,  $G\alpha_{i3}$ ,  $G\alpha_t$ ,  $G\alpha_z$ ,  $G\alpha_g$ ,  $G\alpha_o$ ),  $G\alpha_{q/11}$  ( $G\alpha_q$ ,  $G\alpha_{11}$ ,  $G\alpha_{14-16}$ ) and  $G\alpha_{12/13}$  [11] (Fig. 1.3). Among them,  $G\alpha_s$  and  $G\alpha_{i/o}$  regulate the production of cAMP by stimulating or inhibiting the downstream effector of adenylate cyclase, respectively.  $G\alpha_{q/11}$  mediates signaling through the PLC pathway and  $G\alpha_{12/13}$  induces a Rho-dependent response [12]. The size of the  $G\alpha$  subunits ranges from 39 to 45 kilodaltons (kDa), and all  $G\alpha$  subunits, except photoreception-specific transducin ( $G\alpha_t$ ), contain a post-translational modification with a 16-carbon palmitate near the N-terminus. The myristoylation at the N-terminus is also observed for  $G\alpha_i$  family of proteins. The lipid modification of the  $G\alpha$  subunit is important for its localization to specific cell membrane regions and for regulating interactions with other proteins [13, 14].

The dimerization between  $G\beta$  and  $G\gamma$  subunit to form a  $G\beta\gamma$  heterodimer are obligate in nature, and they can only be dissociated under denaturing conditions [15]. The proper folding of the  $G\beta$  subunit also requires the  $G\gamma$  subunit [16]. As for the  $G\alpha$  subunit, all  $G\gamma$  subunits are post-transnationally prenylated, which ensures membrane localization of the  $G\beta\gamma$  heterodimer [17]. Most  $G\beta$  and  $G\gamma$  subunits can be paired with each other to form the heterodimer, however there are exceptions. For instance,  $G\beta_1$  subunit can couple with both  $G\gamma_1$  and  $G\gamma_2$  subunit, while the  $G\beta_2$  subunit can only bind to the  $G\gamma_2$  subunit [18].

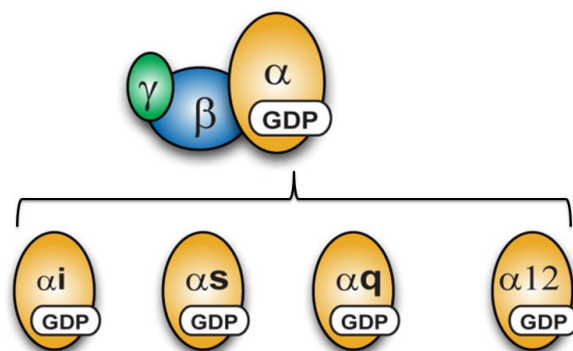


**Fig. 1.3. G $\alpha$  subunit families.** The classification of heterotrimeric G proteins is based on the primary sequence similarity in the G $\alpha$  subunit.

#### 1.4 Heterotrimeric G protein structure

The structures of many G $\alpha$  subunits from the four classes have been solved in different conformations such as the inactive GDP-bound state (Fig. 1.4a) [19], the transition state with GDP-AlF $_4^-$  [20], the active GTP $\gamma$ S-bound (G $\alpha$ -GTP $\gamma$ S) state (Fig. 1.4b) [19], the heterotrimeric state with G $\beta\gamma$  subunit [21], as well as the effector-bound state in complex with RGS [22], AC [23], GRK2 [24] and PLC $\beta$ 3 [25]. The structural information clearly indicates that all G $\alpha$  subunits adopt one completely conserved fold with two distinct domains: a GTPase domain composed of five  $\alpha$ -helices surrounding a  $\beta$ -sheet of six antiparallel strands, and a helical domain formed by six  $\alpha$ -helices (Fig. 1.4a-b). The bound GDP or GTP is sequestered between GTPase domain and helical domain. The GTPase domain possesses the catalytic capability to hydrolyze GTP and also provides most of the binding surface interacting with G $\beta\gamma$  subunits, receptors, and effector proteins. The helical domain is unique for the G $\alpha$  subunit and distinguishes it from other members of the G protein superfamily, such as the monomeric Ras protein superfamily and elongation factors G (EF-G) [26]. Structurally, the helical domain forms a lid over the nucleotide-binding pocket, which may be critical to stabilize the nucleotide and prevent the release of GDP [27].

Comparison of nucleotide-dependent changes in the G $\alpha$  subunit revealed three prominent flexible regions named Switch I (residues 177-187 in G $\alpha_{i1}$ ), II (residues 199-219 in G $\alpha_{i1}$ ) and III (residues 231-242 in G $\alpha_{i1}$ ), respectively (Fig. 1.4a-c) [28, 29]. All three Switch sites are located in the GTPase domain, although Switch I connects the GTPase domain with the helical domain, and adopts different conformations during the G $\alpha$  activation (Fig. 1.4a-c). In the inactive GDP-bound state, Switch II and III are completely disordered, but undergo disorder-to-order conformational changes upon binding of GTP $\gamma$ S (Fig. 1.4a-c). This is especially true for Switch II incorporating the whole  $\alpha$ 2-helix which is stabilized by the interaction of the  $\gamma$ -phosphate of GTP to adopt the helical conformation [26]. These regions are also primarily sites for binding with the G $\beta\gamma$  subunit, RGS proteins and effectors [21, 30]. The conformational alternation is also observed in the N-terminal and C-terminal of the G $\alpha$  subunit.

The 32 residues of the N-terminal and the C-terminal 10 residues are disordered in the active  $G\alpha$ -GTP $\gamma$ S state, while forming a compact micro-domain in the inactive  $G\alpha$ -GDP state (Fig. 1.4a-c) [19]. In addition, the N-terminal of  $G\alpha$ -GDP is unfolded into an extended helix conformation upon binding with the  $G\beta\gamma$  subunit (Fig. 1.5) [21].

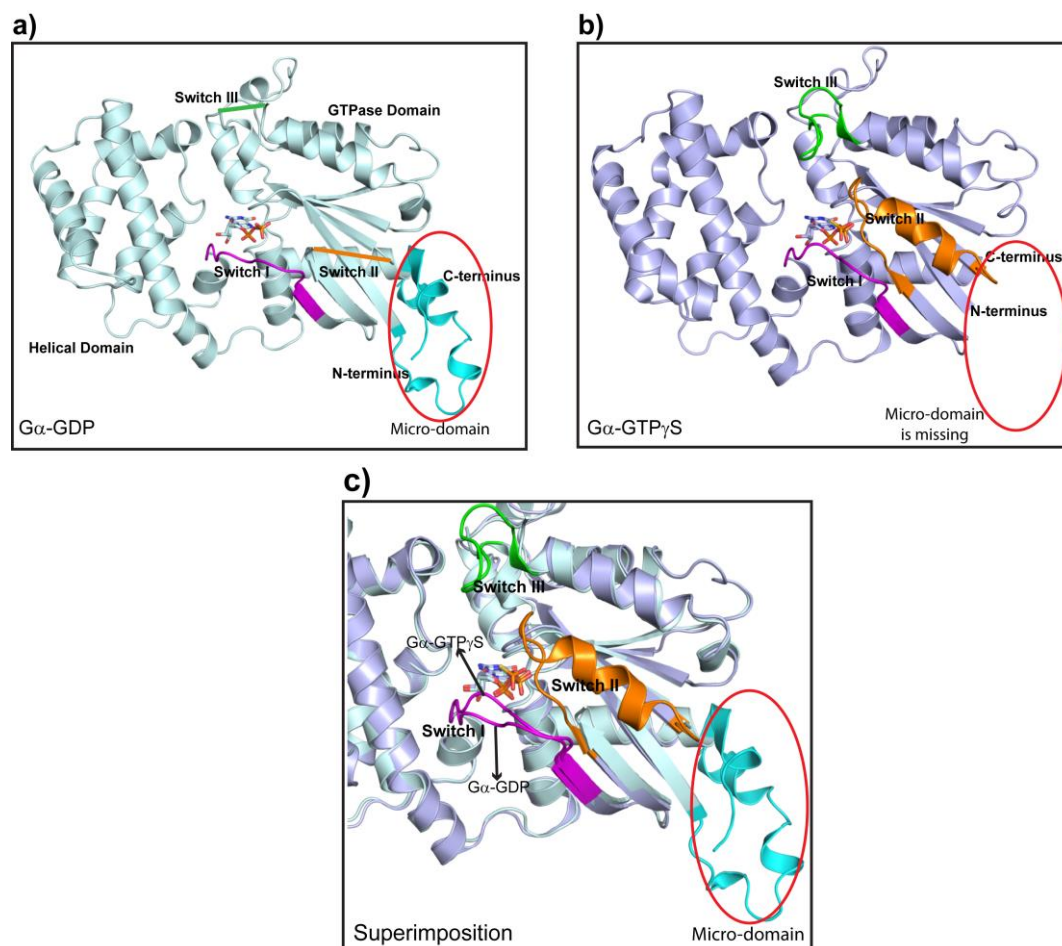


**Fig. 1.4. Structures of  $G\alpha$  subunit.** a-b, Crystal structures of the  $G\alpha$  subunit in GDP-bound state (a) (PDB 1GDD) and GTP $\gamma$ S-bound state (b) (PDB 1GIA). c, Superimposition of a, b. The switch I, II and III regions are colored in magenta, orange and green in a, b and c, respectively. The N- and C-terminus forming the micro-domain in the GDP-bound state is colored in cyan and marked with a red ellipse.

All  $G\beta$  subunits are built up of a seven-bladed propeller structure composed of the typical WD-40 sequence repeats and an  $\alpha$ -helical N-terminus (Fig. 1.5) [18, 31]. The  $G\gamma$  subunit is composed of two short  $\alpha$ -helices joined by a loop (Fig. 1.5). The N-terminal helix of  $G\gamma$  forms a coiled-coil interaction with the N-terminal  $\alpha$ -helix of  $G\beta$ , and the C-terminal helix of  $G\gamma$  makes extensive contacts with blades five and six of  $G\beta$  (Fig. 1.5) [18, 31]. The  $G\beta\gamma$  heterodimer binds to the hydrophobic pocket formed by Switch I and II regions of  $G\alpha$ -GDP, as well as along with the extended N-terminal of  $G\alpha$ -GDP, to form the heterotrimeric complex (Fig. 1.5) [21]. Currently, none of the G protein heterotrimer structures show the direct evidence of  $G\alpha$ - $G\gamma$  contact. One of the major functions of the  $G\beta\gamma$  subunit is to act as the guanine nucleotide dissociation inhibitor (GDI) to inhibit the spontaneous activation of the  $G\alpha$  subunit by preventing the dissociation of bound-GDP from the nucleotide-binding pocket [32].



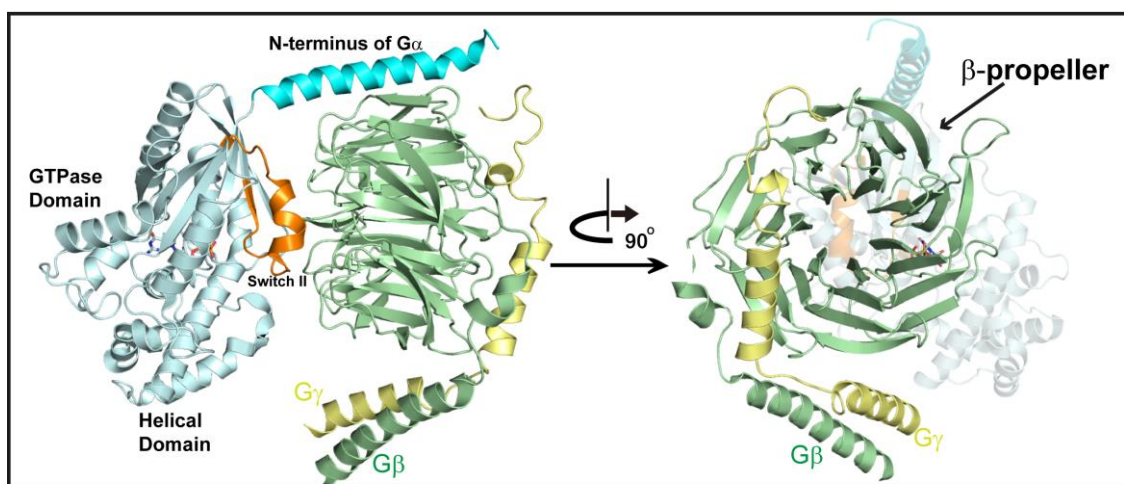


**Fig. 1.5. Structure of heterotrimeric G protein.** The structure of heterotrimeric G protein (PDB 1GP2) is composed of the  $G\alpha$  (pale cyan),  $G\beta$  (pale green) and  $G\gamma$  (pale yellow) subunits. The switch II region of  $G\alpha$  (orange) subunit undergoes disorder-to-order transition upon binding of the  $G\beta$  subunit. The N-terminus of  $G\alpha$  subunit (cyan) is unfolded into an extended helix conformation upon binding by the  $G\beta\gamma$  subunit. The structure of  $G\beta$  subunit is the prototypical  $\beta$ -propeller fold and the  $G\gamma$  subunit is composed of two short  $\alpha$ -helices joined by a loop.

## 1.6 GPCR-G complex state

The GPCR-mediated nucleotide exchange in the  $G\alpha$  subunit can be considered as a two-step process: the release of GDP from the nucleotide-binding site of the  $G\alpha$  subunit leading to a GPCR-bound “empty pocket” ternary GPCR-G protein complex state, GTP binding to the nucleotide-free  $G\alpha$  which causes the dissociation of the  $G\alpha$  subunit resulting in the active  $G\alpha$ -GTP state. In comparison with the well-characterized nucleotide-bound state, the GPCR-G protein interactions in the nucleotide-free complex state are less understood.

Earlier studies such as mutagenesis [33, 34], studies of G protein chimeras [35, 36], chemical crosslinking [37] and proteolysis experiments [38] identified that the binding interface of the G protein to receptor is mainly located in the C-terminus of  $\alpha 5$ -helix and the adjacent  $\alpha 4$ - $\beta 6$  loop of the  $G\alpha$  subunit which interacts with the cytoplasmic pocket opened by receptor-activation. The NMR and crystallographic studies of the  $G_t$  C-terminal peptide bound to rhodopsin further proved this assumption [39, 40]. Additionally, the replacement of  $\alpha 3$ - $\beta 5$  loop of the  $G_{\alpha_s}$  subunit with the homologous amino acids alters the specificity toward  $\beta_2$ -adrenergic receptor ( $\beta_2$ AR), suggesting the role of  $\alpha 3$ - $\beta 5$  loop in coupling with the receptor [41]. The recent chemical crosslinking of the muscarinic M3 receptor to  $G_q$  identified the N- and C-terminus, as well as  $\beta 2$ - $\beta 3$  in the  $G_{\alpha_q}$  subunit as the interaction points of the G protein with the receptor [42]. On the receptor side, the intracellular loops 2 (IL2), IL3 and IL4 of the receptor were identified as the primary specificity determinants for the G protein coupling selectivity [43]. The process of activation was shown to involve a rotation and translation of the C-terminal helix  $\alpha 5$ , increase in the mobility in the vicinity of the nucleotide binding site as well as changes in the dynamics of the Switch I, II and III regions [44-47].



The striking breakthrough in uncovering the interaction between receptor and G protein was the emergence of the first crystal structure of the  $\beta_2$ AR- $G_s$  complex [48] (Fig. 1.6). The  $\beta_2$ AR- $G_s$  structure qualitatively confirms that the natively disordered C-terminus of  $G\alpha_s$  forms an alpha helix which penetrates into the cytoplasmic core of transmembrane bundle to make extensive contacts with transmembrane helices 3 (TM3), TM5 and TM6 of  $\beta_2$ AR. The crystal structure also identified a few less extensive interactions between IL2, TM5 of the receptor and  $\alpha$ N/ $\beta$ 1 hinge,  $\beta$ 2- $\beta$ 3 loop, residues in  $\alpha$ 4 of  $G\alpha_s$ . However, the structure does not display any direct contacts between receptor and  $G\beta\gamma$  subunit, although  $G\beta\gamma$  subunit has also been shown to bind to receptor and stabilize the receptor- $G\alpha$  interface in previous cross-linking [49, 50] and mutagenesis studies [51].

In addition, the  $\beta_2$ AR- $G_s$  structure [48] displays the first structural view of the intermediate state of  $G\alpha$  in the nucleotide-free conformation characterized by the large displacement of the helical domain against the GTPase domain (Fig. 1.6), which is consistent with the recent result that the domain separation between the helical and GTPase domains is required for the receptor activation, as suggested by the double electron resonance (DEER) study in a rhodopsin- $G_i$  model system [52]. The results from Rosetta-based simulation [53] and electron microscopy [54] method further indicate that the helical domain in the receptor-bound state exists in a dynamic equilibrium between multiple conformations.

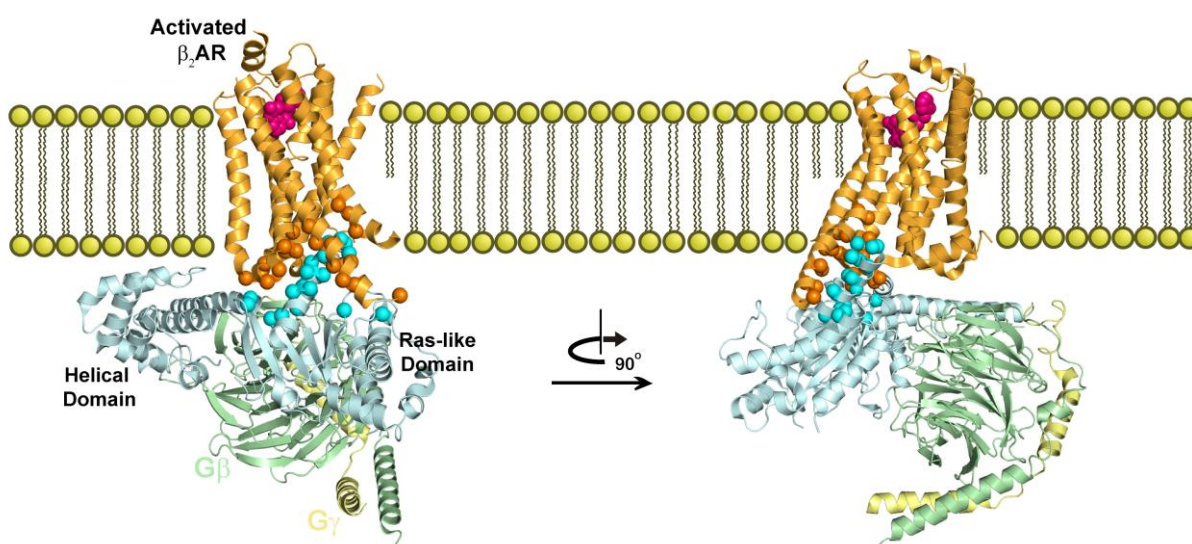


**Fig. 1.6. Structure of GPCR-G protein complex.** The crystal structure of  $\beta_2$ AR- $G_s$  (PDB 3SN6) is the first structure of a G protein in the receptor-bound complex state. The activated  $\beta_2$ AR receptor,  $G\alpha_s$ ,  $G\beta$  and  $G\gamma$  subunits are colored in bright orange, pale cyan, pale green and pale yellow, respectively. The interacting residues located in  $G\alpha_s$  and  $\beta_2$ AR are displayed as spheres and colored in cyan and orange, respectively.

## 1.7 Hypothesized mechanism of receptor-mediated G protein activation

Until now, three models of how the activated receptor causes the G protein to release GDP from the  $G\alpha$  subunit have been proposed. The ‘sequential release’ model [55, 56] stipulates that the coupling with receptor causes a transient conformational change in helix  $\alpha 5$  of the  $G\alpha$  subunit which induces GDP release (Fig. 1.7a). This model solely depends on receptor/ $G\alpha$  contacts. Especially, helix  $\alpha 5$  in the  $G\alpha$  subunit appears to be constituted of two highly conserved modules with distinct functions: an interface module which is important to directly couple with the receptor through its C-terminus by the movement of the rotation and translation, and an transmission module which affects the GDP release by communicating with the GDP-binding pocket through the  $\alpha 5$ - $\beta 6$  loop containing the guanidine-ring-binding TCAT motif, as suggested by mutagenesis [57-60], insertion of the glycine linker [61], site-directed spin labeling [53, 62], and the crystal structure [48].

The alternative two models include the  $G\beta\gamma$  subunit as an active participant in GDP release to open an exit route for the guanine nucleotide to leave the complex. In the ‘lever arm’ model [63], the receptor utilizes the N-terminal helix of  $G\alpha$  as a lever arm to pull  $G\beta\gamma$  away from  $G\alpha$ , which causes the disruption of the binding interface between Switch I and II regions of  $G\alpha$  and  $G\beta\gamma$ , resulting in GDP release (Fig. 1.7b). The ‘gear-shift’ model [64] proposes that the receptor uses the N-terminal helix of  $G\alpha$  to enforce a tighter packing of  $G\beta\gamma$  and  $G\alpha$ , which allows the N-terminus of  $G\gamma$  to engage in displacing the helical domain away from the nucleotide-binding site and triggers GDP release (Fig. 1.7c). In support of these models, several alanine mutations at the Switch interface of  $G\beta$  [65] and C-terminus of  $G\gamma$  [66] showed the significant effect in the receptor-catalyzed nucleotide exchange.

In addition, GDP is tightly sequestered between GTPase domain and helical domain. In order to release GDP, the interruption of the inter-domain interaction seems to be required. The disruption of these interactions by mutagenesis in  $G\alpha_s$  and  $G\alpha_{i1}$  resulted in the increased rates of basal or decreased rates of receptor-catalyzed exchange [67, 68]. A similar effect was also observed in one glycine-proline mutation located in the inter-domain linker [69]. It is also supported by the results from the molecular dynamics simulation that the inter-domain reorientation is required for receptor-mediated activation [70].

A recent modelling study [53] has suggested that G protein activation is associated with the rearrangement of the interfaces between helices  $\alpha 1$  and  $\alpha 5$ , and between  $\alpha 5$  and the loop  $\alpha 5$ - $\beta 6$ . Subsequent experimental mutagenesis studies [71] pinpointed residue F336 in helix  $\alpha 5$  of  $G\alpha_{i1}$  as a particularly important residue for G protein activation, as its mutation increases the rate of spontaneous GDP release. The proposed mechanism involves F336 acting as a relay, transmitting conformational changes via  $\beta 2/3$  and helix  $\alpha 1$  to the phosphate binding loop.

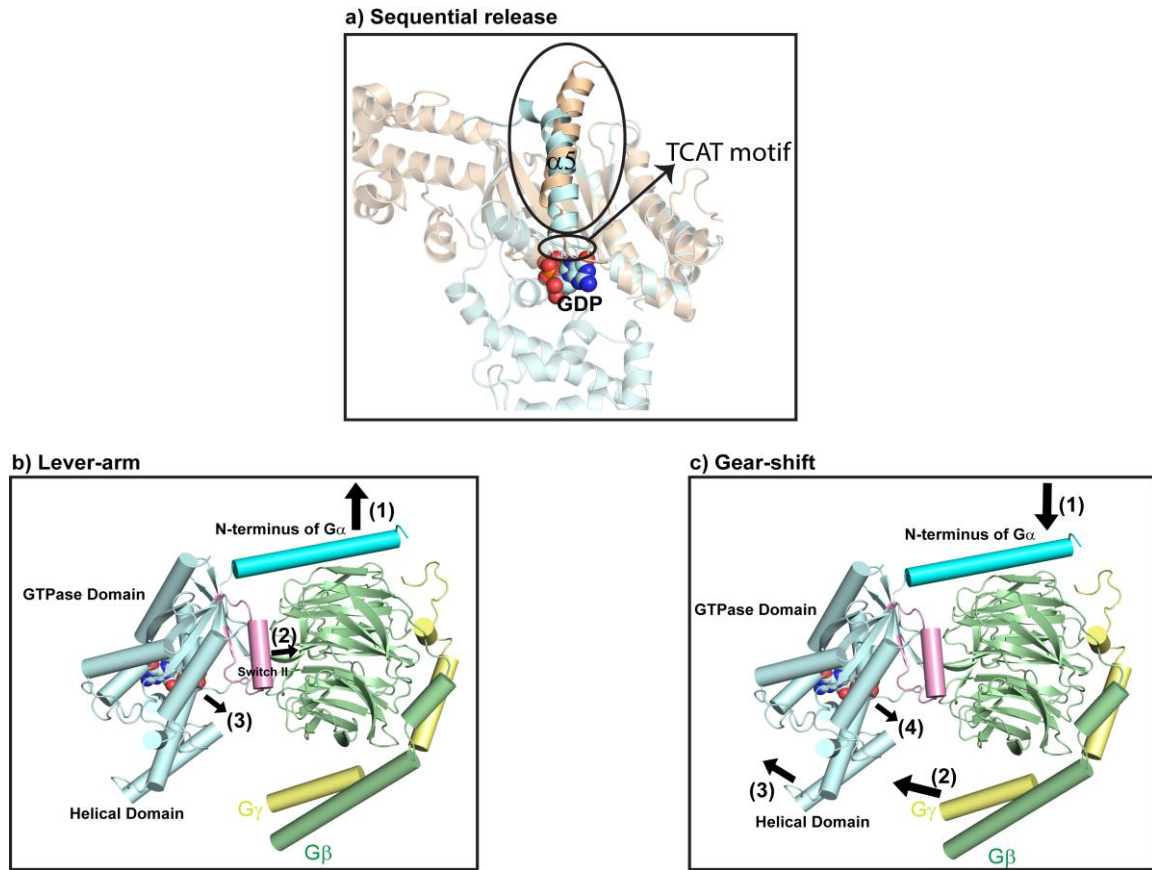


**Fig. 1.7. Proposed mechanisms of receptor-mediated G protein activation.** **a**, Sequential release model. The conformational change in helix  $\alpha_5$  leads to GDP release. The  $G\alpha$  subunit in GDP-bound and receptor-bound states is colored in pale cyan and pale orange, respectively. **b**, Lever-arm model. The receptor uses the N-terminal helix of  $G\alpha$  as a lever arm to pull  $G\beta\gamma$  away from  $G\alpha$  (1), prying Switch II away from the nucleotide-binding pocket (2) and causing GDP release (3). **c**, Gear-shift model. The receptor pushes the N-terminal helix of  $G\alpha$  (1) to force  $G\gamma$  to engage in displacing the helical domain from GTPase domain (2-3), leading to GDP release (4).

## 1.8 Aim of the thesis

Although the GPCR-mediated G protein activation has been extensively studied by biochemical, biophysical, mutagenesis and computational methods, we still do not have a complete picture of how GPCRs propagate the signal through the distal C-terminal region of  $G\alpha$  to cause the allosteric release of GDP.

The primary goal of my project is to understand the G protein activation by providing the complete molecular mapping of the  $G\alpha_{i1}$  subunit at a single amino acid resolution. To achieve the single amino acid resolution, I decided to perform a HTP Ala mutagenesis to replace each residue in the  $G\alpha_{i1}$  subunit with Ala. Once the Ala mutants' library covering the whole sequence of  $G\alpha_{i1}$  was created, I could use the developed HTP purification method to prepare the recombinant Ala mutants in the HTP format. To characterize each Ala mutant's effect, I decided to measure the stability effect of each Ala mutant of  $G\alpha_{i1}$  both in the nucleotide (GDP and  $GTP\gamma S$ ) -bound and receptor-bound states by utilizing the developed HTP thermal shift assay and HTP native gel electrophoresis (NPAGE) -based assay. Comparison of the energetics of the GDP-, receptor- and  $GTP\gamma S$ -bound states allows me to obtain the most detailed data set to understand the process of G protein activation to date.

In this thesis, the experiments to achieve this goal and the detailed interpretation of the experimental results are described. The thesis is started with an introduction of how to prepare the recombinant WT  $G\alpha_{i1}$  in large quantity with the active conformation, followed by the characterization of the recombinant WT  $G\alpha_{i1}$  in the receptor-bound state. After that, the methodology, application and results of my developed HTP Ala mutagenesis scanning, HTP thermal shift assay and HTP NPAGE-based assay are addressed. In the end, the detailed discussion based on the analysis of experimental results is provided. The thesis is then concluded with future prospects resulting from my work.

## Chapter 2 Materials and methods

### 2.1 Expression and purification of recombinant WT $G\alpha_{i1}$

Human G protein alpha subunit ( $G\alpha_{i1}$ ) was cloned into the pJ411 vector (DNA 2.0), incorporating an N-terminal 10×histidine tag (His-tag) followed by a lipoyl domain tag (HLT) and a TEV cleavage site (Fig. 2.1). In addition a similar construct without HLT was prepared (Fig. 2.1). The sequenced plasmid was transformed into *Escherichia coli* (*E.coli*) BL21 (DE3) strain. The bacterial cells were grown in LB or TB media at 37°C. When the OD<sub>600</sub> reached 0.6, the protein expression was induced by addition of 1 mM isopropyl-β-D-thiogalactopyranoside (IPTG) and the cells were further incubated for 20 h at 20 °C. After harvesting cells by centrifugation, the cell pellets were resuspended in buffer A (25 mM Tris-HCl pH 7.4, 0.5 M NaCl, 50 mM imidazole, 10% glycerol) and disrupted by sonication. The supernatant was loaded onto a 5 ml His-Trap FF crude column (GE Healthcare). The column was washed with buffer A and eluted with 25 mM Tris-HCl, pH 7.4, 0.5 M imidazole, 0.5 M NaCl and 10% glycerol. After the cleavage of the histidine tag, the cleaved  $G\alpha_{i1}$  protein was further purified by size exclusion chromatography (HiLoad Superdex 200, GE Healthcare).

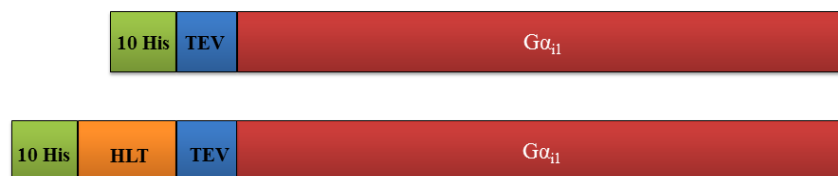


**Fig. 2.1. Design of WT  $G\alpha_{i1}$  expression construct.** 10×His-tag, TEV cleavage site and HLT are colored in green, blue, and orange, respectively. Human  $G\alpha_{i1}$  is colored in dark red.

### 2.2 Preparation of native $G\beta\gamma_t$ subunit

$G\beta\gamma_t$  was separated from endogenous transducin ( $G_t$ ) as previously described [72]. Briefly, dark-adapted bovine retinas (W L Lawson) were exposed to light at 4 °C overnight. The rod outer segment (ROS) membrane was collected by 25-30% (w/w) sucrose gradient. After isotonic and hypotonic washes,  $G_t$  was dissociated from ROS membrane by addition of GTP (Sigma-Aldrich). The collected  $G_t$  was filtered through a 0.22 μm membrane (Millipore Corp) and dialyzed against dialysis buffer (10 mM Tris-HCl, pH 7.4, 2 mM MgCl<sub>2</sub> and 1 mM DTT) containing 50% glycerol.  $G\beta\gamma_t$  was further separated from the purified  $G_t$ . The separation was performed in a column packed with Blue-Sepharose resin (GE Healthcare) by a linear salt gradient (0-500 mM NaCl) in dialysis buffer supplemented with 30% glycerol. The collected  $G\beta\gamma_t$  was concentrated and stored at -80 °C.

### **2.3 Preparation of native rhodopsin**

Native rhodopsin was extracted from dark-ROS membranes which were prepared according to Okada's method [73]. The collected dark-ROS membranes were solubilized with 80 mM  $\beta$ -dodecyl-D-n-maltoside (DDM) in the solubilization buffer (50 mM sodium acetate, pH 6, 1 mM EDTA, 2 mM 2-mercaptoethanol, 3 mM  $\text{CaCl}_2$ , 3 mM  $\text{MgCl}_2$ , 3 mM  $\text{MnCl}_2$  and 100 mM NaCl) at 4 °C overnight. After centrifugation at 30,000 rpm in a Ti70 rotor, the supernatant was diluted with solubilization buffer to a final concentration of 0.4% DDM. The diluted sample was loaded to a column packed with ConA Sepharose resin (GE Healthcare) which was equilibrated with the washing buffer (solubilization buffer supplemented with 0.02% DDM). After extensively washing with the washing buffer, the native rhodopsin was eluted with the solubilization buffer supplemented with 0.02% DDM and 0.2 M  $\alpha$ -D-methylmannoside. The eluted native rhodopsin was concentrated and stored at -80 °C.

### **2.4 Expression of constitutively active rhodopsin at bioreactor scale**

The N2C, M257Y, D282C rhodopsin mutant (RhoM257Y) was expressed in stably transfected HEK293S-GnT1-cells [74] constructed as described previously [75]. In contrast to our previous reports we expressed the RhoM257Y in fully instrumented 20 L stirred-tank bioreactors (Sartorius, Germany) under controlled conditions (120 rpm, pH 7.2,  $\text{CO}_2$  30% air saturation) to be able to produce sufficient protein for crystallization screening. Typically, 5 days after inoculation from shaker flask cultures the cell density reached  $4\text{--}5 \times 10^6$  viable cells/ml (PEM medium (Life Technologies, USA) with 5% FBS, 4 mM glutamine, G418 and blasticidin as selection markers). Protein expression was induced by addition of tetracycline in 500 ml of PEM medium (final concentration of 2  $\mu\text{g/ml}$  tetracycline). 800 ml concentrated feeding solution (Roche, proprietary composition) was added to avoid nutrient limitations. 48 h post-induction the culture was supplemented with sodium butyrate (final concentration of 3 mM butyrate) and with additional feeding solution (400 ml). Cells were harvested 72 h post-induction by centrifugation at 3,000 g for 10 min at 4 °C (1 L beakers, Beckman). Cell pellets (700–900 g in total) were washed once in PBS and frozen in 50 ml Falcon tubes until purification of the complex.

### **2.5 Purification of RhoM257Y- $G_t$ and RhoM257Y- $G_t$ complex**

Purification of RhoM257Y- $G_t$  complex was performed essentially in the same way as described previously [76] using the N2C/D282C/M257Y mutant bovine opsin (OpsinM257Y) instead of the N2C/D282C/E113Q mutant. Briefly, the whole HEK293S-GnT1 $\Gamma$  cells, stably expressing OpsinM257Y, were solubilized in DDM. After separating the supernatant, OpsinM257Y was first immobilized onto the 1D4-antibody immunoaffinity sepharose and reconstituted with 11-*cis* retinal to form the ground state RhoM257Y. The ground state RhoM257Y was mixed with purified  $G_t$  and irradiated for 10 to 15 min through a 495 nm long-pass filter, converting the inverse agonist 11-*cis* retinal to the full agonist all-trans retinal and forming RhoM257Y- $G_t$  complex on the sepharose resin. The resulting RhoM257Y- $G_t$  complex was detergent-exchanged from 0.02% DDM to 0.02% lauryl-

maltose neopentyl glycol (LMNG) and eluted from the resin by incubating with 1D4-elution peptide (TETSQVAPA). The eluent was further purified by size-exclusion chromatography. Adding 25 mU/ml Apyrase (New England Biolabs) during the light activation improved the efficiency of the RhoM257Y/G<sub>t</sub> complex formation by preventing re-binding of the GDP that was released from G<sub>α<sub>t</sub></sub> after the binding of G<sub>t</sub> to the active RhoM257Y. Heterotrimeric G<sub>i</sub> protein was formed by mixing purified G<sub>α<sub>i1</sub></sub> and Gβγ<sub>t</sub> subunits at equimolar ratio for 30 min on ice, and used for the formation of RhoM257Y-G<sub>i</sub> complex in the same way as RhoM257Y-G<sub>t</sub> complex.

## 2.6 CD measurement

The secondary structure of the recombinant WT G<sub>α<sub>i1</sub></sub> was analysed by Chirascan™-plus CD Spectrometer using a 1 mm path length cell. 12.5 μM recombinant WT G<sub>α<sub>i1</sub></sub> was dialyzed overnight in 25 mM Sodium Phosphate pH 7.4 and 200 mM NaCl. CD signal was recorded from 200 nm to 300nm at 20 °C with a 1 nm bandwidth and a sampling time 1 s per step. The spectra were analysed for the fractional content of secondary structures by CDNN software (Applied Photophysics Ltd).

## 2.7 Mass spectrometry

To determine the MW of the recombinant WT G<sub>α<sub>i1</sub></sub>, the LC-MS measurements were performed by Alain Blanc (Chemist FH) at the Center for Radiopharmaceutical Sciences of Paul Scherrer Institut.

## 2.8 Analysis of nucleotide content of WT G<sub>α<sub>i1</sub></sub> by perchloric acid

The standard GDP nucleotide was purchased from Sigma-Aldrich. To prepare the protein sample, 5 μM recombinant WT G<sub>α<sub>i1</sub></sub> was denatured by 5% perchloric acid and the precipitant was removed by centrifugation at 13,000 rpm for 10 min. UV spectra were recorded in Cary 300 UV-visible spectrophotometer.

## 2.9 G protein activation assay

G protein activation was measured by monitoring changes of the intrinsic tryptophan fluorescence in the G<sub>α</sub> subunit by receptor-catalysed exchange of GDP/GTPγS or by forming transient GDP-AlF<sub>4</sub><sup>-</sup>-G<sub>α</sub> state. All measurements were performed in a final volume of 1 ml (10×2 mm cuvette with a stirring bar) using Varian Cary Eclipse fluorescence spectrophotometer with settings of λ<sub>ex</sub> = 295 nm and λ<sub>em</sub> = 340 nm. The heterotrimeric G<sub>i</sub> protein was reconstituted by mixing equimolar amounts of the recombinant G<sub>α<sub>i1</sub></sub> and native Gβγ<sub>t</sub> on ice for 30 min. The native G<sub>t</sub> was prepared from bovine retinas. After forming the protein complex of Rho\*-G by irradiation by orange light (>495 nm), the basic fluorescence of Rho\*-G was monitored for 5 min followed by the addition of 10 μM GTPγS or 2 μl AlF<sub>3</sub> (final Conc.: 840 μM NaF and 10 μM AlCl<sub>3</sub>). The fluorescence intensity was continuously recorded for 1 h.

The measurements of the apparent affinity between rhodopsin and G<sub>i</sub> and G<sub>t</sub> were carried out with 1 or 30 nM native rhodopsin (purified from bovine retina) in 50 mM Bis-Tris, pH 7.3, 130 mM NaCl, 1

mM MgCl<sub>2</sub>, 1 mM DTT and 0.01% DDM. The entire set of experiments was repeated with increasing concentrations of G<sub>i</sub> or G<sub>t</sub>. The initial G protein activation rate was determined by fitting the fluorescence intensity to an exponential association curve  $y = y_0 + a[1 - \exp(-k_r't)]$  using Origin 8.5, where  $k_r'$  is the apparent rate constant and  $t$  is the time in seconds. Apparent rate constant ( $k_r'$ ) of the initial fluorescence increase was plotted against G protein concentrations. The data were fitted by Michaelis-Menten equation:  $k_r' = (V_{max} \cdot [G]) / (K_m + [G])$ . To measure the activity of WT G $\alpha_{i1}$ , the assays were performed with 10 nM native rhodopsin and 250 nM reconstituted G<sub>i</sub> in 10 mM Tris-HCl, pH 7.4, 0.01% DDM, 100 mM NaCl, 1 mM MgCl<sub>2</sub>, and 1 mM DTT.

### 2.10 CPM fluorescence assisted thermostability assay

Thermal dissociation was monitored by the formation of the thiol-specific maleimide fluorochrome CPM (N-[4-(7-diethylamino-4-methyl-3-coumarinyl) phenyl]maleimide) [77] attached to the protected cysteine residues between G $\alpha_t$  or G $\alpha_{i1}$ , and G $\beta\gamma_t$ . For RhoM257Y-G<sub>t</sub>, thermostability assays were performed using Eclipse fluorimeter (Varian) equipped with a multicell holder. 2  $\mu$ l of purified RhoM257Y-G<sub>t</sub> (1 mg/ml) was diluted into 98  $\mu$ l ice cold buffer (100 mM NaCl, 10 mM Hepes pH 7.5 and 0.02% LMNG). Immediately before the measurement, CPM (3 mg/ml in DMSO) was diluted 1:30 into buffer and 10  $\mu$ l of the diluted CPM was added to the reaction mix. Cuvettes were placed into the fluorimeter and fluorescence intensity ( $\lambda_{ex}$ : 387 nm,  $\lambda_{em}$ : 464 nm) was monitored while ramping temperature from 4 °C to 90 °C at the rate of 2 °C/min. The resulting curve was fit using a sigmoidal Boltzmann equation to obtain the dissociation temperature ( $Td_{50}$ ) values. For RhoM257Y-G<sub>i</sub>, the thermostability assay was performed using Rotor GeneQ (Qiagen). 5  $\mu$ g of purified RhoM257Y-G<sub>i</sub> was diluted into 120  $\mu$ l ice cold buffer (10 mM Hepes, pH 7.5, 100 mM NaCl and 0.01%LMNG). 10  $\mu$ l of the freshly prepared 40:1 dilution of CPM into measuring buffer was added immediately before the measurement. CPM stock was prepared at 3 mg/ml in DMSO. Fluorescence intensity ( $\lambda_{ex}$ : 365 nm,  $\lambda_{em}$ : 460 nm) was monitored while ramping temperature from 25 °C to 90 °C at the rate of 4 °C/min. The resulting curves were analyzed by the Rotor GeneQ package software.

### 2.11 Analysis of rhodopsin-G protein complex by FSEC

The experiments were performed by fluorescence-detection size-exclusion chromatography (FSEC) method. For RhoM257Y-G<sub>i</sub>, 1  $\mu$ l of complex (1 mg/ml) was diluted into 100  $\mu$ l of buffer composed of 100 mM NaCl, 10 mM Hepes pH 7.5, and 0.01% LMNG and loaded onto superdex 200 packed in a Tricorn 10/200 column (GE Healthcare) equilibrated with 10 mM Hepes pH 7.5, 100 mM NaCl, and 0.01% LMNG. The elution profile was monitored by protein-intrinsic fluorescence with  $\lambda_{ex}$ : 280 nm,  $\lambda_{em}$ : 340 nm. For the fluorescence-detection size-exclusion chromatography-based thermostability assay (FSEC-TS) [78], 1  $\mu$ g of RhoM257Y-G<sub>i</sub> in 100  $\mu$ l of the buffer was incubated at 4 °C to 60 °C for 30 min, ice-cooled for 5 min, and then centrifuged at 9,000 g for 5 min. The peak heights were normalized and then fit to a sigmoidal dose-response curve to obtain  $Td_{50}$  values.



### **2.12 HTP alanine mutagenesis scanning**

The plasmid containing WT  $G\alpha_{i1}$  with an N-terminal 10×His-tag followed by a TEV cleavage site was chosen as the cloning template. Primers for the scanning mutagenesis were designed using the program AAscan [79] and ordered from Integrated DNA Technologies as desalted oligonucleotides. 1×Phusion High-Fidelity PCR Master Mix with HF buffer (Thermo Scientific) complemented with 170 pg DNA template per reaction was distributed to a 96-well PCR plate (Eppendorf) as 17  $\mu$ l per reaction. Then, 1.5  $\mu$ l each of 1  $\mu$ M forward and reverse primers was added to each well. All PCRs were performed using Eppendorf Mastercycler pro S. The PCR reaction products were digested with DpnI overnight. The resulting products were transformed into *E.coli* Mach1 strain and plated. A single colony was picked and sequenced by GATC Biotech. The sequencing results were checked by MutantChecker [79]. The mutagenesis scanning programs are available at [www.psi.ch/lbr/aascan](http://www.psi.ch/lbr/aascan). In the end, all non-alanine residues in the  $G\alpha_{i1}$  subunit were replaced with alanine and alanine residues were substituted by glycine.

### **2.13 HTP culture and purification of $G\alpha_{i1}$ alanine mutants**

The recombinant  $G\alpha_{i1}$  alanine mutants were expressed in BL21 (DE3) competent cells. The cultures were grown at 37 °C in TB media (GERBU Biotechnik GmbH) using 24 well plates (one mutant per well) (Whatman UniFilter Microplates, GE Healthcare). The culture volume was 5 ml per well. When the OD<sub>600</sub> reached 0.6, cells were induced with 0.5 mM IPTG and continued to grow for 20 h at 20 °C. The cell pellets were solubilized with the binding buffer (25 mM Tris-HCl, pH 7.4, 500 mM NaCl, 10% glycerol, 50 mM imidazole, 5 mM 2-mercaptoethanol) and transferred to a 96 Deep-Well plate (Thermo Scientific). The resuspended cells were disrupted by sonication with an 8-pin probe. After clarifying cell lysates by centrifugation, the supernatants were loaded to a 96 Deep-Well filter plate (one mutant per well) preloaded with cobalt chelating resin (GE Healthcare) and equilibrated with the binding buffer. After extensively washing with the binding buffer, the recombinant  $G\alpha_{i1}$  alanine mutants were eluted from resins by the elution buffer (25 mM Tris-HCl, pH 7.4, 500 mM NaCl, 10% glycerol, 500 mM imidazole, 5 mM 2-mercaptoethanol). The eluted proteins were dialyzed against 25 mM Hepes, pH 7.4, 100 mM NaCl and 2 mM DTT by Slide-A-Lyzer MINI Dialysis Device (Thermo Scientific).

### **2.14 Native gel electrophoresis-based thermostability assay (NPAGE-TS)**

The sample was aliquotted and heated at the indicated temperature. For the determination of the  $Td_{50}$  of the Rho257Y-G<sub>i</sub> complex, a heating temperature of 20°C, 25°C, 30°C, 35°C, 40°C, 45°C, 50°C and 55°C were selected. After heating for 30 min, the samples were centrifuged to remove the precipitants. 14  $\mu$ l of each sample was mixed with NativePAGE Sample Buffer (4×) (Invitrogen) and NativePAGE 5% G-250 Sample Additive (Invitrogen), respectively. The mixtures were loaded into 4-16% NativePAGE Bis-Tris-HCl Gel (Invitrogen) and the gel electrophoresis was performed in a 4 °C cold room according to the manufacturer's protocol (Invitrogen). The complex band was integrated using

ImageJ. The integrated density of the complex band was normalized and then fit to a sigmoidal dose-response curve to obtain  $Td_{50}$  values.

### 2.15 HTP measurement of $G\alpha_{i1}$ alanine mutants' effect on receptor-bound state

In each round, WT  $G\alpha_{i1}$  was always prepared in parallel with  $G\alpha_{i1}$  alanine mutants [ $G\alpha_{i1}(\text{Ala})$ ] to form rhodopsin- $G_i$  protein complex [ $\text{Rho}^*-\text{G}_i(\text{WT})$ ] as the reference control. The recombinant  $G\alpha_{i1}$  alanine mutants (12.5  $\mu\text{M}$ ) from HTP purification and the native  $G\beta\gamma_t$  (10  $\mu\text{M}$ ) were reconstituted to form heterotrimer ( $G_i$ ) by incubation in a 96-well PCR plate (one mutant per well) (Eppendorf) on ice for 2 h. Under the dim-red light in the dark room, the purified rhodopsin (18  $\mu\text{M}$ ) was added and mixed with  $G_i$  in the ice cold assay buffer (25 mM Hepes, pH 7.4, 100 mM NaCl, 2mM DTT, 0.02% DDM, 1 mM  $\text{MgCl}_2$ , 0.16 unit/ml apyrase). After the irradiation by orange light (>495 nm) on ice for 10 min, the tetramer complex  $\text{Rho}^*-\text{G}_i(\text{Ala})$  was formed by coupling the activated rhodopsin with  $G_i$  and the formed  $\text{Rho}^*-\text{G}_i(\text{Ala})$  complex was further incubated in the dark at 4 °C overnight. The reaction volume was 50  $\mu\text{l}$  for each alanine mutant. 20  $\mu\text{l}$  of each  $\text{Rho}^*-\text{G}_i(\text{Ala})$  complex was transferred to another 96-well PCR plate and heated for 30 min in the PCR machine (Eppendorf Mastercycler Gradient) at 36.3 °C. After centrifuging at 3000 rpm for 10 min at 4 °C, 14  $\mu\text{l}$  of formed  $\text{Rho}^*-\text{G}_i(\text{Ala})$  complex (4 °C) and 14  $\mu\text{l}$  of heated  $\text{Rho}^*-\text{G}_i(\text{Ala})$  complex (36.3 °C) were mixed with NativePAGE Sample Buffer (4 $\times$ ) (Invitrogen) and NativePAGE 5% G-250 Sample Additive (Invitrogen), respectively. The mixtures were loaded onto 4-16% NativePAGE Bis-Tris-HCl Gels (Invitrogen) and the gel electrophoresis was performed in a 4 °C cold room according to the manufacturer's protocol (Invitrogen). Protein markers were used with NativeMark Unstained Protein Standard (Invitrogen). The gel bands of  $\text{Rho}^*-\text{G}_i$  complex were integrated and quantified by ImageJ software. The complex formation efficiency (CF) (%) was obtained from the normalization of integrated density of  $\text{Rho}^*-\text{G}_i$  complex band [ $\text{ID}_c(\text{Ala or WT}), 4\text{ °C}$ ] with integrated density of  $\text{Rho}^*-\text{G}_i(\text{WT})$  complex band [ $\text{ID}_c(\text{WT}), 4\text{ °C}$ ]. The complex stability (CS) (%) was defined as the normalization of integrated density of  $\text{Rho}^*-\text{G}_i$  complex band [ $\text{ID}_c(\text{Ala or WT}), 36.3\text{ °C}$ ] with integrated density of  $\text{Rho}^*-\text{G}_i(\text{WT})$  complex band [ $\text{ID}_c(\text{Ala or WT}), 4\text{ °C}$ ].

$$\text{CF}(\text{Ala}) = \frac{\text{ID}_c(\text{Ala}, 4^\circ\text{C})}{\text{ID}_c(\text{WT}, 4^\circ\text{C})} \times 100\%$$

$$\text{CS}(\text{WT}) = \frac{\text{ID}_c(\text{WT}, 36.3^\circ\text{C})}{\text{ID}_c(\text{WT}, 4^\circ\text{C})} \times 100\%$$

$$\text{CS}(\text{Ala}) = \frac{\text{ID}_c(\text{Ala}, 36.3^\circ\text{C})}{\text{ID}_c(\text{Ala}, 4^\circ\text{C})} \times 100\%$$

The  $\Delta\text{CF}$  (%) and  $\Delta\text{CS}$  (%) were defined as:

$$\Delta\text{CF} = \text{CF}(\text{Ala}) - \text{CF}(\text{WT})$$

$$\Delta\text{CS} = \text{CS}(\text{Ala}) - \text{CS}(\text{WT})$$

## 2.16 HTP differential scanning fluorimetry to measure thermostability

The thermostability of each  $G\alpha_{i1}$  alanine mutant in nucleotide-bound state was measured by HTP differential scanning fluorimetry (DSF). The samples were prepared on ice. 10  $\mu$ l of recombinant  $G\alpha_{i1}$  alanine mutant stocks (0.7  $\mu$ g/ $\mu$ l) were dispensed into a 96-well PCR plate (one mutant per well) (Eppendorf) and mixed with 100  $\mu$ l ice-cold assay buffer (25mM Hepes, pH 7.4, 100mM NaCl, 2mM DTT) containing 5 $\times$  SYPRO-orange (Invitrogen) and nucleotides (1 mM GDP or 100  $\mu$ M GTP $\gamma$ S). After mixing, 110  $\mu$ l reaction mixture of each alanine mutant was divided into 0.2 ml PCR tubes (Qiagen) as three samples of 35  $\mu$ l. The DSF experiments were performed with Rotor GeneQ (Qiagen) by ramping from 25  $^{\circ}$ C to 95  $^{\circ}$ C at the rate of 3  $^{\circ}$ C/min. The melting temperature ( $T_m$ ) was defined as the inflection point of the melting curve as analyzed by the Rotor Gene Q Series Software. The  $T_m$  value of each  $G\alpha_{i1}$  alanine mutant [ $T_m(\text{Ala})$ ] in addition of nucleotides was averaged from three individual experiments.

The  $\Delta T_m$  value was defined as:

$$\Delta T_m = T_m(\text{Ala}) - T_m(\text{WT})$$

In each round, WT  $G\alpha_{i1}$  was always prepared in parallel with  $G\alpha_{i1}$  alanine mutants as the reference control.

In addition, the thermal shift of WT  $G\alpha_{i1}$  in titration with GDP and GTP $\gamma$ S were also performed with HTP DSF.

## 2.17 Analysis of heterotrimer formation by FSEC

The recombinant  $G\alpha_{i1}$  alanine mutants (6  $\mu$ M) and  $G\beta\gamma_t$  (2  $\mu$ M) were reconstituted to form heterotrimer ( $G_i$ ) in 100  $\mu$ l running buffer (25 mM Hepes, pH 7.4, 100 mM NaCl) overnight on ice. 80  $\mu$ l of reconstituted  $G_i$  was injected to superdex 200 packed in a Tricorn 10/200 column (GE Healthcare) equilibrated with the running buffer. The elution profile was monitored by protein-intrinsic fluorescence with  $\lambda_{\text{ex}}$ : 280 nm and  $\lambda_{\text{em}}$ : 340 nm at a flow rate of 1 ml/min. The retention time of the reconstituted  $G_i$  was integrated with UNICORN 5.2 software (GE Healthcare).

## 2.18 Modelling of Rhodopsin- $G_i$ complex

**Homology modelling of G alpha i.** The sequences of G alpha i and G alpha s were aligned using Clustal Omega [80]. This initial alignment was manually refined using Chimera [81] to adjust some of the gaps in the loop regions. Using this alignment, G alpha i was modelled with Modeller [82] using the structure of  $G_s$  bound to the  $\beta_2$  adrenergic receptor [48] as a template. Residues missing in the template were refined using the loop optimization method in Modeller. All models were subjected to 300 iterations of variable target function method optimization and thorough molecular dynamics and simulated annealing optimization and scored using the discrete optimized protein energy potential.

The 20 best-scoring models were analysed visually, and a suitable model (in terms of low score and structure of the loops) was selected.

**Homology modelling of active rhodopsin.** The sequences of bovine rhodopsin and the human  $\beta_2$  adrenergic receptor were aligned using Clustal Omega [80]. This initial alignment was manually refined using Chimera [81] to adjust some of the gaps in the loop regions. Using this alignment, rhodopsin was modelled with Modeller [82] using the structure of  $\beta_2$  adrenergic receptor bound to  $G_s$  [48] as a template. Residues missing in the template were refined using the loop optimization method in Modeller. All models were subjected to 300 iterations of variable target function method optimization and thorough molecular dynamics and simulated annealing optimization and scored using the discrete optimized protein energy potential. The 20 best-scoring models were analysed visually, and a suitable model (in terms of low score and structure of the loops) was selected.

**Modelling of the rhodopsin- $G_i$  complex.** The models of  $G_i$  and rhodopsin were superimposed to the structures of  $G_s$  and the  $\beta_2$  adrenergic receptor [48], keeping the  $G_{\beta}$  and  $G_{\gamma}$  subunits. In addition to the crystallographic waters resolved in the structure of rhodopsin, we added additional ordered water molecules, as observed in the high-resolution structure of the adenosine  $A_{2A}$  receptor [83]. Cysteines 322 and 323 were palmitoylated. Glu, Asp, Arg and Lys residues were set as charged, except Glu122 (3.37) and Asp83 (2.50) [84]. Topology and parameter definitions for palmitoyl-cysteine and retinal bound via protonated Schiff-base link to lysine [85-87] were obtained from the parameter/topology repository of NAMD [88]. The complex was embedded in a solvated and pre-equilibrated lipid bilayer consisting of 360 molecules of 1-palmitoyl-2-oleoyl-sn-glycerol-3-phosphatidylcholine (POPC) and approx. 50.000 water molecules. Sodium and chloride ions were added to a concentration of 0.15 M NaCl, and then additional ions were added to achieve charge neutrality. The system measured roughly  $120 \times 120 \times 160 \text{ \AA}^3$ , with a total of approximately 215'000 atoms. This system was equilibrated as follows: first a short (0.5 ns) simulation was performed in which only the lipid tails were allowed to move, in order to induce the appropriate disorder of a fluid-like bilayer. Then, the geometry of the entire system was optimized by 1000 steps of energy minimization, followed by two equilibration steps with the protein constrained (0.5 ns) and without constraints (0.5 ns). In order to equilibrate the complex, the system was subjected to 20 ns of unrestrained molecular dynamics. Simulations were carried out using NAMD 2.8 (14) with the CHARMM27 all-hydrogen force field [89] at constant pressure (1 atm), and using a time step of 2 fs.

### 2.19 Sequence alignment of $G_{\alpha_i}$ subunits

The sequence used are human  $G_{\alpha_{i1}}$  (UniProt: P63096), human  $G_{\alpha_{i2}}$  (UniProt: P04899), human  $G_{\alpha_{i3}}$  (UniProt: P08754), bovine G transducin (UniProt: P02698), human  $G_{\alpha_s}$  (UniProt: P63092), human  $G_{\alpha_o}$  (UniProt: P09471), human  $G_{\alpha_{olf}}$  (UniProt: P38405), human  $G_{\alpha_q}$  (UniProt: P50148), human  $G_{\alpha_z}$  (UniProt: P19086), human  $G_{\alpha_{i1}}$  (UniProt: P29992), human  $G_{\alpha_{i2}}$  (UniProt: Q03113), human  $G_{\alpha_{i3}}$

(UniProt: Q14344), human  $G\alpha_{14}$  (UniProt: O95837) and human  $G\alpha_{15}$  (UniProt: P30679). The sequences were first aligned by Clustal2 (<http://www.ebi.ac.uk/Tools/msa/clustalw2/>). The final alignment was performed with Jalview software [90] using Clustal algorithm (Fig. 2.2).

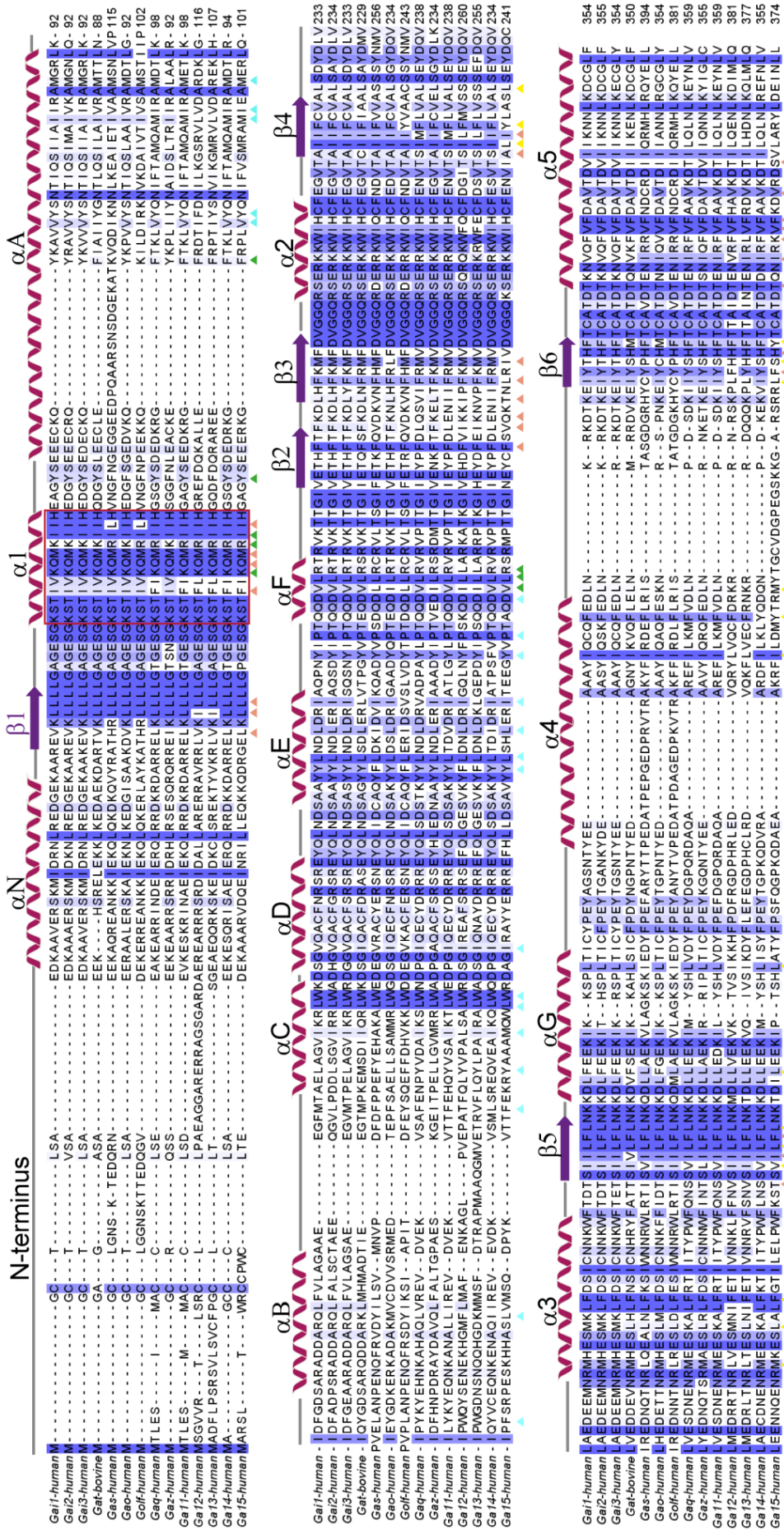


**Fig. 2.2. Multiple Sequence alignment of Gα subunits.** Sequence alignment was performed with Jalview software based on Clustal algorithm. The conservation of residues is highlighted in blue: the darker the color, the more conserved the residues. The residues which are involved in stabilization of cluster I and c cluster II of the GTPase domain are indicated as light coral and yellow triangles, respectively. The residues which are involved in stabilization of cluster III of the helical domain and the inter-domain interface are indicated as cyan and green triangles.

## Chapter 3 Results

### 3.1 Characterization of recombinant WT $G\alpha_{i1}$

#### 3.1.1 Expression and purification of recombinant WT $G\alpha_{i1}$

In the beginning of designing the expression construct for WT  $G\alpha_{i1}$ , I fused a lipoyl domain tag (HLT) to the N-terminus of WT  $G\alpha_{i1}$  followed by the protease cleavage site. Fusion with HLT has been previously shown to enhance protein solubility and expression [91]. The initial expression test showed that WT  $G\alpha_{i1}$  fused with HLT could be expressed well at 20 °C rather than 37 °C at which protein was expressed in inclusion bodies. In the final optimized expression and purification condition, the intact WT  $G\alpha_{i1}$  could be purified, yielding around 10-15 mg from one liter LB media with a monodisperse profile as shown by gel-filtration (GF) chromatography (Fig. 3.1). I also designed another expression construct which incorporated only one N-terminal 10-histidine tag (His-tag) followed by TEV protease site. This His(10)-TEV- $G\alpha_{i1}$  construct showed lower expression yield in LB media compared to the HLT-fused construct. The expression yield was enhanced by using rich media, which finally could also provide around 15-20 mg intact  $G\alpha_{i1}$  from one liter TB rich media. In consideration of the increased expression yield and simplified purification by avoiding the remove of the fused HLT, the His(10)-TEV- $G\alpha_{i1}$  construct was finally chosen for developing HTP mutagenesis scanning.

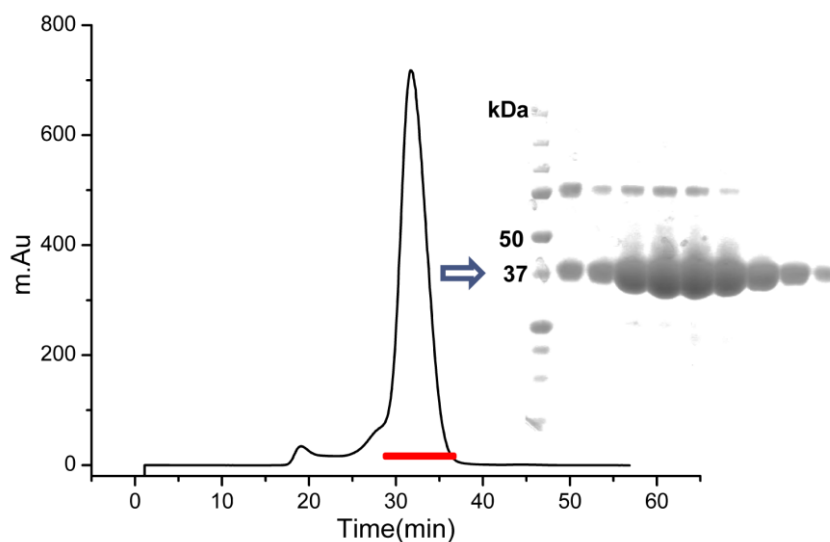


**Fig. 3.1. SDS-PAGE and GF profile of recombinant WT  $G\alpha_{i1}$  (intact).** The digested WT  $G\alpha_{i1}$  was further purified by size-exclusion chromatography. The fractions from the center peak region were analyzed by SDS-PAGE.

#### 3.1.2 Biophysical Characterization of recombinant WT $G\alpha_{i1}$

To characterize the biophysical properties of purified WT  $G\alpha_{i1}$ , first I performed CD spectroscopy to determine the secondary structure of WT  $G\alpha_{i1}$ . The CD measurement clearly shows that the purified WT  $G\alpha_{i1}$  is well-folded and mainly composed of alpha helical secondary structure (Fig. 3.2a), which is consistent with its domain architecture as demonstrated by many crystal structures of the  $G\alpha_{i1}$  subunit [30]. Meanwhile, I also verified the molecular weight (MW) of purified WT  $G\alpha_{i1}$  by mass

spectrometry (MS). The MW measured by MS is 40564 Dalton (Da) which is almost same as the calculated MW (40505 Da) from  $G\alpha_{i1}$  sequence (Fig. 3.2b), indicating the purified WT  $G\alpha_{i1}$  is well preserved after the protease cleavage. Additionally, I also measured the melting temperature ( $T_m$ ) of WT  $G\alpha_{i1}$  by differential scanning fluorimetry (DSF) (Fig. 3.2c). The determined  $T_m$  value of WT  $G\alpha_{i1}$  is  $48.6 \pm 0.03$  °C. Interestingly, the determined  $T_m$  values of WT  $G\alpha_{i1}$  fused with either HLT or 10-histidine tag is  $48.4 \pm 0.03$  °C and  $48.3 \pm 0.6$  °C, respectively (Fig. 3.2c), which is almost identical with the  $T_m$  value of intact WT  $G\alpha_{i1}$ , implicating that the fused HLT or His-tag does not affect the overall thermal stability of WT  $G\alpha_{i1}$ .

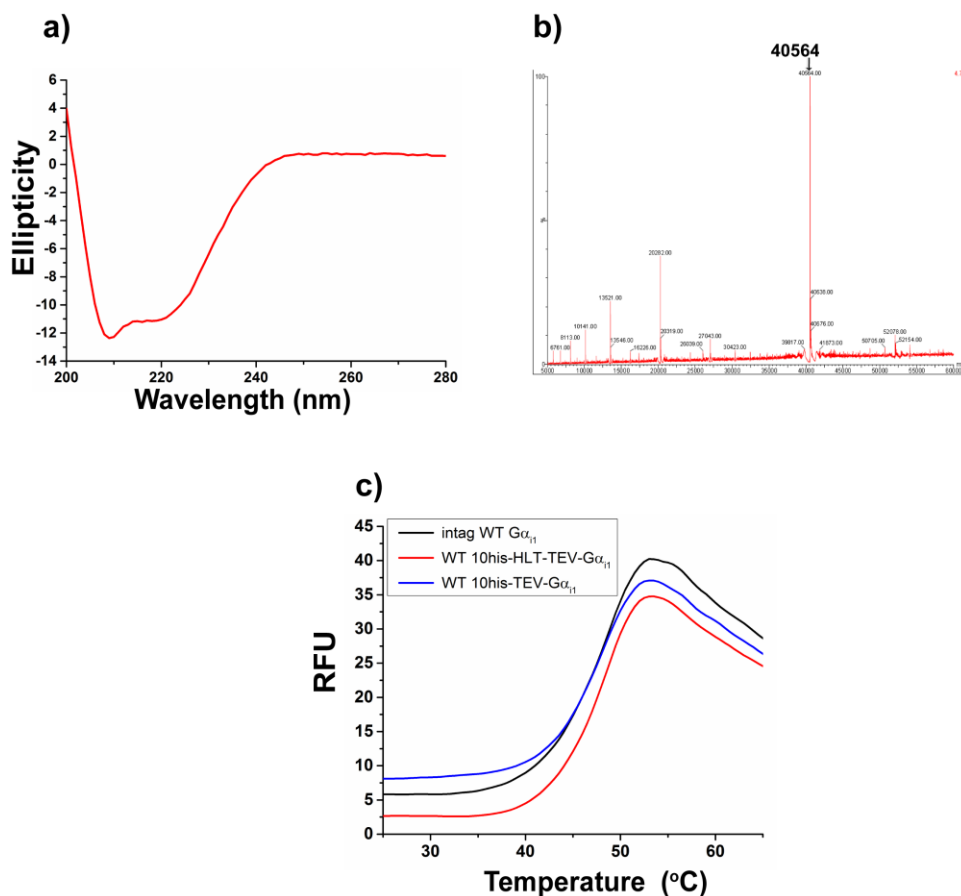


**Fig. 3.2. Characterization of biophysical property of recombinant WT  $G\alpha_{i1}$ .** a, CD spectroscopy of purified WT  $G\alpha_{i1}$ . b, Mass spectroscopy of purified WT  $G\alpha_{i1}$ . c,  $T_m$  measurements of WT  $G\alpha_{i1}$  (intact), WT  $G\alpha_{i1}$  fused with HLT and WT  $G\alpha_{i1}$  fused with 10-histidine tag.

### 3.1.3 Analysis of the GDP content in recombinant WT $G\alpha_{i1}$

One hallmark of the inactive state of the G protein alpha subunit is the presence of a tightly bound GDP molecule in the nucleotide-binding pocket. To determine whether the expressed and purified WT  $G\alpha_{i1}$  is, in fact, bound with GDP, the purified WT  $G\alpha_{i1}$  was denatured by perchloric acid [92] followed by centrifugation to remove the precipitant. The GDP concentration in the supernatant was measured by UV spectroscopy (Fig. 3.3a). In comparison with the standard plot of GDP nucleotide (Fig. 3.3b), the determined stoichiometry of GDP binding with WT  $G\alpha_{i1}$  is around 1:1 ratio as



expected, indicating that the nucleotide-binding pocket of purified WT  $G\alpha_{i1}$  is well-conserved and occupied by GDP nucleotide.

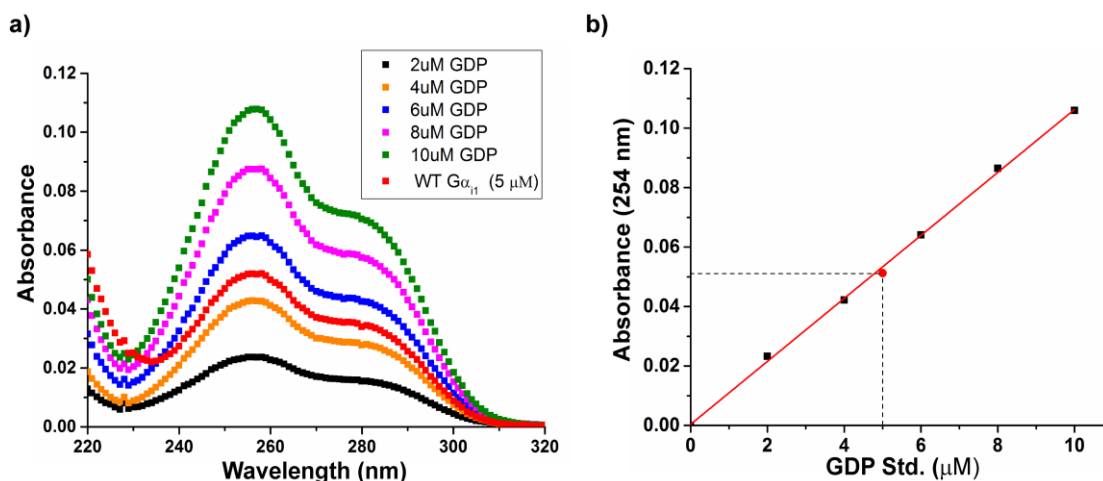


**Fig. 3.3. Determination of bound-GDP in purified WT  $G\alpha_{i1}$ .** a, UV spectra of standard GDP nucleotides. b, Standard curve: plotting of absorbance at 254 nm against concentration of standard GDP nucleotide. By using the standard curve, the absorbance (254 nm) of supernatant of 5  $\mu$ M purified WT  $G\alpha_{i1}$  denatured by perchloric acid corresponds to 5  $\mu$ M standard GDP nucleotide.

### 3.1.4 Verification of the functional activity of recombinant WT $G\alpha_{i1}$

Previous research has shown that one tryptophan (Trp) (W211 in  $G\alpha_{i1}$ ), which was located in the Switch II region of the G protein alpha subunit and which is conserved in all G proteins, could be used as a fluorescence sensor to monitor G protein activation [93]. The conformational changes in the Switch II region that occur upon activation decrease the exposure of W211 to the aqueous environment, resulting in an increase in fluorescence. Based on this, two classical intrinsic fluorescence assays have been performed to confirm whether the purified  $G\alpha_{i1}$  can undergo an activation-dependent conformational alteration or not. One typical assay is to utilize aluminum fluoride ( $AlF_4^-$ ) as an analogue of the gamma-phosphate of GTP to trigger the conformational change in the Switch II region of the G protein alpha subunit from the inactive state of  $G\alpha$ -GDP to the transient active state of  $GDP-AlF_4^-G\alpha$ , which can mimic the active GTP-bound state [94, 95]. Another typical assay is designed to induce the conformational change by the receptor-catalyzed GDP/GTP exchange [96-99]. Practically,  $GTP\gamma S$ , a non-hydrolysable analogue of GTP, is used in the experiment. The interaction of G protein with the activated receptor triggers the release of bound-GDP from the  $G\alpha$  subunit and enables  $GTP\gamma S$  binding, resulting in conformational changes and the fluorescence emission. My experimental results clearly show that both of the aluminum fluoride- and receptor-dependent assays can change the intrinsic Trp fluorescence signal from the purified WT  $G\alpha_{i1}$  (Fig. 3.4a-b), indicating that the expressed and purified WT  $G\alpha_{i1}$  maintain the functional integrity and activity expected of  $G\alpha$  proteins.

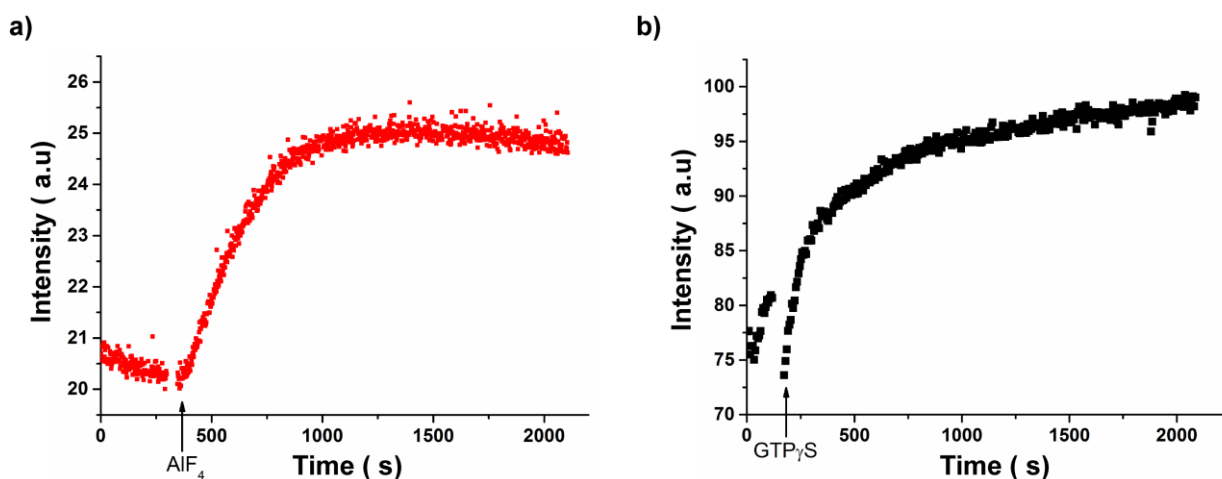


**Fig. 3.4. Intrinsic tryptophan activation of recombinant WT  $G\alpha_{i1}$ .** **a**, Intrinsic tryptophan activation induced by addition of aluminum fluoride. **b**, Intrinsic tryptophan activation stimulated by receptor-catalyzed GDP/GTP $\gamma$ S exchange.

### 3.2 Characterization of recombinant WT $G\alpha_{i1}$ in receptor-bound state

#### 3.2.1 Characterization of the coupling affinity between $G_i$ and rhodopsin

As discussed in the section 3.1, the purified recombinant WT  $G\alpha_{i1}$  undergoes a receptor-mediated conformational change which can be monitored by the increase in intrinsic tryptophan fluorescence, allowing the measurement of the apparent affinity of  $G_i$  to photo-activated rhodopsin [100]. The initial rate of G-protein activation was determined by monitoring the increase in intrinsic tryptophan fluorescence. Plotting the initial rate against the titrated G-protein concentrations in the reaction gave a Michaelis-Menten type hyperbolic function, with a  $K_m$  value obtained after curve fitting representing the apparent affinity of WT  $G\alpha_{i1}$  binding to photo-activated rhodopsin. Unexpectedly, the obtained  $K_m$  value with 0.01% DDM at 20 °C was around 8.6 nM (Fig. 3.5a), indicating an apparently high binding affinity between  $G_i$  protein and rhodopsin. To see whether the temperature or detergent concentration affected the binding affinity, I also performed the  $G_i$  protein activation at 25 °C with 0.01% DDM and 20 °C with 0.05% DDM. The  $K_m$  values under these conditions were 7.7 nM and 9.9 nM, respectively, similar to the value at 20 °C with 0.01% DDM (Fig. 3.5b-c). This suggests that the molecular interaction between  $G_i$  and rhodopsin is relatively tight and stable at these temperatures and detergent concentrations. In parallel, I also characterized  $G_t$  activation at 20 °C with 0.01% DDM. In comparison with  $G_i$  protein activation,  $G_t$  protein showed an apparently faster reaction rate and the addition of 500 nM  $G_t$  still did not reach the highest reaction rate. Despite the difficulties in measuring  $G_t$  activation due to limited material, the  $K_m$  value for  $G_t$  coupling was estimated to be 860 nM (Fig. 3.5d). Although the exact  $K_m$  value of  $G_t$  activation is not determined from the experiment, previous research has reported that the  $K_m$  values of  $G_t$  activation in 0.008% DDM and 0.01% DDM were 0.8  $\mu$ M and 2.3  $\mu$ M, respectively [100]. Taken together,  $G_i$  protein reconstituted from the recombinant WT  $G\alpha_{i1}$  shows the higher binding affinity with rhodopsin. It indirectly suggests that the rhodopsin- $G_i$  complex may be much more stable than rhodopsin- $G_t$  complex.

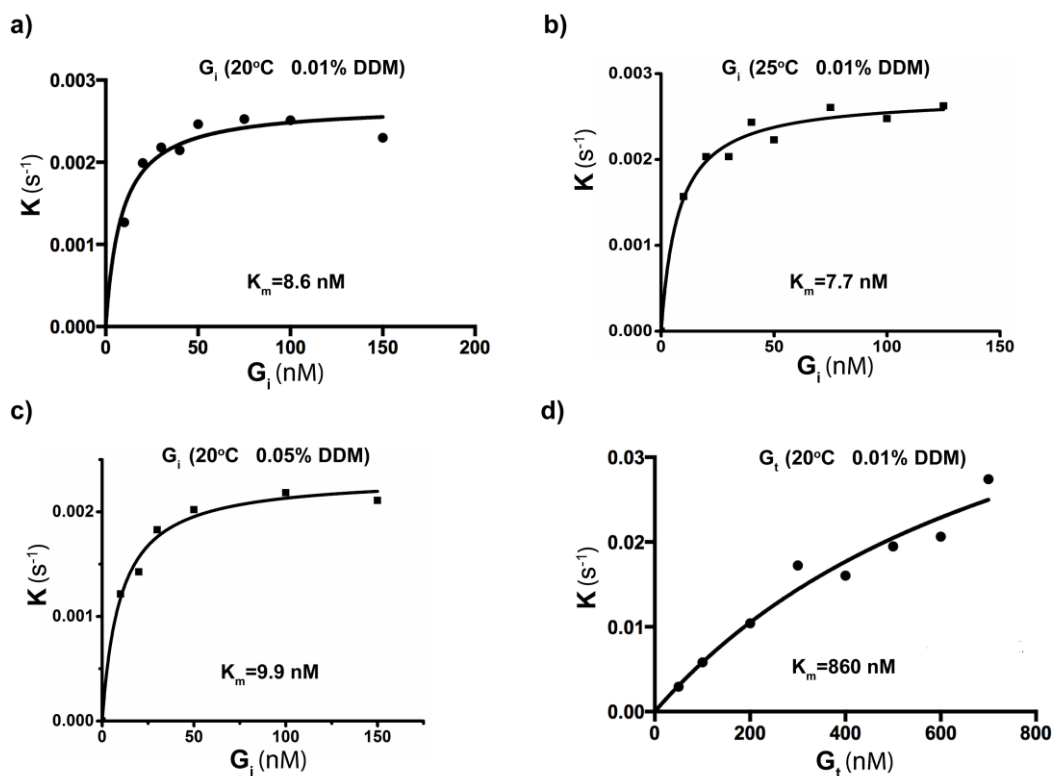


**Fig. 3.5.**  $G_t$  and  $G_i$  activation by rhodopsin using Trp fluorescence assay. **a-c**, The Michaelis-Menten constant ( $K_m$ ) of  $G_i$  to the photoactive rhodopsin at 20 °C with 0.01% DDM (**a**), 25 °C with 0.01% DDM (**b**), and 20 °C with 0.05% DDM (**c**). **d**,  $K_m$  of  $G_t$  activation is 860 nM.

### 3.2.2 Characterization of the thermostability of the rhodopsin- $G_i$ complex

In these experiments, an engineered construct of bovine opsin was used which combined a constitutively activating mutation (M257Y) together with a thermostabilizing cysteine double mutant (N2C/D282C) forming a disulfide bridge. This construct was shown to maintain both constitutive activity and high thermal stability, without changing the retinal binding, G-protein activation, activation pathways, or structure of the protein [101-104]. To be able to measure the thermostability of rhodopsin- $G_i$  complex, I have established few analytical methods in my lab.

The first method is the thermal shift assay based on binding of the thiol-specific maleimide CPM to cysteines that become exposed during unfolding of the protein [77]. Melting curves of the RhoM257Y- $G_i$  complex obtained with this assay showed a clear transition of the fluorescence signal at 40.5 °C and a later transition at 58 °C (Fig. 3.6a). Among the 10 cysteines which the  $G\alpha_{i1}$  subunit possesses, there are two cysteine residues that are supposedly protected upon complex formation: one located at the boundary between  $G\beta\gamma_t$  subunit, and the other one within the C-terminus. The latter one will be buried deep within the G-protein binding pocket in the rhodopsin, assuming the C-terminus of the  $G\alpha_{i1}$  subunit binds similarly as in the structure of the RhoM257Y co-crystallized with  $G\alpha$ -CT peptide [75]. Upon complex dissociation, these cysteines will be exposed and become available for reaction with the fluorescent dye. Therefore, the first transition is thus likely due to dissociation of the

complex and the derived  $T_m$  can present the dissociation temperature ( $T_{d50}$ ) of RhoM257Y-G<sub>i</sub> complex. The second transition likely stems from unfolding of the complex components, as both active rhodopsin and the G-protein subunits unfold between 50°C and 60°C.

The  $T_{d50}$  of RhoM257Y-G<sub>i</sub> complex was also measured by two additional methods: the fluorescence-detection size-exclusion chromatography-based thermostability assay (FSEC-TS) [78] (Fig. 3.6b), and the native gel electrophoresis-based thermostability assay (NPAGE-TS) (Fig. 3.6c). The equal amount of RhoM257Y-G<sub>i</sub> complex was heated in the different temperature, followed by the injection to size-exclusion column or by the visualization with the native PAGE. The  $T_{d50}$  of RhoM257Y-G<sub>i</sub> complex derived from FSEC-TS and NPAGE-TS was 45 °C and 43 °C, which were similar with the one from the thermal shift assay.

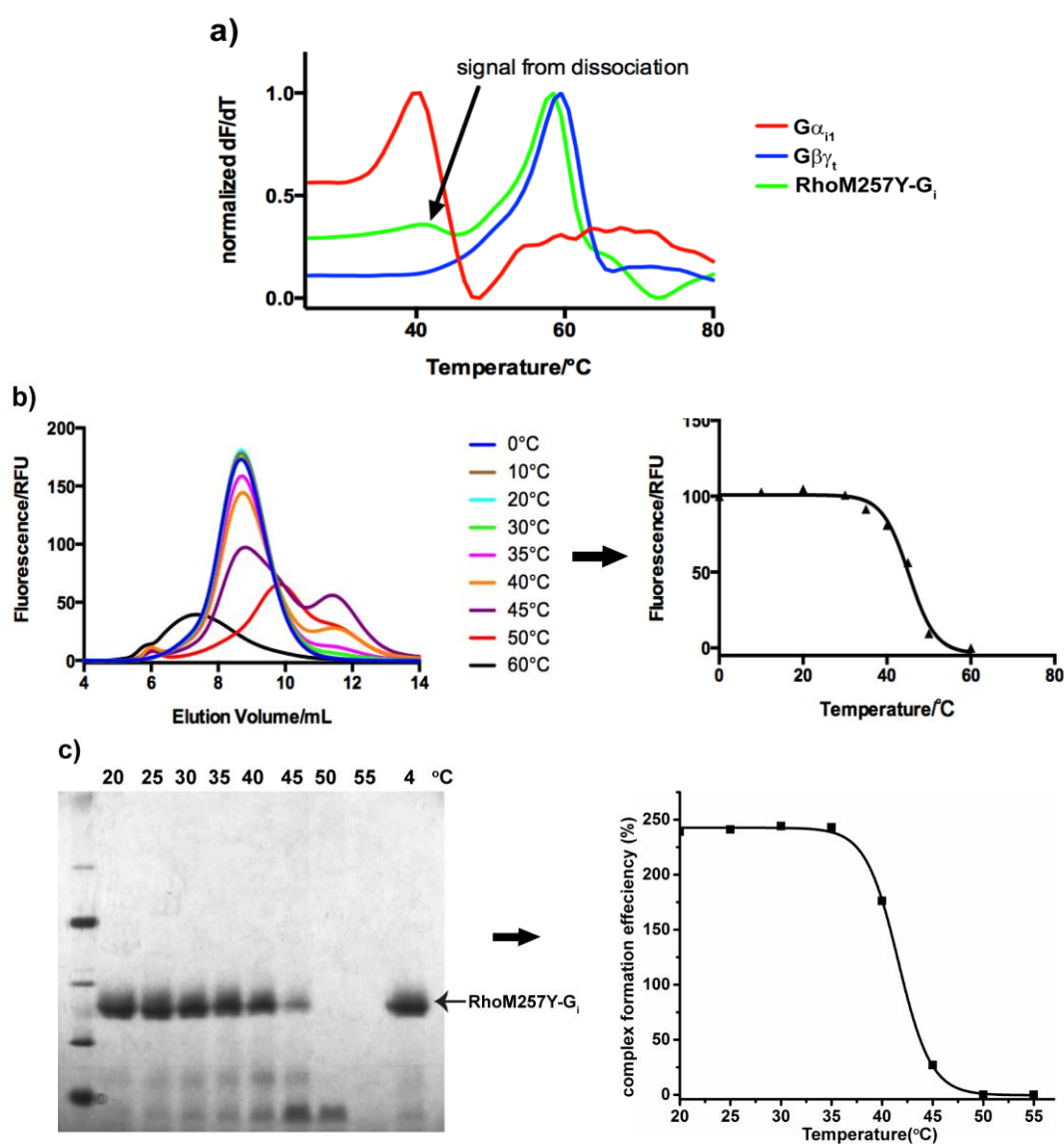


**Fig. 3.6. Characterization of thermal stability of rhodopsin-G<sub>i</sub>.** a-c, Measurement of thermal stability of RhoM257Y-G<sub>i</sub> by the CPM based thermal shift assay (a), FSEC-TS (b) and NPAGE-TS (c).

I also measured the  $Td_{50}$  of RhoM257Y-G<sub>t</sub> complex. The derived  $Td_{50}$  from the thermal shift assay showed two transitions of the fluorescence signals at 22°C and at 56°C (Fig. 3.7a). The first transition is likely due to dissociation of the complex, as the second transition likely stems from unfolding of active rhodopsin and Gβγ<sub>t</sub> subunit (Fig. 3.6a). This interpretation of the melting curves correlates well with the data from the FSEC-TS method indicating a dissociation of the complex between 20°C and 30°C (Fig. 3.7b).

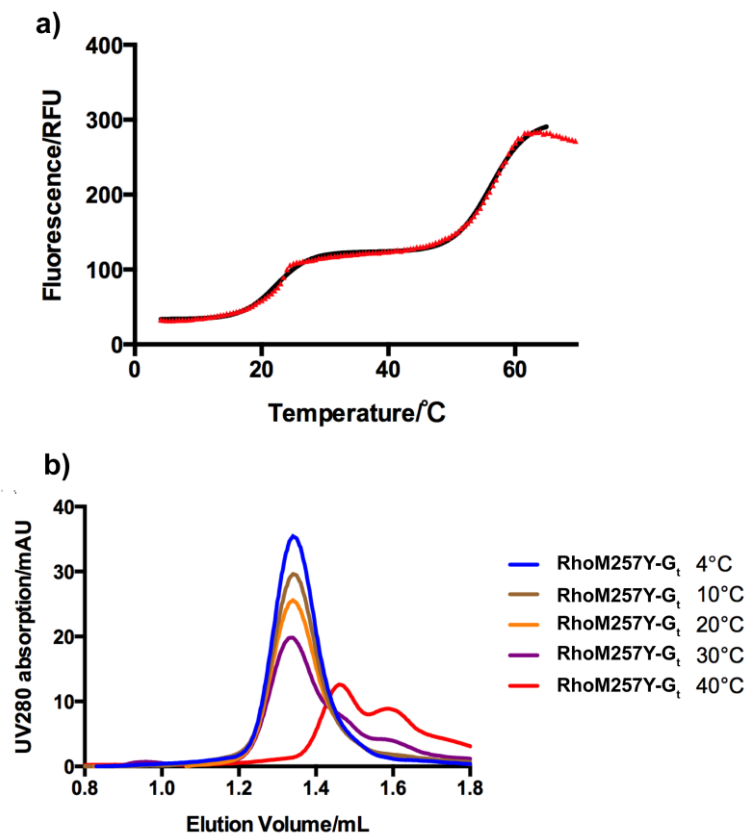


**Fig. 3.7. Characterization of thermal stability G<sub>t</sub> complex.** a-b, Measurement of thermal stability of RhoM257Y-G<sub>t</sub> by the CPM-based thermal shift assay (a) and by FSEC-TS (b).

### 3.2.3 Characterization of the activity of rhodopsin-G<sub>i</sub> complex

In addition to measuring the apparent affinity and thermal stability of rhodopsin-G<sub>i</sub> complex, I also tested the purified RhoM257Y-G<sub>i</sub> complex for specific dissociation upon binding of the non-hydrolysable GTP analogue GTPγS and AlF<sub>4</sub><sup>-</sup>. Indeed the profile obtained by analytical size exclusion chromatography showed a near complete dissociation of the complex upon specific binding of GTPγS and AlF<sub>4</sub><sup>-</sup>, indicative of a high activity in the purified RhoM257Y-G<sub>i</sub> complex (Fig. 3.8a). Resistance to detergents is another critical factor for the crystallization of membrane proteins as it allows the screening of a larger crystallization space. I therefore tested detergent resistance of the purified RhoM257Y-G<sub>i</sub> complex by diluting it into a range of detergents. After incubation for 30 minutes the diluted complexes were analyzed for their structural integrity by FSEC (Fig. 3.8b). While dissociated in relatively harsh detergents, the complex survived in a number of detergents.

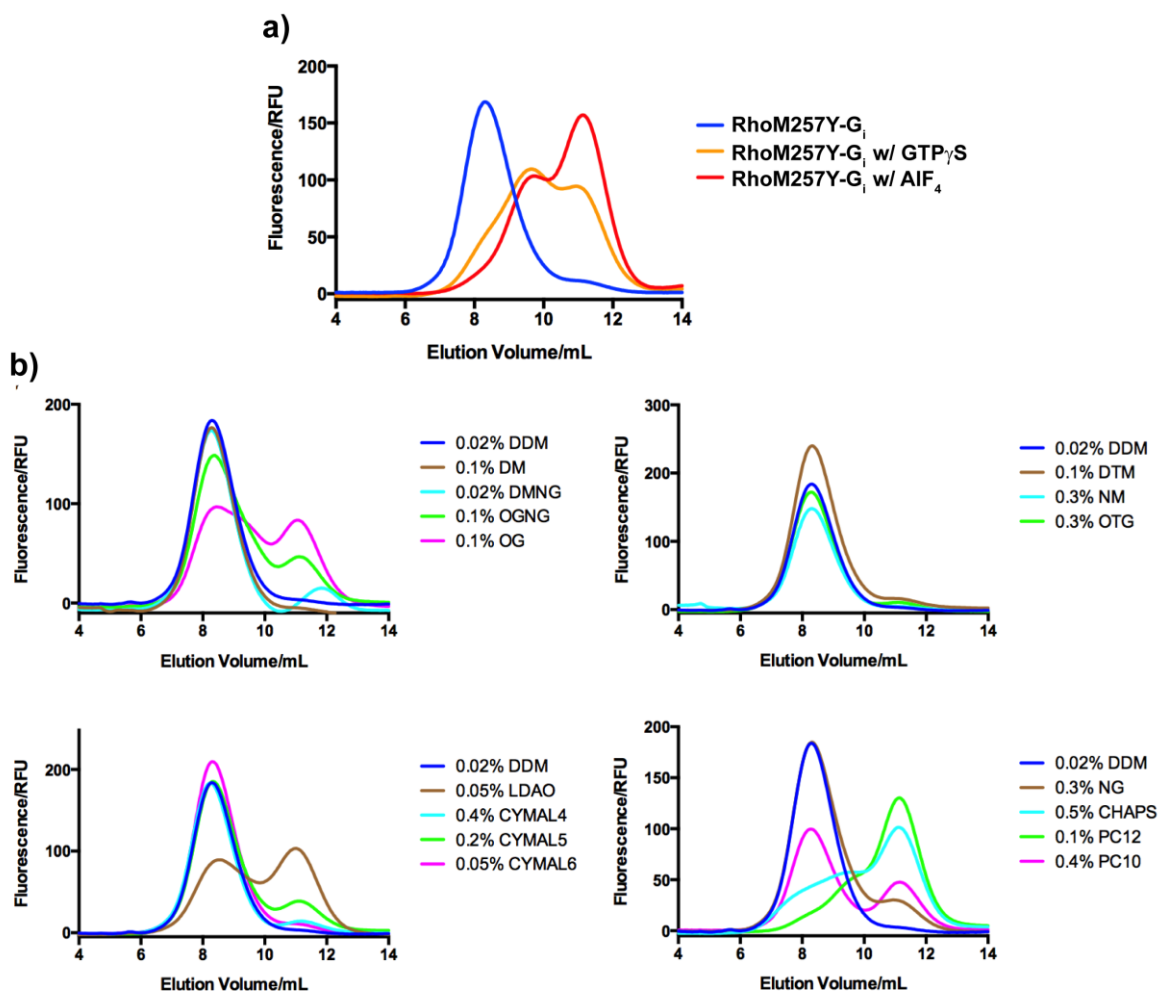


**Fig. 3.8. Characterization of the activity of rhodopsin-G<sub>i</sub> complex.** a, FSEC assay: The G<sub>i</sub> in RhoM257Y-G<sub>i</sub> complex adopts the active conformation showing dissociation upon incubating with GTP $\gamma$ S or GDP and AIF<sub>4</sub>. b, RhoM257Y-G<sub>i</sub> complex is resistant to wide variety of detergents. DDM, dodecyl- $\beta$ -D-maltopyranoside; DM, decyl- $\beta$ -D-maltopyranoside; DMNG, decyl maltose neopentyl glycol; OGNG, octyl glucose neopentyl glycol; OG, octyl- $\beta$ -D-glucopyranoside; DTM, decyl- $\beta$ -D-thiomaltopyranoside; NM, nonyl- $\beta$ -D-maltopyranoside; OTG, octyl- $\beta$ -D-thioglucoylpyranoside; LDAO, lauryldimethylamine-oxide; CYMAL, cyclohexyl-1-hexyl- $\beta$ -D-maltopyranoside; NG, nonyl- $\beta$ -D-glucopyranoside; CHAPS, 3-[(3-cholamidopropyl) dimethylammonio]-1-propanesulfonate; PC, phosphatidylcholine.

### 3.2.4 Preparation of rhodopsin-G<sub>i</sub> complex in large scale

The high expression of active WT G $\alpha_{i1}$  (section 3.1) and the stability of the Rho\*-G<sub>i</sub> complex allows preparation of the receptor-bound G $\alpha_{i1}$  protein complex in large quantities. Therefore, I established an optimized procedure for the complex preparation (Fig. 3.9). The activated rhodopsin-G<sub>i</sub> complex was prepared by first solubilizing HEK293S-GnTII<sup>-</sup> cells expressing the N2C/M257Y/D282C opsin in 1.25% DDM (w/v), centrifuging the material to remove nuclei and insoluble fractions, and applying the supernatant fraction to a 1D4-antibody immunoaffinity matrix as described previously [76, 102]. The heterotrimeric G<sub>i</sub> was reconstituted by combing the recombinant G $\alpha_{i1}$  with G $\beta\gamma_t$  separated from native G<sub>t</sub>. The immobilized opsin was then reconstituted with 11-*cis*-retinal to ground-state rhodopsin while still bound to the resin. Free (unbound) retinal was washed away and excess G<sub>i</sub> (typically 1.5 times molar ratio of rhodopsin) was added. Complex formation was induced by isomerization of 11-*cis*-

retinal to the full agonist all-trans-retinal using a xenon lamp with a 495nm long-pass filter to prevent isomerization of unbound retinal. After extensive washing of the resin, rhodopsin in complex with  $G_i$  was released from the immunoaffinity matrix by incubating with the 1D4-elution peptide resembling the C-terminus of rhodopsin (TETSQVAPA). The eluted fraction was concentrated and further purified by size-exclusion chromatography to remove free components. Initially size-exclusion chromatography showed that the preparation contained a relatively large amount of free rhodopsin, supposedly due to dissociation of the complex by re-binding of GDP to  $G\alpha_{i1}$ . Adding apyrase, an enzyme that hydrolyzes GDP to GMP and phosphate, during the light activation improved the efficiency of the RhoM257Y- $G_i$  complex formation by preventing re-binding of GDP. After the improvement the protein was eluted as a symmetric peak from the size exclusion column that contained all components of the RhoM257Y- $G_i$  complex. A typical yield from 40 g of cell pellet was 6-9 mg of RhoM257Y- $G_i$  complex with the purity suitable for biophysical characterization and high-throughput crystallization screening. In addition, it has been confirmed in my lab that the rhodopsin- $G_i$  complex also could be prepared with the native rhodopsin isolated from bovine retina in a large amount with the similar purity and stability as RhoM257Y- $G_i$  complex.

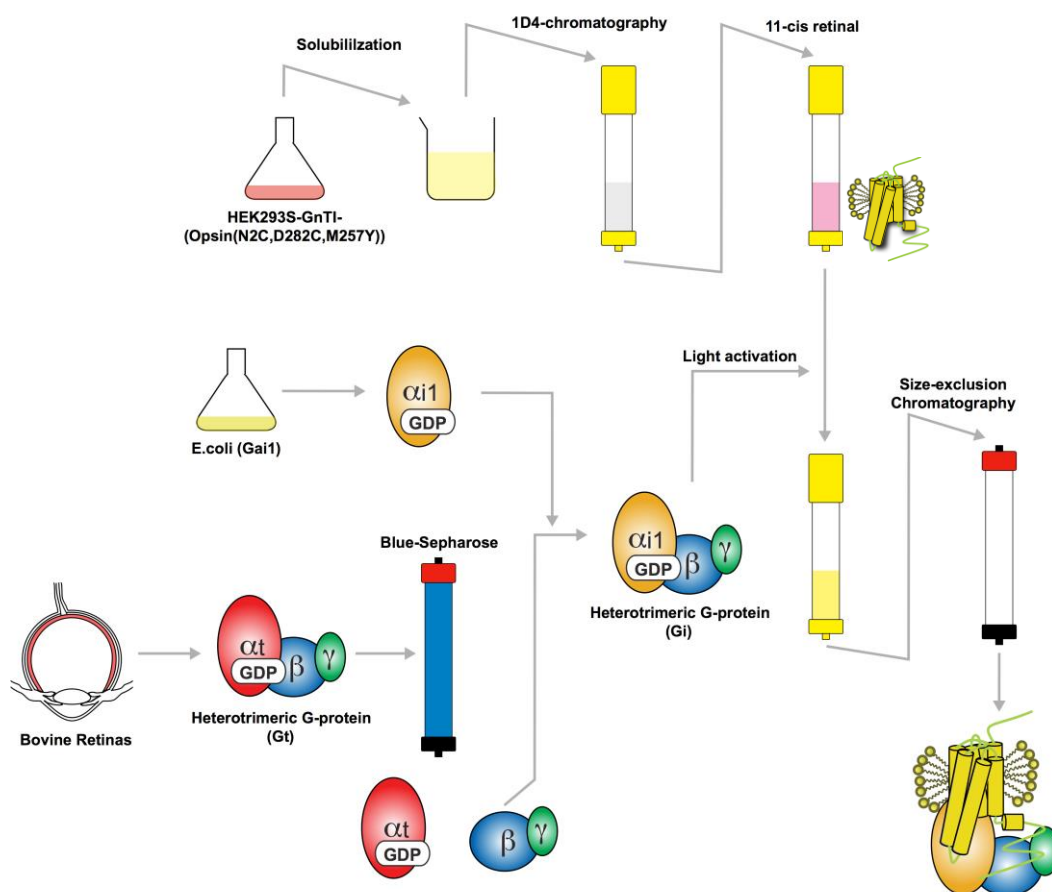


**Fig. 39. Preparation diagram of RhoM257Y- $G_i$  complex.** A typical 1D4 immuno-affinity purification and preparative size-exclusion chromatography of RhoM257Y- $G_i$  from recombinant OpsinM257Y and reconstituted  $G_i$  (combining the recombinant  $G\alpha_{i1}$  with native  $G\beta\gamma$ ).



### 3.3 HTP alanine mutagenesis scanning of $G\alpha_{i1}$

#### 3.3.1 Mutagenesis strategy and workflow

A convenient way of performing site-directed mutagenesis is an adaptation [105] of the original ligation-independent cloning protocol [106]. The target plasmid is amplified with two primers which contain the mutation site (Fig. 3.10), leading to a linear PCR product with short identical sequence at both ends. Transformation into *E. coli* Mach1, NovaBlue or TG1 strains leads to end repair which restores a circular plasmid containing the introduced mutation [107, 108]. While the exact mechanism of this reaction is not well understood, from my experience the above-mentioned cell strains are more efficient than other cell strains commonly used for DNA manipulation. The repair requires a minimal primer overlap of 13 bp. The mutation site could be located anywhere in the pair of primers and not necessarily in the overlap region, however, certain limitations are discussed below. Unlike the PCR product, the original template is methylated. This allows digestion of the template with DpnI in order to minimize the background. Alternatively, the PCR template may be methylated enzymatically at CpG dinucleotides and is eliminated by certain strains of *E. coli* that contain wt McrBC restriction system [109]. After transformation and plating with appropriate antibiotics, several single colonies are sent for sequencing as bacterial slabs on a 96-well plate. If mutagenesis was not successful after three attempts, alternative methods were used to generate the remaining mutants.

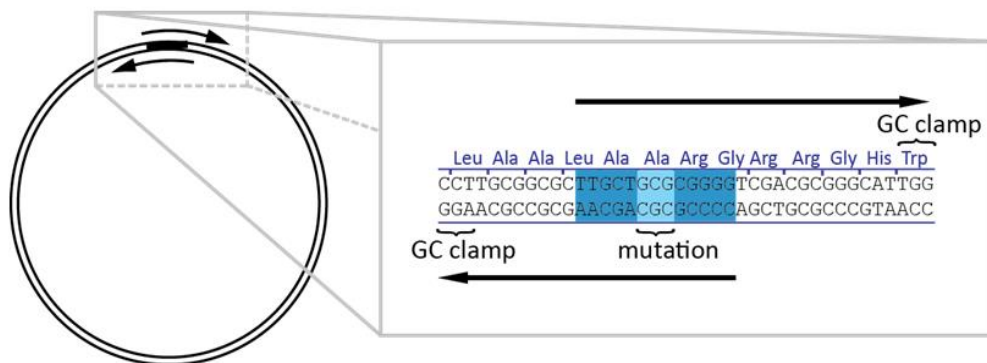
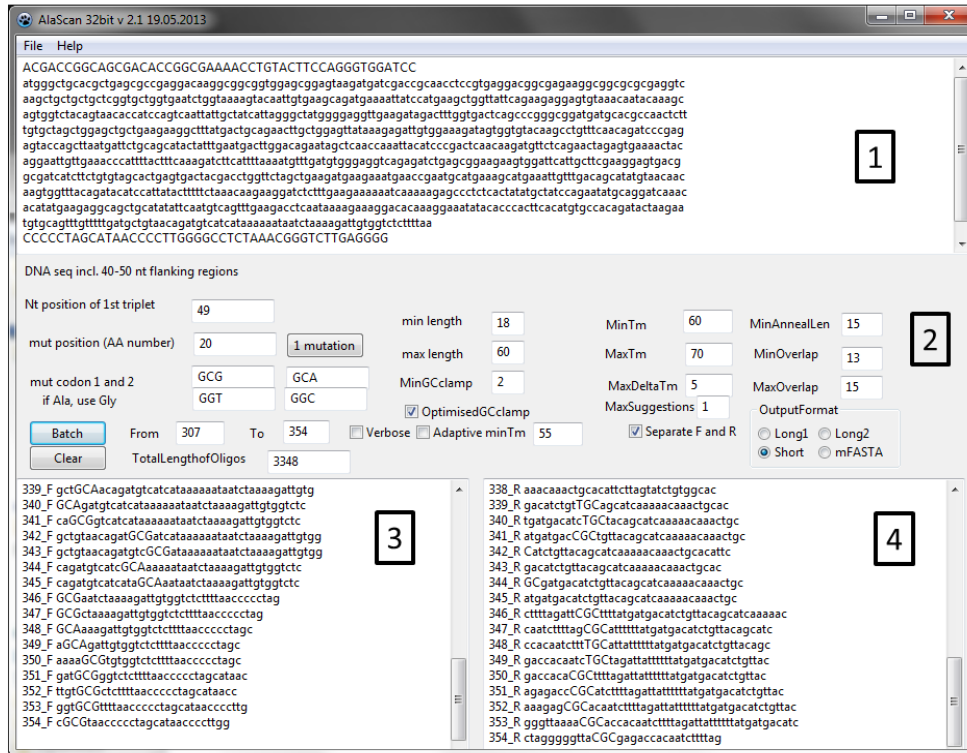


Fig. 3.10 Mutagenesis by overlapping PCR reaction.

#### 3.3.2 Primer design by AAscan

The software interface (Fig. 3.11) includes a text box for entering the template DNA sequence, the choice of codons to be used for mutagenesis, fields to define the region of the protein sequence to be mutated, various options used in primer design described above and, finally, different options for the output data format. The template sequence for scanning mutagenesis include the flanking regions of 50-60 bp (but at least with a length equivalent to the number of bp given in the field “**max length**”) as the primers may anneal outside of the protein coding region, if the position to be mutated is close to the protein termini. The flanking regions are shown in capital letters in Fig. 3.11.





**Fig. 3.11. AAscan software interface.** (1) Input text box for reference sequence. (2) Options for primer design. (3) Output window containing primer forward and (4) reverse primers.

The position of the 1<sup>st</sup> nucleotide in the protein coding sequence needs to be specified so that the software can convert the amino acid position to nucleotide coordinates. For example, if the 48 bp of the vector upstream of the protein coding sequence are included, the position of A from the first ATG is 49. Two different codons for mutagenesis need to be specified for the desired substitution, and the program will choose the one that introduces the least number of mismatches. If the template codon is already encoding an alanine, the codon will be mutated to another amino acid, for example glycine. Two alternative codon choices are provided. Of course, the mutations can be designed for any desired amino acid, not only alanine. If only one codon encodes a particular amino acid, or use of a particular codon is preferred, the same codon needs to be entered. If more than two codons encode a particular amino acid, the two preferred codons are selected based on the expression organism and goals of the project. To design the primers, either a single amino acid position or a range needs to be specified. AAscan designs the shortest primers with a length in between the “min length” and “max length” entered by the user. The  $T_m$  is designed to be as close to the “min $T_m$ ” as possible, not exceeding the “max $T_m$ ”. The maximal difference between melting temperatures of forward and reverse primers may not exceed the value given in “MaxDeltaTm”.  $T_m$  is calculated according to the following formula [110]:

$$T_m = 64.9^\circ\text{C} + 41^\circ\text{C} \times (\text{number of G's and C's in the primer} - 16.4) / \text{length of the primer}$$

Two melting temperatures are reported. The first ( $T_m$ ) is relevant for the initial cycles of the PCR when the primer anneals to the original template DNA, with mismatches in the mutation site. The second  $T_m$  value ( $T_{mfull}$ ) is relevant for the later stages of the PCR, when sufficient product was already amplified and the full length sequence of the primer anneals to the newly synthesized template without mismatches. The increased stability of primers may lead to a change in the efficiency of the PCR reaction.

In addition, several further parameters are taken into account: “MinAnnealLen” is the minimal distance from the mutation codon to the 3’ end of the primer, and in my experience it should be at least 15bp. “minGCclamp” is the minimal number of G or C bases at the 3’ end of the primer. The “minGCclamp” can be set to 0 if the GC clamp is not required. If the checkbox “OptimisedGCclamp” is selected, “OptimisedGCclamp” score is calculated according to the rules formulated in [111]. Depending on the combination of the last three nucleotides of the 3’ end of the primer, score is assigned as follows: [GC][GC][GC]=0; [ATGC][ATGC][AT]=1; [ATGC][AT][GC]=2; and [AT][GC][GC]=3. The score of 0 corresponds to the worst GC clamp and 3 to the best, respectively. In this context, [ATGC] means any nucleotide, [AT] means A or T, and [GC] means G or C, respectively. “MinOverlap” and “MaxOverlap” is the length of the overlap sequence between the ends of the resulting PCR fragment. The default range is 13 to 15 bp. If the overlap is too short (<11 bp), this will result in decreased efficiency of end repair [112], while too long overlaps may lead to undesired self-annealing of primers, formation of wrong PCR products and decrease in overall PCR efficiency. The number of primer pairs designed for the mutation of every specified amino acid position is defined by the filed “Maxsuggestion”. When generating primers in batch mode, this parameter is generally set to “1”. The “Adaptive  $T_m$ ” option can be used when for some positions in the gene no primers can be generated within the constraints of maximal length and minimal  $T_m$ . For these positions only, the program will decrease the “min $T_m$ ” value by 1 °C until it can generate a primer pair satisfying all constraints. However, a better alternative is to increase the maximum length of the primer.

Different output formats of the primer design are applicable. The “Long1” format provides the sequence of the suggested primer on the coding strand, with capitalized mutation site and introduced mutations denoted by an “X”, a list of parameters describing its properties such as length,  $T_m$  excluding mismatches,  $T_m$  of the full length primer, GC clamp score, annealing length from the mutation site to the 3’ end, and the actual sequence of the primer to be ordered, reverse-complemented if needed. “Long2” format provides the same information in tabular format convenient for import into spreadsheets. “Short” generates a list of oligo names and sequences (reverse-complemented if needed) to be ordered— convenient for generating orders. “FASTA” generates a FASTA formatted list of primers. “Separate F and R” checkbox creates two separate lists of forward

and reverse oligonucleotides which can be useful for ordering. “Verbose” activates additional information printout which may helpful for primer design. The results of the primer design from one or both output text boxes can be copied to the clipboard and pasted in the order form. “File/Open” and “File/Save” menu items allow opening and saving of the projects (sequences and options). The data are saved in binary format and manual editing of the data file is not supported.

### 3.3.3 MutantChecker: sequencing results analysis

The amount of sequencing results which needed to be analyzed stimulated the development of a software to align and identify mutations semi-automatically (Fig. 3.12). Mutant checker is a software designed to align and identify mutations semi-automatically which facilitates analysis of large numbers of sequencing results. It aligns the sequencing results to the reference sequence using an empirical likelihood function that is defined as a number of perfect matches in a sliding track of 7 nucleotides along the whole length of reference sequence. This function (Eq. 1) does not allow gaps, as I am looking only for mutations, and not deletions or insertions.

$$score = \sum_{i=1}^{N-6} \prod_{j=i}^{i+6} match(seq_1[j] \text{ AND } seq_2[j]) \quad (\text{Eq. 1})$$

For every possible offset between two sequences to be compared, an overlap region is copied into  $seq_1$  and  $seq_2$ . The length of the overlap region is  $N$ . The match function compares if the nucleotides  $seq_1[i]$  and  $seq_2[i]$  at position  $i$  are the same (result=1) or different (result=0). By combining the match function over a sliding window of 7 nucleotides, the software calculates if all 7 nucleotides are the same. The sliding window is then moved by one nucleotide, and calculations are repeated. The total score for the alignment with a given offset is a sum of individual scores. The maximal score corresponds to the best alignment. The function has significant differentiating power between right and wrong alignments. If the sequencing results contain the desired mutation and no additional rearrangements, then there will be only one possible alignment. On the other hand, if during recombination event in the cell part of the sequence was duplicated, there will be two or more possible alignment positions reported on a graph. The MutantChecker can also reverse complement the sequence if the sequencing was done with reverse primers, for mutations close to the C-terminus of the protein. The software can also process batches of sequences which dramatically speed up the analysis of sequencing results.

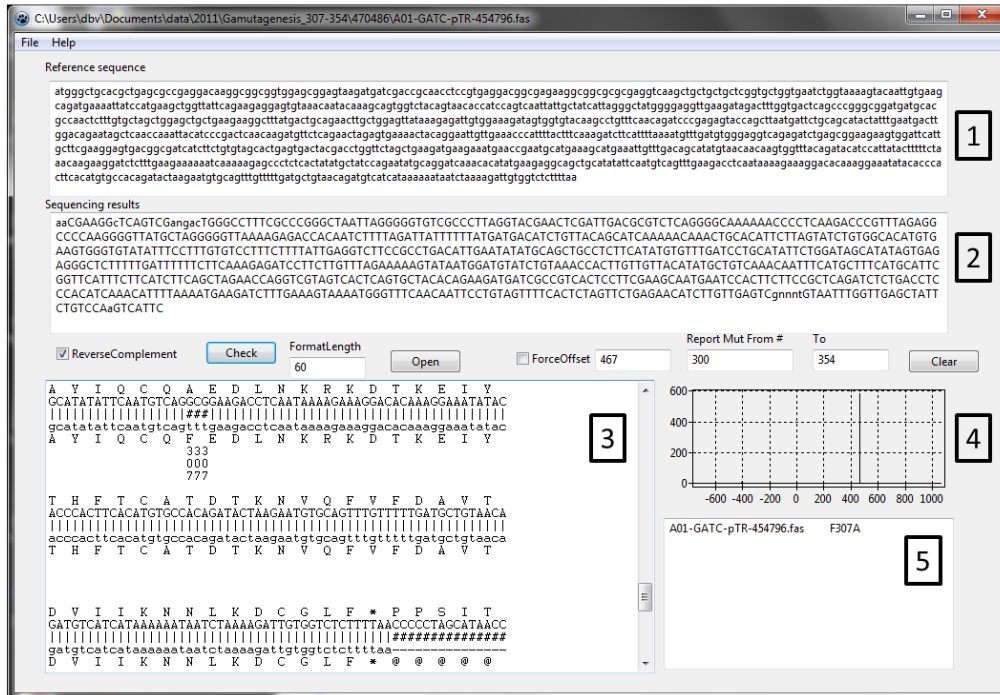


**Fig. 3.12. Mutant Checker interface.** (1) Input text box for reference sequence, starting with the beginning of the expressed sequence (first ATG). (2) Input text box for sequencing results. The sequence is reverse complemented for the analysis if the “ReverseComplement” checkbox is activated. (3) Output windows of aligned sequences, DNA to protein translation of both reference sequences showing identified mutations and their position, based on the reference sequence. (4) Graphical output of the alignment score function vs offset between to sequences. A single peak indicates only one possible alignment, while multiple peaks indicate several alternative alignments and non-productive clone. (5) Identified mutations, within the specified region.

### 3.3.4 PCR cloning primer design software

Seamless cloning has gained acceptance as a very convenient cloning method which allows seamless integration of the desired DNA sequences into a vector [107, 113]. Versions of this method also allow deletion or replacement of a part of a sequence with a single PCR reaction. At the core of the method is a PCR amplification of the vector backbone and, in a separate reaction, amplification of the desired inserts, so that the ends have identical sequences overlapping by about 15 bp. During the PCR stage it is also possible to have additional sequences included in the primer, for example a coding sequence for a protease restriction site.

The cloning primer design software (Fig. 3.13) simplifies the task of designing such primers. The inputs of the software are the approximately 50 bp long vector sequences upstream and downstream of the insert, as well as the sequence of the insert. There is also a possibility to include additional sequences between the insert and the vector. Such short sequences will be included in the primers and may be useful for insertion or replacement of restriction sites, protease cleavage sites or purification tags.

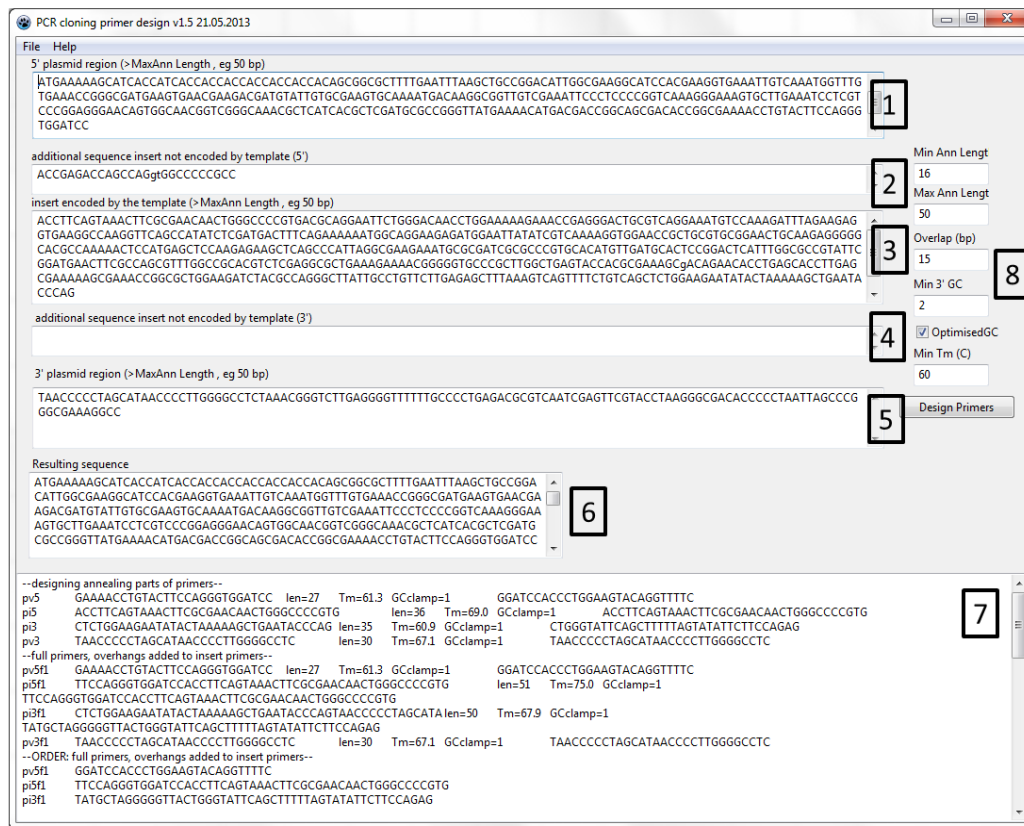


**Fig. 3.13. PCR cloning primer design software interface.** (1) Upstream portion of the vector, up to the cloning position. (2) Additional sequence to include between the vector and the 5' end of the target gene, eg protease cleavage site. (3) Sequence of the target, encoded by the template. (4) Additional sequence to include between the 3' end of the target gene, eg protease cleavage site. (5) Downstream portion of the vector. (6) Resulting sequence, i.e. (1)+(2)+(3)+(4)+(5). (7) Output window containing information about primer design and primers to be ordered. pv5 is the primer annealing to the 5' end of the vector, pi5 is primer annealing to the 5' end of the insert, pv3 and pi3 are primers annealing to the 3' end of the vector and the insert, correspondingly.

The software designs primers to amplify the vector and the insert. It subsequently adds the desired inclusions and the required 15 bp overlaps needed for homologous recombination. It offers the user several options of primer pair design which may be advantageous in different situations (Fig. 3.14). When cloning several different inserts into the same vector, it makes sense to have a primer pair for vector amplification and various primer pairs for amplification of the inserts. The opposite would be desired if the same insert was cloned into different vectors. In a third case, where due to the insertion of the relatively long additional DNA sequence the primers are long, it may be advantageous to have a balanced length of primers due to the technical difficulties of producing very long primers. In this case, four primers of balanced lengths would be advantageous when primers with long additional DNA sequences are designed.

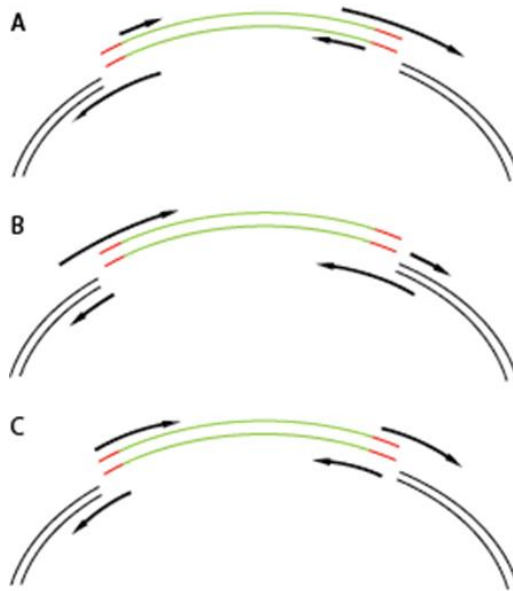


**Fig. 3.14. Various strategies for primer design.** Green – insert, black – vector, red – additional sequences complementary to the primer overhangs are incorporated between the insert and the vector. Overhangs can be added either to (A), the insert-replicating primers or (B) they can be split or (C) added to both primers.

### 3.3.5 Optimization of PCR conditions and HTP Ala mutagenesis workflow

I have optimized the PCR reaction conditions for obtaining single bands at 5-8 kb (linearized vectors) on 0.7% or 1% agarose gels. However, visually detectable bands were not essential to obtain mutant clones.

All solutions were strictly kept on ice. 1X Phusion® High-Fidelity PCR master mix with GC or HF buffer, or KOD polymerase with its supplied buffer, were supplemented with 400 mM TMSO and 12 pg/μl DNA template for amplification. 17 μl PCR master mix were combined with each 1.5 μl of both forward and reverse primer at stock concentration of 1 μM in each well of 96-well micro-plate. For the PCR with a vector of approximately 8 kbp, I used a touchdown protocol [114], the detailed conditions were as follows: Initial denaturation at 98 °C for 30 sec, then 20 step-down thermal cycles consisting of the denaturation at 98 °C for 20 sec, annealing from 60 °C down to 50 °C for 30 sec with 0.5 °C per cycle decrement, and extension at 72 °C for 2 min, followed by 20 thermal cycles (98 °C for 20 sec, 54 °C for 30 sec, 72 °C for 2 min), and final extension at 72 °C for 5 min. Afterwards reactions were kept at 10 °C. DpnI digestion was also optimized to reduce the background. I have incubated 20 units of DpnI in 20 μl PCR mixture overnight at 37°C.

I have used the *E.coli* strain Mach1 for all DNA manipulations. The chemically competent cells had an efficiency of  $>10^7$  colonies/μg of pBR322 DNA for reliable results. Transformation steps were also

optimized by adding 4  $\mu$ l of PCR product into another 96-well microplate filled with 50  $\mu$ l Mach1 cell suspensions. After 25min on ice, the mixture was incubated in the PCR machine at 42 °C (heat shock) for 45 s and then placed back on ice for 2min. The transformed cells were then transferred to a 96 deep-well plate filled with 600  $\mu$ l S.O.C. media and incubated at 37 °C for 2 hr. 100  $\mu$ l of 650  $\mu$ l samples were plated on LB agar plate with appropriate antibiotics and incubated at 37 °C overnight. A single colony of each mutant was transferred into a 96 well Agar plate with appropriate antibiotics and sequenced by the GATC Biotech Company (Fig. 3.15).

To minimize sequencing costs, I have sent one or two clones for sequencing, and sent additional ones only if the first round of sequencing did not yield the desired mutation. It has been relatively easy to achieve 80% success rate – on average only about two colonies for each mutant had to be sequenced. Sending more clones for sequencing yields missing mutants, however some proved to be very difficult to obtain. If repeating the whole mutagenesis procedure with alternative polymerase still did not produce the desired mutant, I resorted to alternative mutagenesis strategies. Finally, I obtained 289 out of 354 alanine mutants of  $G\alpha_{11}$  in three rounds of mutagenesis. The remaining 65 mutants were ordered as synthetic constructs.

The most common problem I have observed at the sequencing level was insertion of tandem repeats of the mutagenesis primer at the mutation site [115]. Reducing the amount of template DNA to 0.2 ng seems to minimize this artefact. The second commonly observed problem was deletion of a part of a sequence, either upstream or downstream of the mutation site. Both problems are easily detectable by mutant checker software or by manual alignment of the sequencing results to the reference sequence. I have observed that the “problematic” mutants tend to cluster, and in several cases there was a stretch of amino acid positions for which I was not able to obtain alanine mutants by this technique. As the primers generated for the neighboring positions have to a large degree identical sequence, it is possible that certain sequence related features lead to undesired side products of the mutagenic PCR.

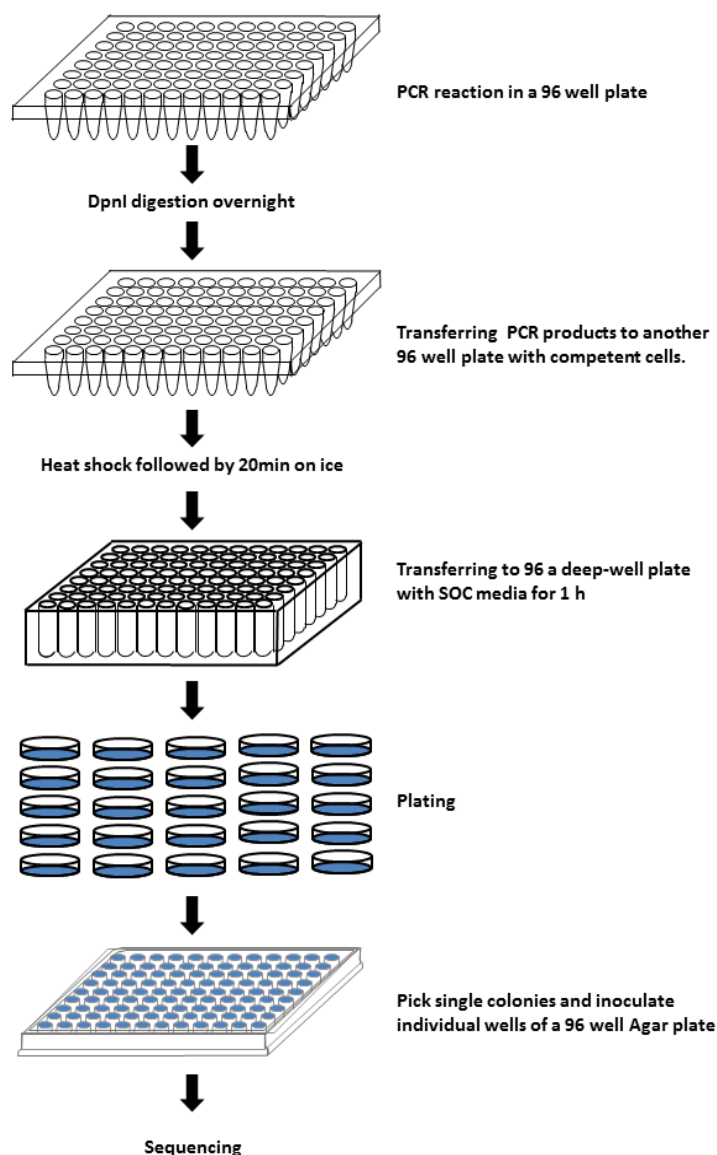


**Fig. 3.15. Workflow of HTP alanine mutagenesis scanning.** The PCR reaction was performed in the 96 well format. The reaction products were digested by DpnI, followed by transformation into *E.coli* MachI and plating. Single colonies were picked and sent for sequencing.

### 3.4 Probing $G\alpha_{i1}$ activation at single amino acid resolution

#### 3.4.1 Development of HTP purification

To facilitate the purification of 354  $G\alpha_{i1}$  alanine mutants, I developed an HTP purification method in 96-well format (Fig. 3.16a). In the development of the method, the major problems were in performing efficient cell lysis, and in simultaneous protein purification in the HTP format. To solve these problems, first I bought and installed one 96-pin probe in our sonicator for HTP sonication. Unfortunately, this 96-pin sonication probe could not efficiently lyse the cells because of the power limitation of our sonicator. After that, I found that an 8-pin sonication probe can efficiently lyse eight



alanine mutants at a time. To carry out the HTP protein purification, I utilized a 96-well filter plate preloaded with the metal ion affinity chromatography (IMAC) media to perform HTP IMAC purification. After loading His(10)-tagged alanine mutants (one mutant per well), the bound recombinant proteins could be conveniently and efficiently washed and eluted from the 96-well filter plate by utilizing multi-channel pipettes. By this method, 48  $G\alpha_{i1}$  alanine mutants per day can be simultaneously prepared with a yield of 200  $\mu\text{g}$  from 10 mL *E.coli* cell culture. The purified recombinant alanine mutants are of high purity, as judged by coomassie-stained SDS-PAGE (Fig. 3.16b), and can be directly applied to further HTP assays. Most  $G\alpha_{i1}$  alanine mutants were well-expressed and purified, however the R142A, Y230A, K270A and D272A were severely aggregated and could not be used in further assays.

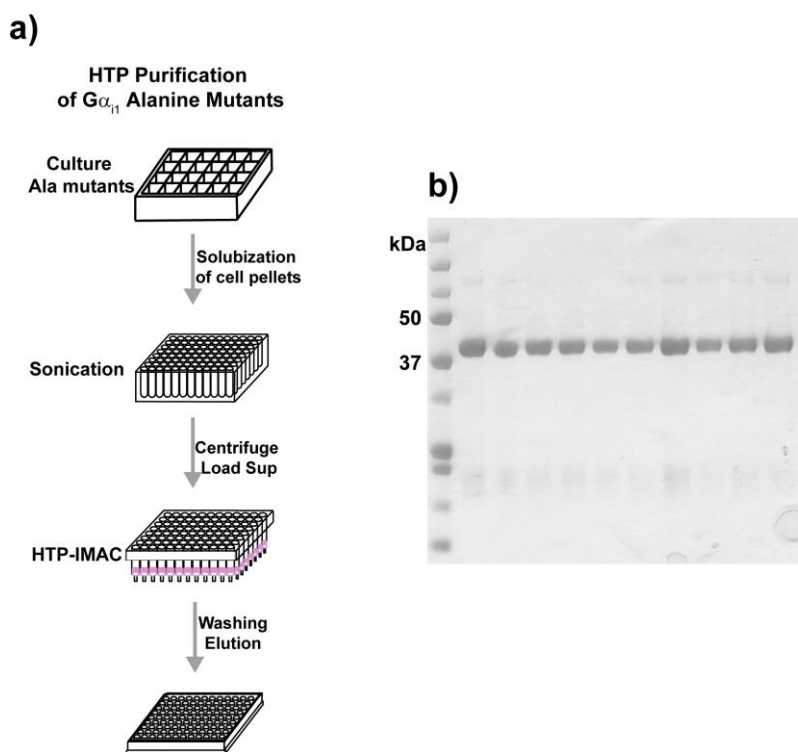


**Fig. 3.16.** HTP purification of  $G\alpha_{i1}$  alanine mutants. **a**, HTP purification flowchart. **b**, SDS-PAGE analysis of the purified alanine mutants by HTP purification.

### 3.4.2 Thermal shift analysis of WT $G\alpha_{i1}$

To characterize the thermostability of each  $G\alpha_{i1}$  alanine mutant in nucleotide-bound state, I first performed thermal shift assay of WT  $G\alpha_{i1}$  in titration with different concentrations of GDP and GTP $\gamma$ S. In titration with GDP, the thermal shift concentration-response curve shows that there is a significant transition shift by 2  $^{\circ}\text{C}$  upon addition of 2  $\mu\text{M}$  GDP (Fig. 3.17a-b). After an initial sharp rise, increasing GDP concentration shifts the transition progressively at a slower rate (Fig. 3.17a-b). However, as for GTP $\gamma$ S, the melting curves with titration of GTP $\gamma$ S are characterized, at low GTP $\gamma$ S concentration (less than 2  $\mu\text{M}$ ), by two transition regions: the derived  $T_m$  value of the first transition region is the same as WT apo- $G\alpha_{i1}$ , and the  $T_m$  value of the second transition region is 70  $^{\circ}\text{C}$  (Fig.

3.17c). With increasing concentration of GTP $\gamma$ S, the second transition remains, however the first transition region disappears (Fig. 3.17c). Interestingly, the derived  $T_m$  values of the second transition curves are not affected by the titration concentration of GTP $\gamma$ S, indicating that GTP $\gamma$ S has the higher binding affinity with  $G\alpha_{i1}$  comparing with GDP (Fig. 3.17d). Based on the thermal shift analysis,  $T_m$  values upon addition of 1mM GDP and 0.1mM GTP $\gamma$ S are finally chosen as to reflect the thermostability of WT  $G\alpha_{i1}$  in GDP-bound state [ $G\alpha_{i1}$ (WT)-GDP] and in GTP $\gamma$ S-bound state [ $G\alpha_{i1}$ (WT)-GTP $\gamma$ S], respectively. The mean  $T_m$  values of  $G\alpha_{i1}$ (WT)-GDP and  $G\alpha_{i1}$ (WT)-GTP $\gamma$ S are  $63.7 \pm 0.3$  °C and  $70.5 \pm 0.3$  °C derived from 25 and 24 individual measurements, respectively (Fig. 3.17e-f).

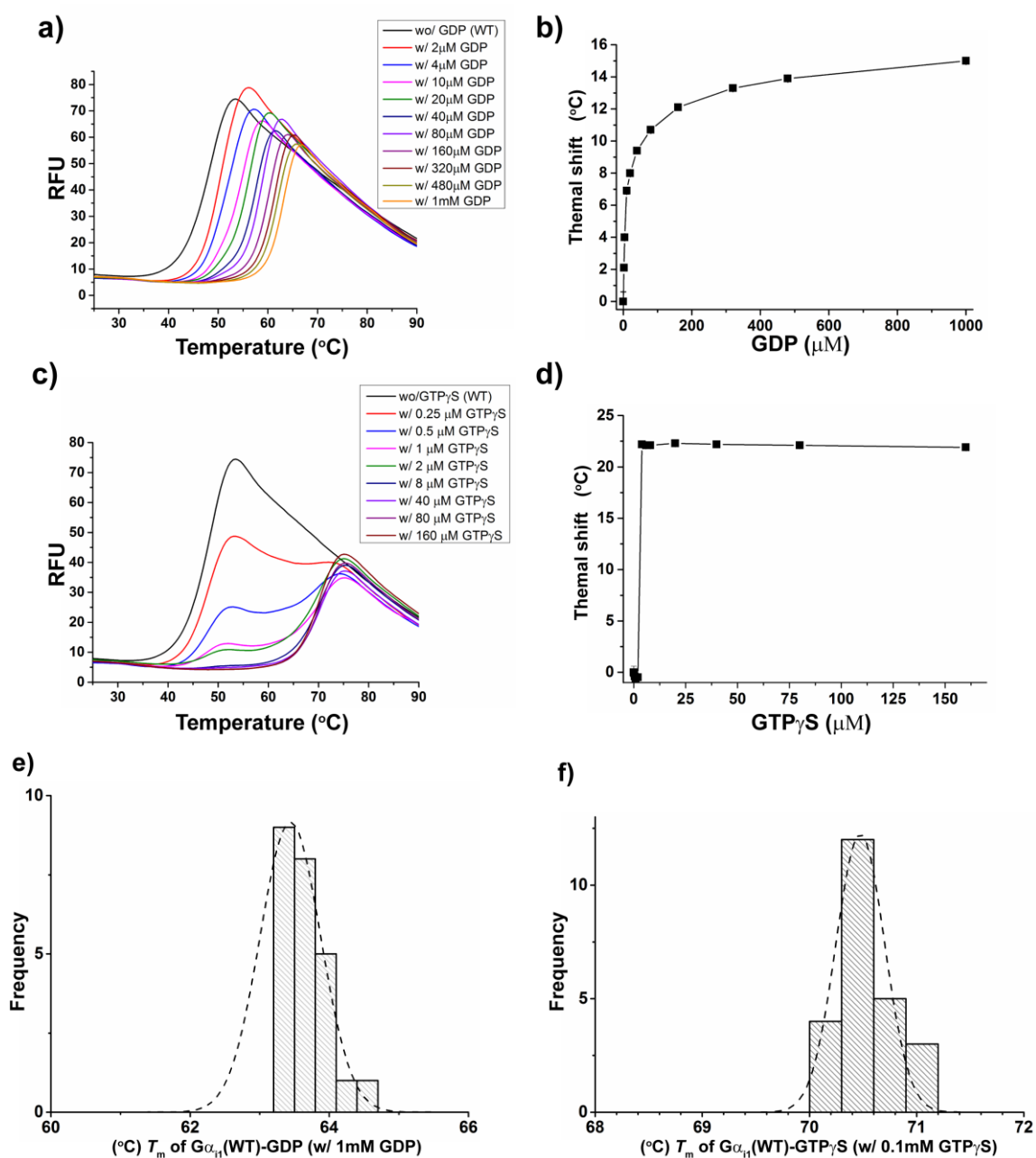
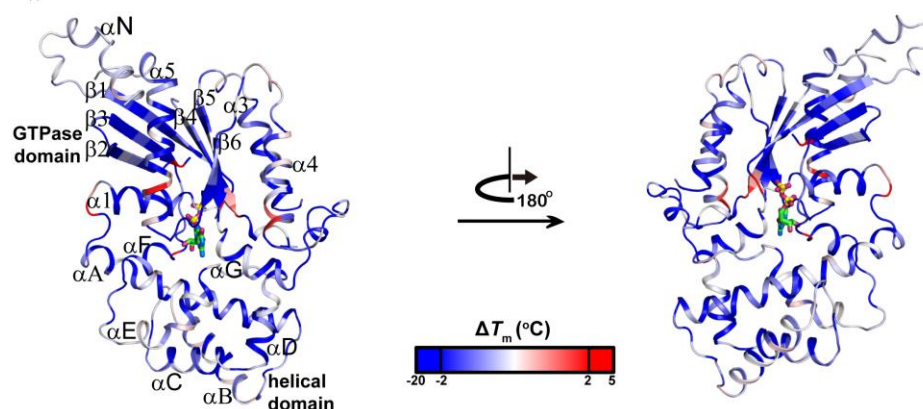


**Fig. 3.17. Thermal shift analysis of WT  $G\alpha_{i1}$ .** a-d, Melting profile of WT  $G\alpha_{i1}$  in titration with GDP (a) and GTP $\gamma$ S (c), and the correlated thermal shift concentration-response curve as b, d, respectively. e-f, Statistics analysis of thermal stability of WT  $G\alpha_{i1}$  in GDP-bound (e) and GTP $\gamma$ S-bound state (f).

### 3.4.3 Characterization of thermostability of $G\alpha_{i1}$ alanine mutants in the nucleotide-bound state

Based on the established thermostability conditions from WT  $G\alpha_i$ , the  $T_m$  value of each  $G\alpha_{i1}$  alanine mutant in the presence of 1mM GDP or 0.1mM  $GTP\gamma S$  are regarded to reflect the thermostability in the GDP-bound [ $G\alpha_{i1}(\text{Ala})\text{-GDP}$ ] and GTP-bound [ $G\alpha_{i1}(\text{Ala})\text{-GTP}\gamma S$ ] state, respectively. Thus, the thermostability effect of each  $G\alpha_{i1}$  alanine mutant can be measured, compared and directly visualized by mapping the  $\Delta T_m$  values to the crystal structures of nucleotide-bound  $G\alpha_{i1}$  (Fig. 3.18a-b).

a)  $G\alpha_{i1}\text{-GDP}$



b)  $G\alpha_{i1}\text{-GTP}\gamma S$

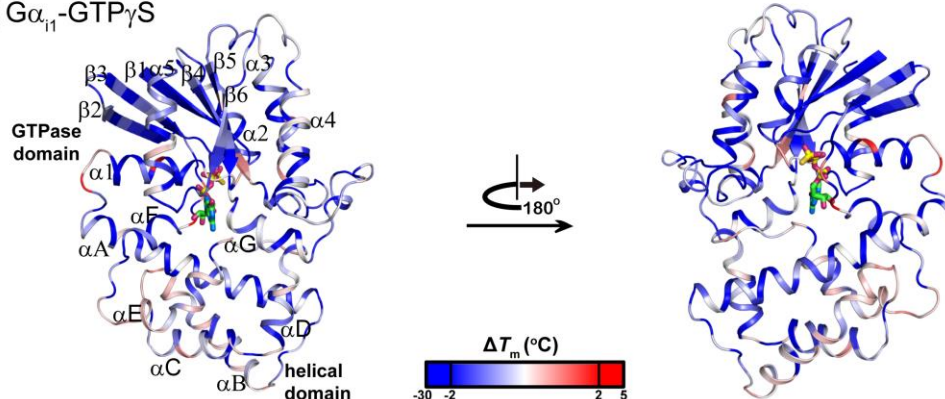


**Fig. 3.18. Characterization of thermostability of  $G\alpha_{i1}$  alanine mutants in nucleotide-bound state.** a-b,  $\Delta T_m$  values of each single alanine mutant of  $G\alpha_{i1}$  in addition of GDP and  $GTP\gamma S$  were mapped to the crystal structure of GDP-bound  $G\alpha_{i1}$  (PDB 1GDD) (a) and  $GTP\gamma S$ -bound  $G\alpha_{i1}$  (PDB 1GIA) (b). Blue: destabilizing effect by the alanine replacement; red: stabilizing effect by the alanine replacement.

About 65% of  $G\alpha_{i1}$  alanine mutants in GDP-bound state and 72% of alanine mutants in  $GTP\gamma S$ -bound state leave the  $\Delta T_m$  value unchanged (between  $\pm 2$  °C of WT level) (Fig. 3.19a-b), while the alanine mutants which exhibit a  $T_m$  of more than 2 °C below WT level are regarded as destabilizing for both GDP- and  $GTP\gamma S$ -bound states. Additionally, the comparison of  $\Delta T_m$  distribution shows that the destabilization effect caused by the alanine mutation in the  $GTP\gamma S$ -bound state are smaller than those in the GDP-bound state, implicating that  $G\alpha_{i1}$  in the GTP-bound state is more stable than GDP-bound state. Furthermore, among 350 purified  $G\alpha_{i1}$  alanine mutants, D200A is the only alanine mutant which dramatically stabilizes both apo- and GDP-bound state (12 °C and 5 °C, respectively) (Fig. 3.19c). The derived  $T_m$  value of D200A in GDP-bound state is almost the same as in the  $GTP\gamma S$ -bound state. The structural overview shows that D200 is located at the c-terminus of the  $\beta 3$  sheet, which is the

starting point for the Switch III region and is disordered in the GDP-bound state. D200A seems to be able to stabilize the flexible Switch III region, which further enhances the overall stability of the GDP-bound state. The exact reason needs more experimental results, such as solving the crystal structure of D200A by X-ray crystallization.

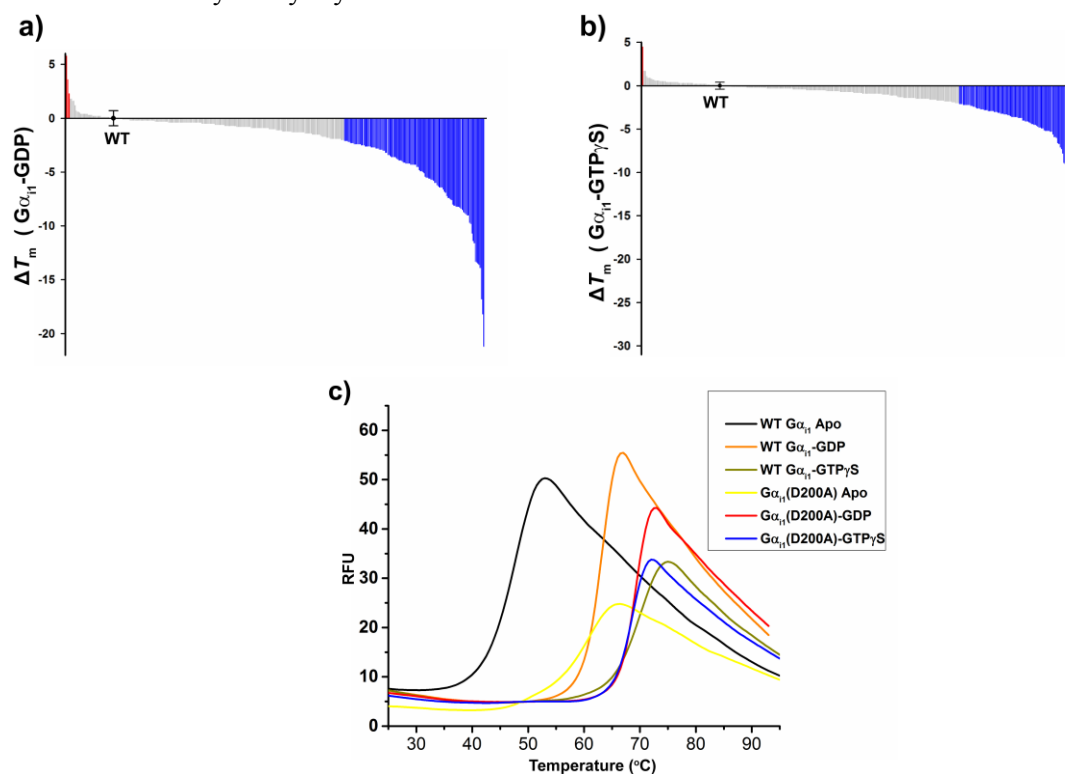


**Fig. 3.19. Distribution of effect on stability of G $\alpha_{i1}$  alanine mutants in the nucleotide-bound.** a-b, Distribution of  $\Delta T_m$  of each single alanine mutant in GDP-bound (a) and GTP $\gamma$ S-bound state (b). c, Thermal shift of D200A in apo and nucleotide-bound state.

#### 3.4.4 Characterization of Rho\*-G $_i$ (WT) complex by native gel electrophoresis

To characterize the effect of each G $\alpha_{i1}$  alanine mutant on receptor-bound state, I started to develop an HTP assay based on native gel electrophoresis (NPAGE). To show the possibility of the NPAGE method, I first characterized Rho\*-G $_i$ (WT) complex reconstituted with WT G $\alpha_{i1}$  and native rhodopsin. The results show that the reconstituted Rho\*-G $_i$ (WT) complex can be clearly visualized in NPAGE as one single band with sharp resolution (Fig. 3.20a). To confirm the functionality of the reconstituted Rho\*-G $_i$ (WT) complex, the complex was incubated with 200  $\mu$ M GTP $\gamma$ S at 20 °C for 30 min followed by NPAGE analysis. The result clearly shows that Rho\*-G $_i$ (WT) complex is completely dissociated upon addition of GTP $\gamma$ S (Fig. 3.20a) indicating that the reconstituted Rho\*-G $_i$ (WT) complex is correctly folded with the empty nucleotide binding pocket and the addition of GTP $\gamma$ S can quickly occupy the empty pocket to dissociate the Rho\*-G $_i$  complex. Moreover, to test the reproducibility of NPAGE method, the formation and analysis of Rho\*-G $_i$ (WT) complex by the NPAGE method was repeated by 33 individual experiments. The distribution of normalized complex

amount (%) of Rho\*-G<sub>i</sub>(WT) can be well-fit by a Gaussian model with an R<sup>2</sup> of 0.9839, with a mean of 100 ± 4% (Fig. 3.21a).

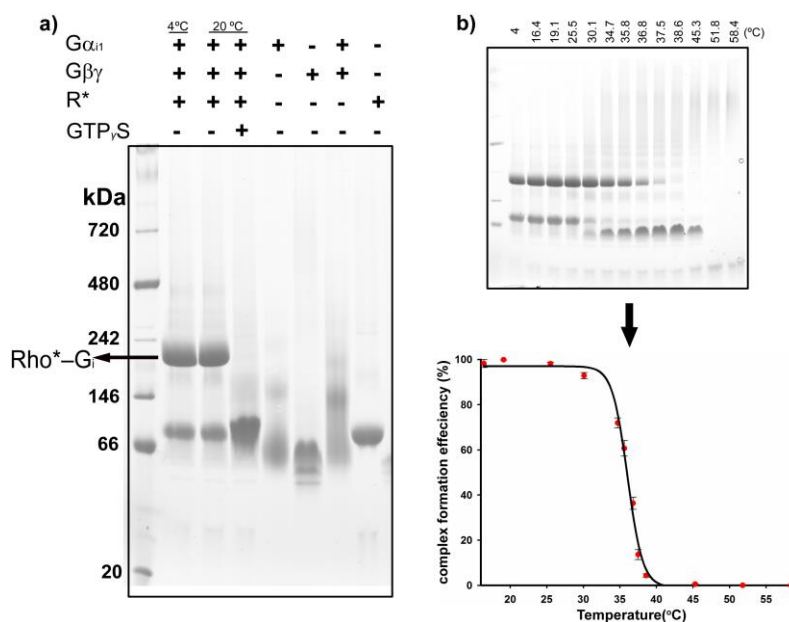


**Fig. 3.20. Characterization of Rho\*-G<sub>i</sub>(WT) complex by native gel electrophoresis. a,** Visualization of R\*-G<sub>i</sub> (WT) complex by NPAGE. **b,** Determination of  $Td_{50}$  of R\*-G<sub>i</sub> (WT) complex by NPAGE.

The thermal dissociation ( $Td_{50}$ ) of Rho\*-G<sub>i</sub>(WT) complex was further characterized by utilizing the established NPAGE method (Fig. 3.20b). Equal amounts of Rho\*-G<sub>i</sub>(WT) complex were simultaneously heated at the indicated temperature and visualized by the NPAGE method. The normalized complex amount was fit with sigmoidal Boltzmann equation to obtain the  $Td_{50}$  value. The determined  $Td_{50}$  value of Rho\*-G<sub>i</sub>(WT) complex is 36.0 ± 0.1 °C. To compare the thermostability effect of each alanine mutant on receptor-bound state, the HTP assay was designed to measure the complex stability (%) (See methods and materials) of Rho\*-G<sub>i</sub> complex formed with each alanine mutant at 36.3 °C. The complex stability of Rho\*-G<sub>i</sub>(WT) at 36.3 °C is determined as 44 ± 3% from 38 individual measurements. The distribution could also be fit well by a Gaussian model with an R<sup>2</sup> of 0.9544 (Fig.3.21b).

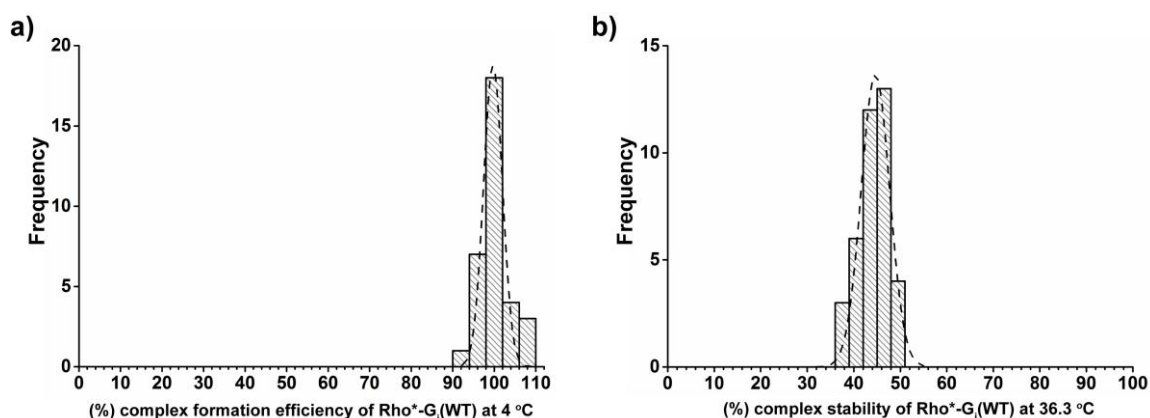


**Fig. 3.21. Statistics analysis of Rho\*-G<sub>i</sub>(WT) complex in receptor-bound state. a-b,** Frequency distribution of complex formation efficiency (at 4 °C) (a) and complex stability (at 36.3 °C) (b) of Rho\*-G<sub>i</sub>(WT) complex.

### 3.4.5 Development of NPAGE assay in HTP format

Based on the NPAGE conditions derived from Rho\*-G<sub>i</sub>(WT) complex, I extended the NPAGE method to the HTP format (Fig. 3.22a). The purified recombinant alanine mutants were directly reconstituted with Gβγ<sub>t</sub> subunit to form the heterotrimer in a 96-well PCR plate (one mutant per well), followed by addition of rhodopsin and the light activation to form Rho\*-G<sub>i</sub>(Ala) complex at 4 °C. The reconstituted Rho\*-G<sub>i</sub>(Ala) complexes in the 96-well PCR plate were further heated in a PCR machine at 36.3 °C for 30 min. To analyze the stability of the mutant complexes, material from each Rho\*-G<sub>i</sub>(Ala) complex, both upon formation at 4 °C and after heating at 36.3 °C, were sequentially loaded onto the native PAGE and analyzed by the NPAGE method (Fig. 3.22b). Thus, each 15-well native PAGE can visualize seven Rho\*-G<sub>i</sub>(Ala) complexes (4°C and 36.3°C for each) (Fig.3.22b). Practically, 24 Rho\*-G<sub>i</sub>(Ala) complexes can be simultaneously visualized in the developed HTP NPAGE assay and 48 Rho\*-G<sub>i</sub>(Ala) complexes can be possibly measured per day.

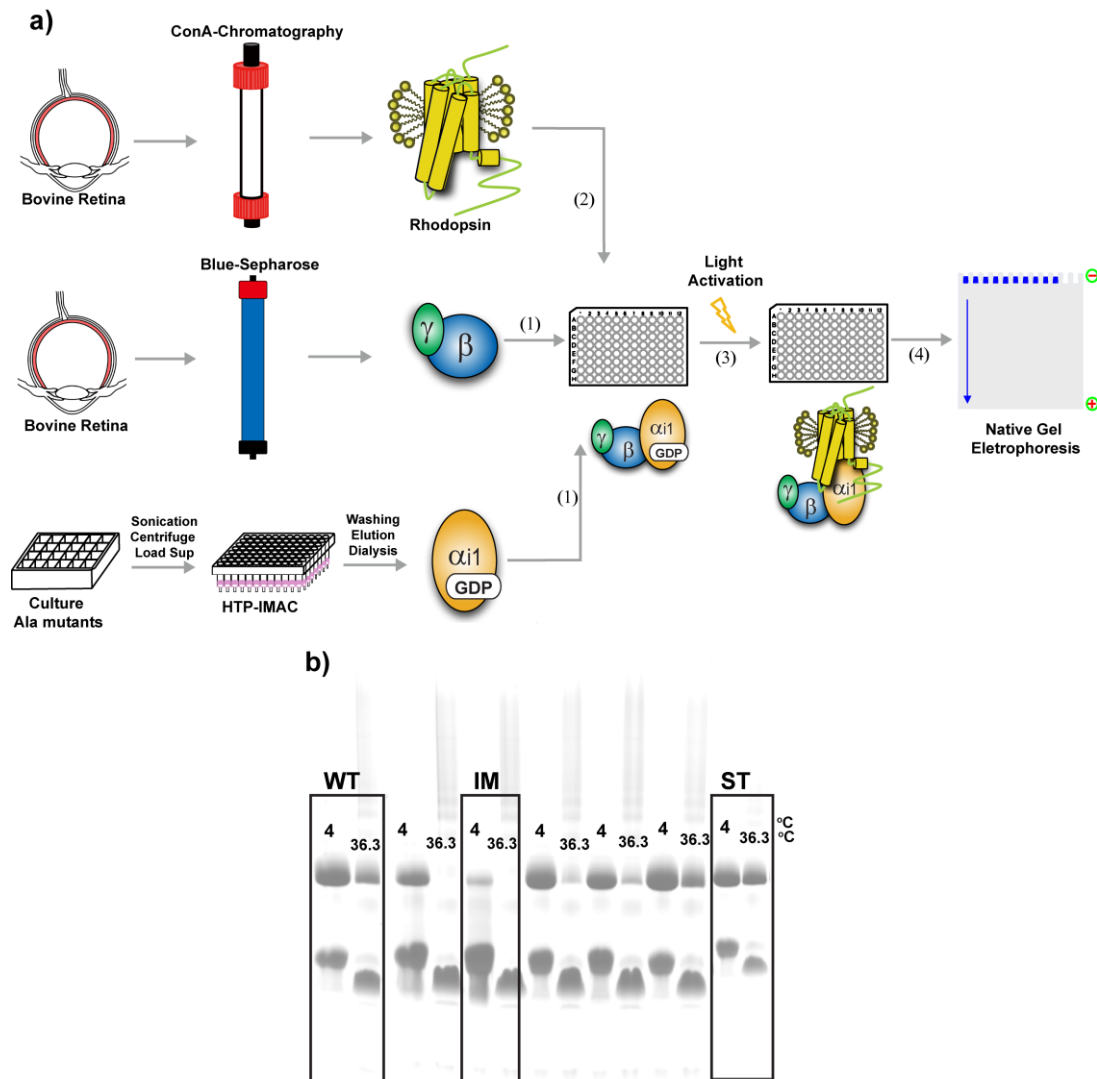


**Fig. 3.22. HTP NPAGE assay for monitoring effect of G $\alpha_{i1}$  alanine mutants on Rho\*-G $_i$  complex. a,** Flowchart of HTP NPAGE assay. **b,** The typical result from HTP NPAGE assay. Each R\*-G $_i$ (Ala) complex after incubation at 4 °C and 36.3 °C were loaded to the native PAGE. The results provided by HTP NPAGE assay can clearly display which alanine mutant is impaired in formation of complex (IM) or stabilizes the complex (ST).



### 3.4.6 Characterization of effects of alanine substitutions in $G\alpha_{i1}$ on receptor-bound state by HTP NPAGE assay

By utilizing the developed HTP NPAGE assay, the complex formation efficiency and complex stability (*see* Materials and methods) of each alanine mutant can be measured, compared, and visualized by mapping the change in complex formation efficiency ( $\Delta$ complex formation efficiency; *see* Materials and methods) and change in complex stability values ( $\Delta$ complex stability; *see* Materials and methods) to the modeled structure of the rhodopsin- $G_i$  complex (Fig. 3.23a-b).

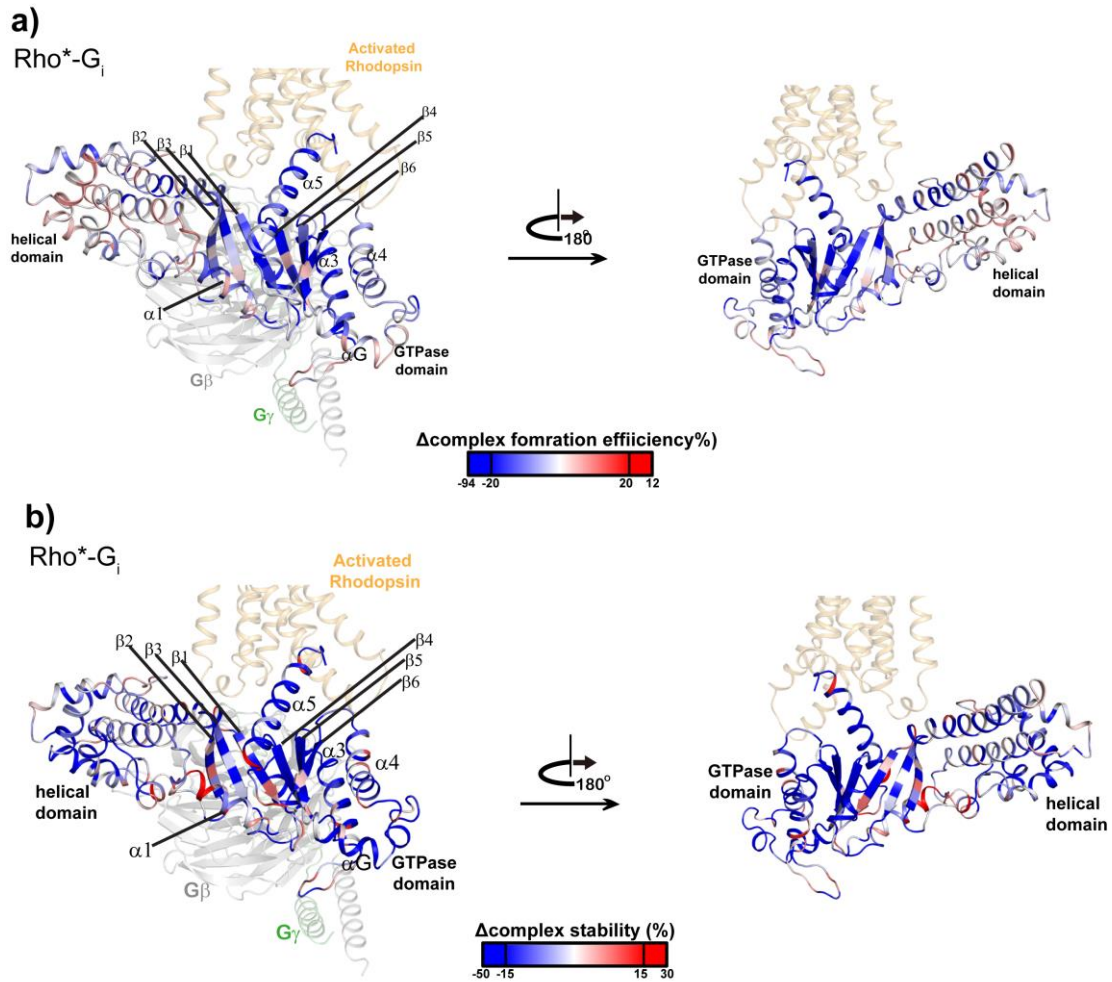


**Fig. 3.23. Characterization of effects of alanine substitutions in  $G\alpha_{i1}$  on receptor-bound state by HTP NPAGE assay. a-b,** Modeling structure of rhodopsin- $G_i$  complex mapped with  $\Delta$ complex formation efficiency (**a**) and  $\Delta$ complex stability values (**b**) of each alanine mutant in the  $G\alpha_{i1}$  subunit. Blue: destabilizing effect by the alanine replacement; red: stabilizing effect by the alanine replacement.

About 73% of  $G\alpha_{i1}$  alanine mutants leave the  $\Delta$ complex formation efficiency value unchanged (between  $\pm 10\%$  of WT level) (Fig. 3.24a). The alanine mutants with less than 20% of WT level are regarded to obviously perturb the complex formation. These mutations are mainly located in the N-terminus,  $\alpha 5$ , and  $\beta$ -sheet network of the GTPase domain of  $G\alpha_{i1}$ , rather than in the helical domain (Fig. 3.23a). As for the distribution of  $\Delta$ complex stability value, about 48% of alanine mutants shows a destabilization of the Rho\*- $G_i$  complex with more than 10% decrease relative to WT level (Fig. 3.24b). These mutants are mainly composed of hydrophobic residues, and sparsely located polar and

charged residues, widely spread throughout the whole G protein alpha subunit (Fig. 3.23b). The top 10 of best alanine mutants with more than 10% increment in complex stability are mainly located in the C-terminus of the  $\alpha 1$ -helix and N-terminus of the  $\alpha 5$ -helix (Fig. 3.23b and Fig. 3.24 c-d).

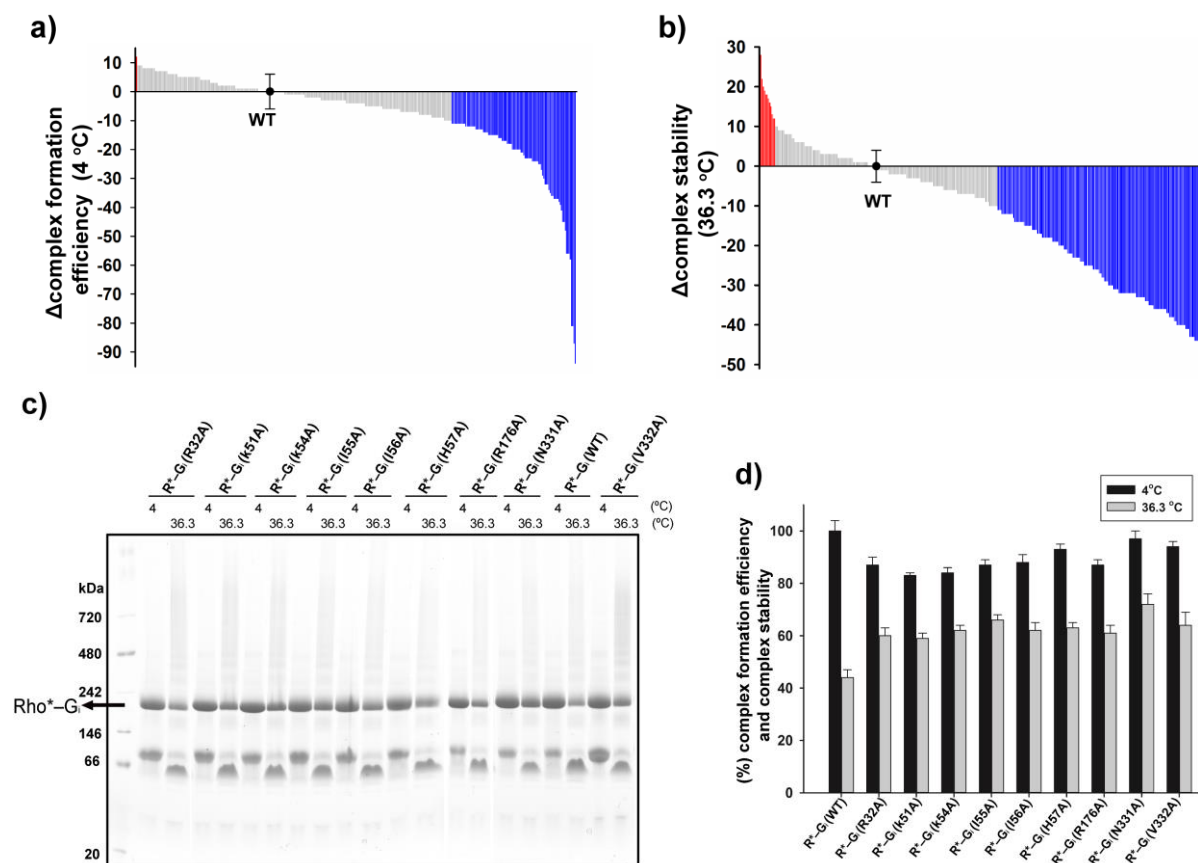


**Fig. 3.24. Distribution of effect on stability and complex formation of  $G\alpha_{11}$  alanine mutants in the receptor-bound state.** a-b, Distribution of  $\Delta$ complex formation efficiency (a) and  $\Delta$ complex stability values (b) of each alanine mutant. c-d, Top 10 of  $G\alpha_{11}$  alanine mutants showing dramatic stabilization in Rho\*- $G_i$  complex were visualized by the native PAGE (c) and compared (d).

### 3.4.7 Characterization of inefficiently coupling alanine mutants in heterotrimer formation

To further exclude the possibility that the inefficient Rho\*-G protein formation may be caused by the insufficient reconstitution of heterotrimer, 48 of the  $G\alpha_{11}$  alanine mutants with the worst complex formation efficiency (less than 20% of complex formation efficiency of WT level) were reconstituted with  $\beta\gamma$  subunit and the formed heterotrimers were examined by FSEC method. Thirteen of the 48 worst coupling  $G\alpha_{11}$  alanine mutants show inefficient heterotrimer reconstitution by FSEC (Fig. 3.25c-d). These mutations were found to be located either in the  $\beta\gamma$  binding interface of  $G\alpha_{11}$  subunit (I19A, S16A, D20A, L23A, K210A, W211), or the nucleotide-binding pocket (G45A, N269A). Some mutants appeared to be not well-folded (I221A, F250A, F259A, F307A, and C351A) as suggested by thermal shift assay. F267A, F336A, and V342A show the oligomer state after reconstituting with  $\beta\gamma$  subunit (Fig. 3.25e-f), while they still shows ability to form Rho\*- $G_i$  complex with 62-82% of WT



level (Table. S1). The remaining of the 48 worst-coupling alanine mutants shows comparable ability to form heterotrimer relative to WT. (Fig. 3.25a-b).

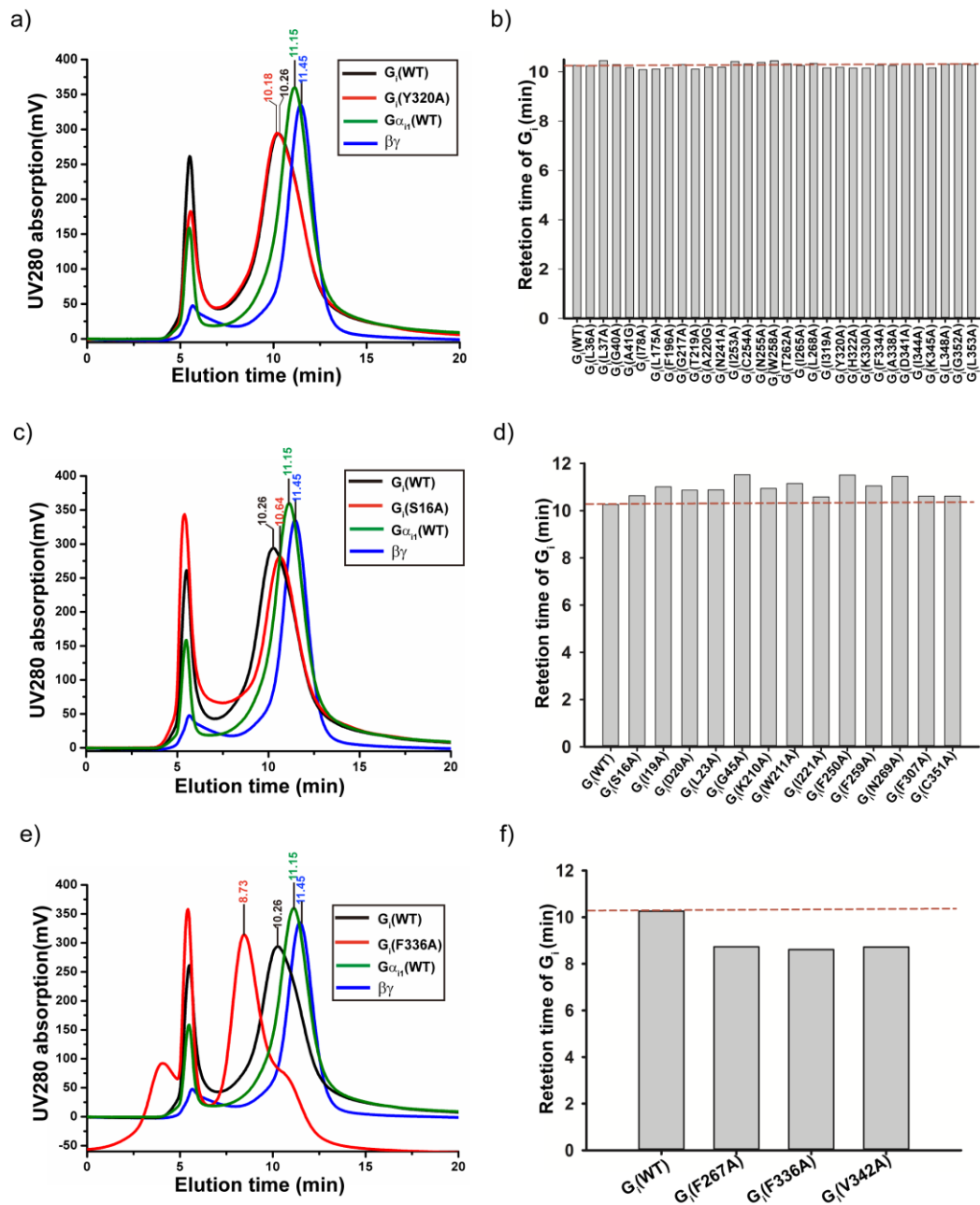


**Fig. 3.25.** Characterization of heterotrimer ( $G_i$ ) formation by FSEC. **a-f**, Characterization of heterotrimer reconstitution of lowest 48  $G\alpha_{i1}$  alanine mutants which were inefficient in formation of Rho\*- $G_i$  complex. The retention time of WT  $G\alpha_{i1}$ ,  $\beta\gamma$  subunit and reconstituted  $G_i$  are 11.15 min, 11.45 min and 10.26 min, respectively. **a-b**, Retention time of alanine mutants which are efficient in  $G_i$  reconstitution. **c-d**, Retention time of alanine mutants inefficient in formation of heterotrimer. **e-f**, Retention time of three alanine mutants forming the oligomer reconstitution.

## Chapter 4 Discussion

### 4.1 Interpretation of alanine scanning mutagenesis of $G\alpha_{i1}$

Mutation of an amino acid to alanine (or, to glycine, if the original amino acid is alanine) changes the stability of a protein or complex due to an alteration of the local structure caused by the removal of

the side chain. Importantly, this change in stability is sensitive to conformational changes. This strategy is the basis of phi-value analysis, a technique developed by Alan Fersht and his colleagues to study energetic and structural details of protein folding intermediates[116]. Here I have adapted this method to study conformational changes of  $G_i$  in the Rho\*- $G_i$  complex relative to  $G_i$  in the GDP bound state, which I used as a reference state.

I found that many mutations (30-50%) destabilize both GDP-bound  $G_{\alpha_{i1}}$  and the Rho\*- $G_i$  complex. These residues are important for the stability and integrity of the protein, and are located in the regions with the same local environment (i.e. conformation) in both states. However, mutations at several positions had different effects on GDP-bound  $G_{\alpha_{i1}}$  and the Rho\*- $G_i$  complex, indicating that they are in regions that undergo conformational changes. This way, I have been able to identify positions that contribute specifically to the stability of  $G_{\alpha_{i1}}$  in each conformation. Additionally, a large effect of the mutation on stability suggests that the side chain was involved in local interactions, indicating a structured environment. Conversely, a small change in stability implies that the side chain is not involved in local interactions. Thus, if several residues in a stretch do not affect the stability, this region is likely to be unstructured. These simple considerations are the basis for interpreting the measured stability changes in structural terms.

#### **4.2 Definition and description of stabilization clusters**

The stabilization cluster is composed of residues that are classified by consideration of both the thermostability effect of the alanine substitution and the orientation of the sidechain. Principally, the sidechains of residues grouped in the stabilization cluster should be spatially proximate to each other. The alanine substitution of residues should have a significant effect on the stability of one or more states, as defined by applying a  $2\sigma$  threshold, i.e. 2 °C below the  $T_m$  of WT  $G_{\alpha_{i1}}$  in nucleotide-bound state or 10% less than the stability of the Rho\*- $G_i$ (WT) complex. Based on these two principles, four stabilization clusters are observed: two in the GTPase domain, one in the helical domain, and one at the interface of the GTPase and helical domains (Fig. 4.1). Stabilization cluster I, in the GTPase domain, is composed of residues from strands  $\beta 1-6$  and helices  $\alpha 1$  and  $\alpha 5$ . Stabilization cluster II, also in the GTPase domain, is composed of residues from strands  $\beta 3-5$ , and helices  $\alpha 4$ ,  $\alpha 5$ , and  $\alpha G$ . Stabilization cluster III is constituted of residues from the helical domain. The fourth inter-domain interface stabilization cluster is comprised of residues located between the GTPase domain and the helical domain. The residues in stabilization cluster I can be classified into three types of residues: alanine substitution destabilizing the nucleotide-bound state but not receptor-bound state; alanine substitution destabilizing the receptor-bound state but not nucleotide-bound state; alanine substitution destabilizing both nucleotide-bound and receptor-bound state. For stabilization clusters II and III, the residues are primarily composed by hydrophobic amino acids, and alanine substitution of most of these positions shows destabilization of both the nucleotide-bound and the receptor-bound states. In

the inter-domain interface stabilization cluster, alanine substitutions mostly destabilize the nucleotide-bound state, while stabilizing the receptor-bound state.

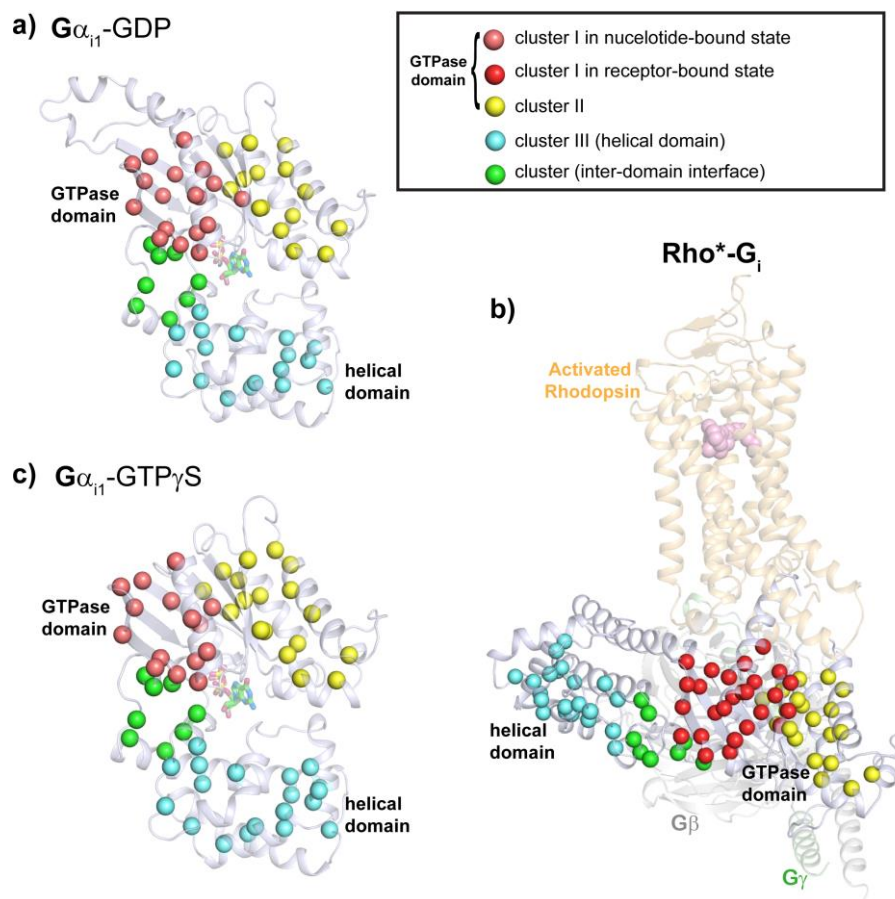


**Fig. 4.1. The observed stabilization clusters in  $G\alpha_{i1}$  subunit. a-c,** Stabilization cluster in the GTPase and helical domains and the inter-domain interface in the GDP, GTP $\gamma$ S and receptor-bound states.

### 4.3 Critical role of N- and C-terminus of $G\alpha_{i1}$ in receptor-mediated response

The N-terminus provides an excellent benchmark for the performance of my method. Mutation of positions 1 to 32 has very little impact on the stability of  $G\alpha_{i1}$  alone, suggesting that this region is unstructured in the absence of the  $G\beta\gamma$  subunit. However, mutation of the residues in the N-terminus that form the interface with  $G\beta\gamma$  in the G protein trimer has a severe impact on the  $Rho^*-G_i$  complex stability, while mutation of the residues facing the solvent do not have such an effect (Table. S1).

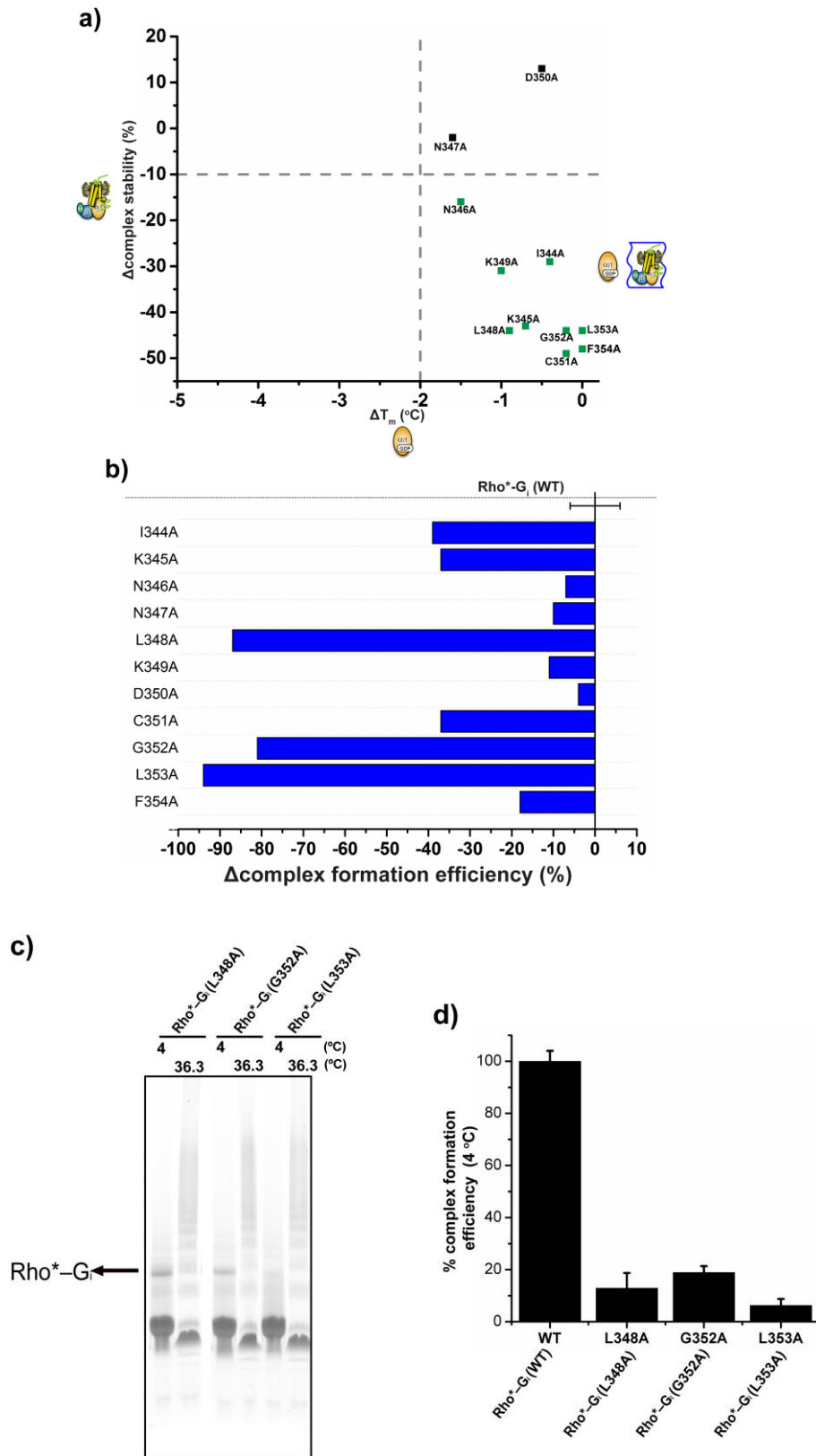


**Fig. 4.2. Effect on nucleotide-bound and receptor-bound states by alanine replacement of the last 11 amino acid of  $G\alpha_{i1}$ .** **a-b**, Thermal stability effect on GDP-bound and receptor-bound state (**a**), and effect on  $Rho^*-G_i$  complex formation (**b**) by alanine mutation of the last 11 residues of C-terminus of  $G\alpha_{i1}$ . The blue wave represents the destabilization effect on one or both states by alanine substitution. The decrease in  $\Delta$ complex formation efficiency is coloured in blue. **c-d**, L328A, G353A and L353A are impaired in complex formation.  $Rho^*-G_i$  complex was visualized by the native PAGE (**c**) and compared (**d**).

Numerous studies have shown that the last eleven residues in the C-terminus of  $G\alpha$  play a critical role in recognizing the receptor [33, 34, 117, 118]. My results are in agreement with these data, showing that most alanine mutations at positions 344-354 significantly affect the formation of the Rho\*- $G_i$  complex (Fig. 4.2b). Particularly, substitution of the conserved L348 and L353 and the less conserved G352 at the end of the C-terminus severely impair coupling with the receptor without affecting the stability of the nucleotide bound states (Fig. 4.2a-d). These data also agree with NMR and crystallographic studies of a  $G_t$  C-terminal peptide bound to rhodopsin and with the crystal structure of the  $\beta_2AR$ - $G_s$  complex, which shows that the C-terminus of  $G\alpha_s$  becomes helical and penetrates into a crevice formed in the cytoplasmic side of the transmembrane bundle upon receptor activation [39, 40, 48, 119]. Interestingly, D350A and N347A did not affect the formation and stability of the Rho\*- $G_i$  complex (Fig. 4.2a-b), showing that not all amino acids in the C-terminus are required for efficient coupling to the receptor. Finally, the absence of a destabilizing effect upon mutating positions 344-354 in the nucleotide bound states strongly suggests that this region is unstructured in the absence of the receptor.

#### **4.4 Receptor coupling rearranges stabilization cluster I in the GTPase domain**

The movement of helix  $\alpha 5$  in the GTPase domain upon formation of the complex [44, 48, 120] results in significant conformational changes around its base, which is packed against the  $\beta$  sheet consisting of strands  $\beta 1$ - $\beta 6$ , and helix  $\alpha 1$ . My data are in agreement with such rearrangement, as shown by the different effect of mutations on the nucleotide bound state and on the complex (Fig. 4.3a). Importantly, my analysis allows me to focus on the individual contribution of each amino acid of this entire region to the stability of the different  $G\alpha_{i1}$  states. This allowed me to detect a number of residues with a concerted role, which I termed as stabilization cluster I, formed by several highly conserved hydrophobic residues from  $\beta 1$ -3 strands, helix  $\alpha 1$  and inward-facing residues of helix  $\alpha 5$ , whose side chains are proximal to each other. In the nucleotide-bound state of  $G\alpha_{i1}$ , cluster I is stabilized by tight hydrophobic packing. Alanine substitution of these residues significantly destabilizes the GDP-bound conformation (3-18 °C) and moderately affects the GTP $\gamma$ S-bound state (1-5 °C) (Fig. 4.3a-b and Table. S1). Especially, mutation of F336 (universally conserved in  $G\alpha$  subfamilies; *see* submitted paper by Flock et al[121]) in helix  $\alpha 5$  is the only substitution that results in a complete impairment of  $G\alpha_{i1}$  stability and of its ability to bind nucleotides (Fig. 4.3a and d). F336A also causes a severe impairment in reconstitution of  $G\alpha_{i1}$  with  $G\beta\gamma$  to form the G protein heterotrimer (Fig. 3.25c). Despite these severe effects on  $G\alpha_{i1}$ , this mutant still forms a relatively stable complex with the receptor (Table. S1). In the structure of the  $\beta_2AR$ - $G_s$  complex, the corresponding phenylalanine has moved from the buried hydrophobic core of  $G\alpha_s$  to contact ICL2 of the receptor [48]. This suggests that F336 plays a critical role in stabilizing the  $G\alpha_{i1}$  subunit in the nucleotide-bound conformation, consistent with the observation that its mutation increases the rate of spontaneous nucleotide release [71]. I

hypothesize that relocation of F336 concomitant with the upward movement and twist of  $\alpha 5$  triggers the reorganization of the cluster I into the receptor-bound state.

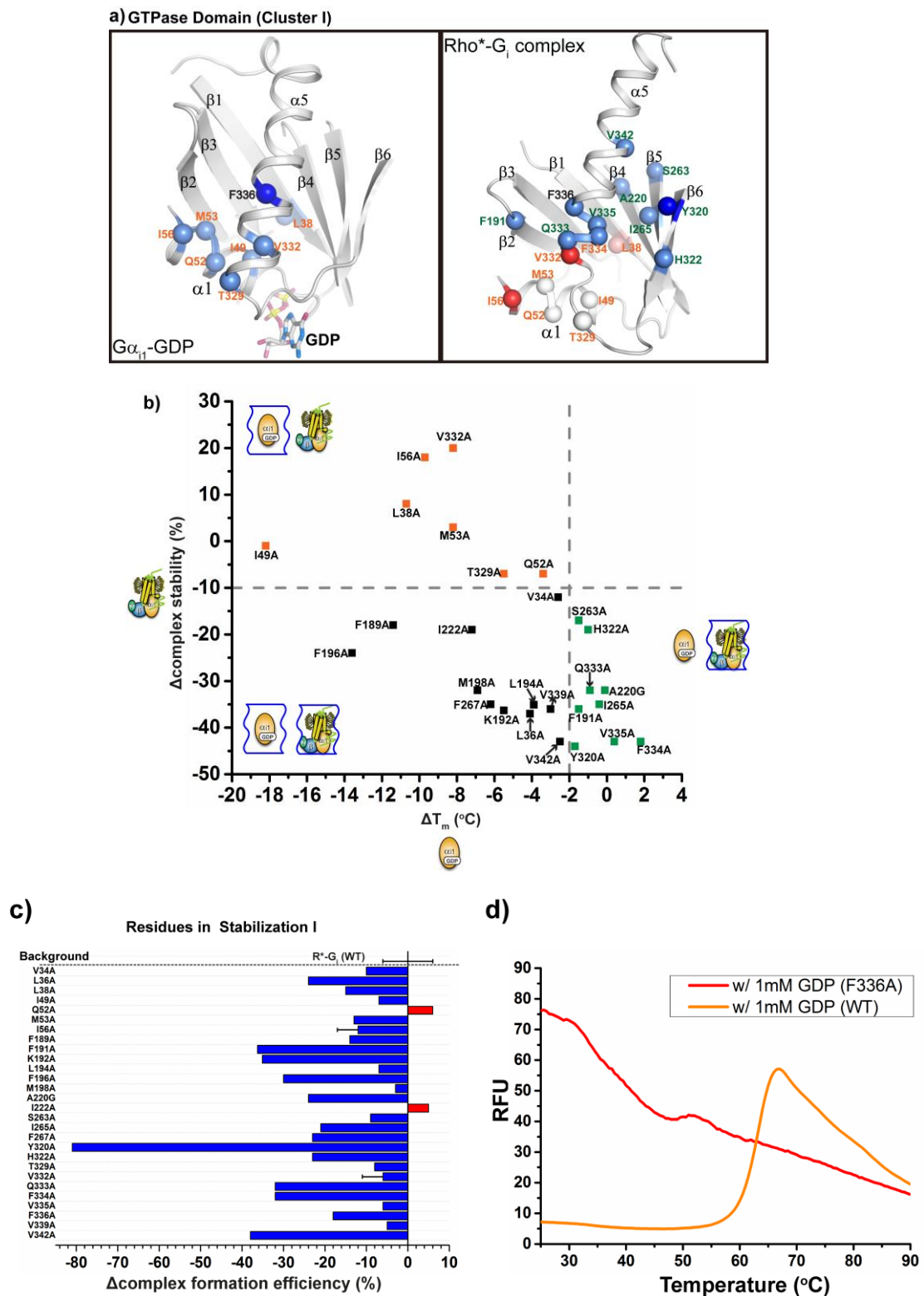


**Fig. 4.3. Stabilization clusters I in GTPase domain.** **a**, Close-up view of stabilization cluster I of GTPase domain in GDP-bound and receptor-bound states. **b-c**, Stability effect on GDP-bound and receptor-bound state (**b**), and effect on Rho\*-G<sub>i</sub> complex formation (**c**) by alanine mutation of residues involved in stabilization cluster I. The blue wave represents the destabilization effect on one or both states by alanine substitution. The increase in  $\Delta$ complex formation efficiency is coloured in red and the decrease is coloured in blue. **d**, Thermal shift assay of F336A.

Upon coupling with the receptor, the structural reorganization of cluster I disrupts the interactions that stabilize helix  $\alpha 1$  (Fig. 4.3a). This is suggested by the fact that mutation of residues I49, M53, and I56 in  $\alpha 1$ , L38 of  $\beta 1$ , T329 and V332 of  $\alpha 5$ , which tether helix  $\alpha 1$  in the  $G\alpha_{i1}$ -GDP state, severely impair its stability, but does not affect the stability of Rho\*-G<sub>i</sub> complex (Fig. 4.3a-b, and Table. S1). Moreover, mutation of the conserved N331 and V332 in helix  $\alpha 5$  increases the stability of the complex by 30% and 20%, respectively (Fig. 3.24c-d, 4.3a-b, and Table. S1). N331 and V332 stabilize the nucleotide bound state by making connections to the helix  $\alpha 1$ . Thus, its mutation destabilizes the nucleotide bound state and stabilizes the receptor bound state. Relocation of these residues results in the disruption of contacts between the base of helix  $\alpha 5$  and helix  $\alpha 1$ , which would lead to the loss of helicity at the base of helix  $\alpha 5$  observed in the  $\beta_2$ AR-G<sub>s</sub> complex. This order-to-disorder transition potentially increases the flexibility of the loop S6- $\alpha 5$ , which contains the guanine-binding TCAT motif, thus perturbing its interaction with GDP.

The loss of local structural stability associated with the disordered C-terminus of helix  $\alpha 1$  and the N-terminus of helix  $\alpha 5$  is compensated by the strengthening of their interactions with the  $\beta 4$ ,  $\beta 5$  and  $\beta 6$  strands and the relocated helix  $\alpha 5$ . This is suggested by the fact that mutation of A220 of  $\beta 4$ , S263 and I265 of  $\beta 5$ , Y320 and H322 of  $\beta 6$ , Q333, F334, V335, and V342 of  $\alpha 5$  dramatically destabilize the Rho\*-G<sub>i</sub> complex (20-50%) without affecting the stability of nucleotide-bound state (Fig. 4.3a-b, and Table. S1). Additionally, many of these mutants show competent heterotrimer reconstitution, while the efficiency in forming the Rho\*-G<sub>i</sub> complex is reduced by 20-80% (Fig. 3.25a-b and Table. S1). Interestingly, a sequence alignment of human G proteins shows that these residues are highly conserved in the G $\alpha$  subfamily (Fig. 2.2; *see* submitted paper by Flock et al[121]). Taken together, this indicates that these residues are not only important for stabilizing the G protein conformation in the receptor-bound state, but also crucial for allosteric regulation of receptor-mediated G protein activation.

#### **4.5 Y320 in cluster I as the signal transduction hub**

Alanine substitution of Y320 in the  $\beta 5$  strand, which is a tyrosine or phenylalanine in G $\alpha$  subfamilies, severely impairs the Rho\*-G<sub>i</sub> complex formation (Fig. 4.4a-b, *see* submitted manuscript Flock et al[121]) while having only a very moderate effect on the nucleotide bound states. Remarkably, Y320A, L348A, G352A and L353A have a similarly strong impact on the formation of the complex (Fig. 4.2c-d and 4.4a-b), but Y320 is the only position which does not interact directly with the receptor (Fig. 4.3a). Also, Y320A shows a well-preserved ability to bind nucleotides and form the heterotrimer (Fig. 3.25a). I hypothesize that mutation of Y320 prevents the formation of an allosteric activation pathway that propagates the signal for GDP release transmitted from the receptor, making Y320 a key signal transduction hub in the mechanism of receptor-mediated G protein activation.

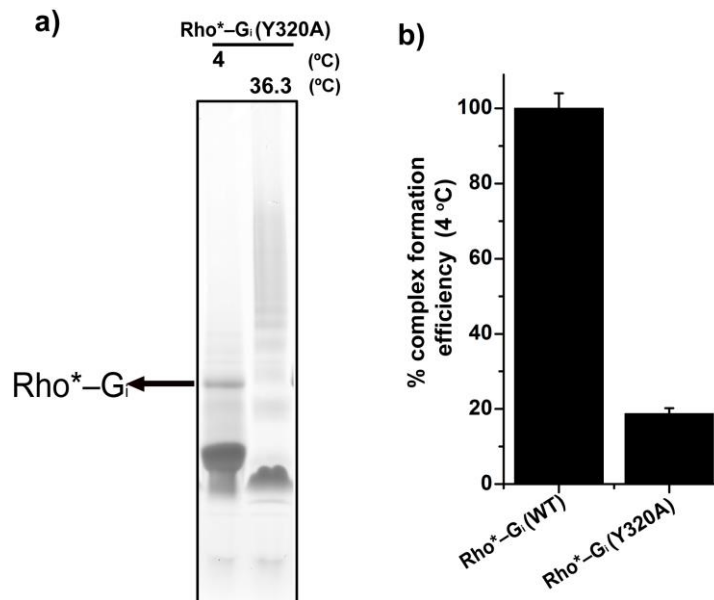


**Fig. 4.4. Y320A impairing in complex formation.** a-b, Rho\*-G<sub>i</sub> complex was visualized by the native PAGE (a) and compared (b).

#### 4.6 The hydrophobic stabilization cluster II in GTPase domain

I have identified a second cluster of residues with a common role in the GTPase domain, which partially overlaps with cluster I and is formed by residues in helices  $\alpha_3$ ,  $\alpha_4$  and  $\alpha_G$  packed against residues in strands  $\beta_4$ ,  $\beta_5$  and  $\beta_6$  (Fig. 4.5a). In contrast to cluster I, most mutations in cluster II destabilize both receptor- and nucleotide-bound states of G $\alpha_{i1}$ . I observed that most mutations destabilize the GDP-bound state by 3-13 °C, the receptor-bound state by 30-40%, and moderately destabilize the GTP $\gamma$ S-bound state by 1-5 °C (Fig. 4.5b and Table. S1). Cluster II is highly conserved among G proteins, and likely forms the structural scaffold of the G $\alpha$  subunit (Fig. 2.2, *see* submitted paper by Flock et al [121]). It should be noted that mutation of residues I221 of  $\beta_4$ , T321 of  $\beta_6$ , M247 and I253 of  $\alpha_3$ , I264, N311 and I319 of  $\alpha_4/\beta_6$  dramatically destabilize Rho\*-G<sub>i</sub> complex without significantly affecting the stability of the GDP-bound state (Fig. 4.5a-b). Mutation of K248 and D251 of  $\alpha_3$  which are located in solvent-exposed surface, also show similar effect (Table. S1). I hypothesize that these residues may form additional stabilizing contacts in the receptor-bound conformation, or are involved in direct interactions with the receptor.



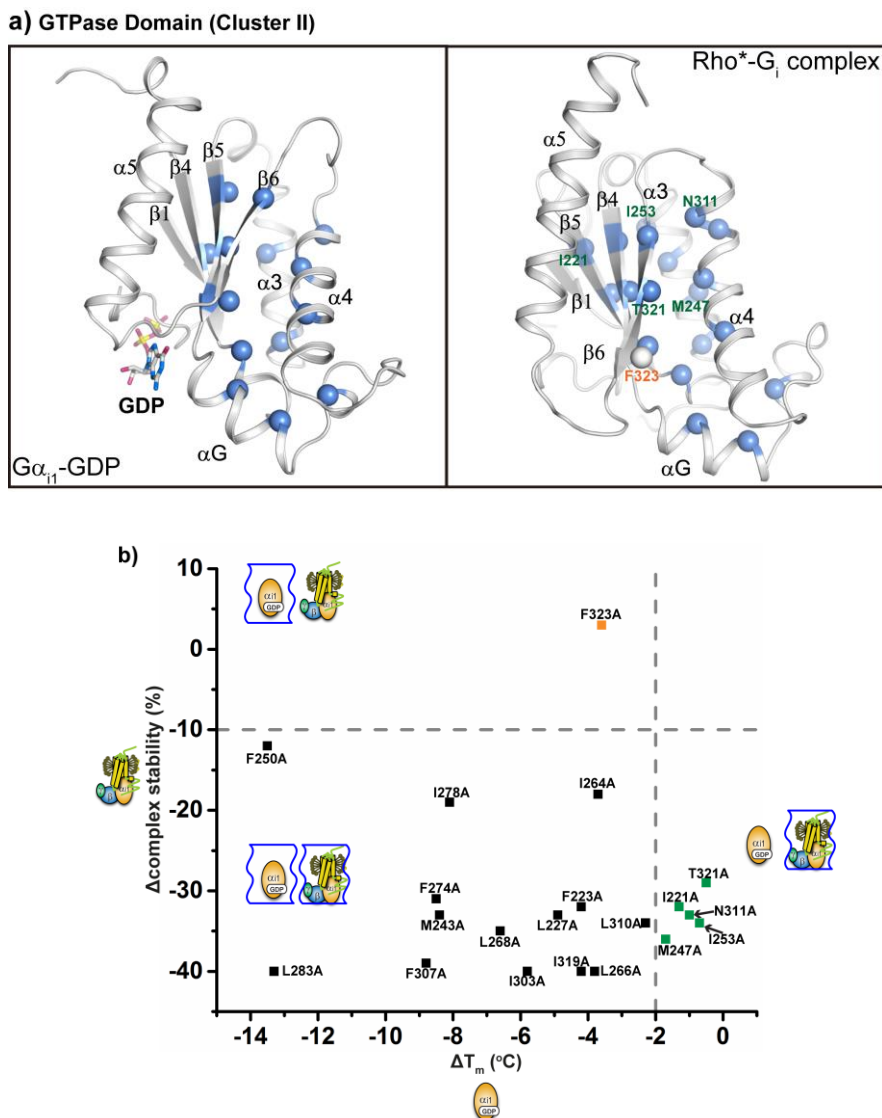


**Fig. 4.5. Stabilization clusters II in GTPase domain.** **a**, Close-up view of stabilization cluster II of the GTPase domain in GDP-bound and receptor-bound states. **b**, Stability effect of alanine mutation of residues involved in stabilization of cluster II on GDP-bound and receptor-bound states. The blue wavy box represents the destabilization effect on one or both states by alanine substitution.

#### 4.7 Hydrophobic packing allows the helical domain to behave as a rigid body and adopt multiple conformations relative to the GTPase domain

A hallmark of G protein activation by the receptor is the release of GDP accompanied by the separation of the GTPase and helical domains. The helical domain consequently displays dynamic equilibrium between multiple conformations relative to the GTPase domain [48, 52, 54, 122]. My data show that a cluster of mostly hydrophobic residues (63-176) of  $G\alpha_{i1}$  stabilizes the helical domain (Fig. 4.6a-b and Table. S1). In contrast to the stabilizing clusters in the GTPase domain, where most mutants affect both the stability and formation of  $Rho^*-G_i$  complex, mutations in the stabilizing cluster III of the helical domain do not affect the formation of the  $Rho^*-G_i$  complex (Fig. 3.23a and Table. S1). The sequence alignment shows that hydrophobic residues are preferred at these positions

in all  $G\alpha$  subtypes (Fig. 2.2). This is consistent with the observation that the helical domain can be expressed independently from the GTPase domain while retaining its ability to activate cGMP phosphodiesterase [123].

However, there are some exceptions. Mutation of A138, L156, L159, R161 and I162 destabilize the  $Rho^*-G_i$  complex, without affecting the stability of GDP- and GTP-bound states (Fig. 4.6a-b and Table. S1). Also, I78A reduces complex formation by 20% and L175A both destabilize GDP-bound state and reduces complex formation (Table. S1). This suggest that subtle internal rearrangements of the helical domain are required to keep its integrity in the  $Rho^*-G_i$  complex.

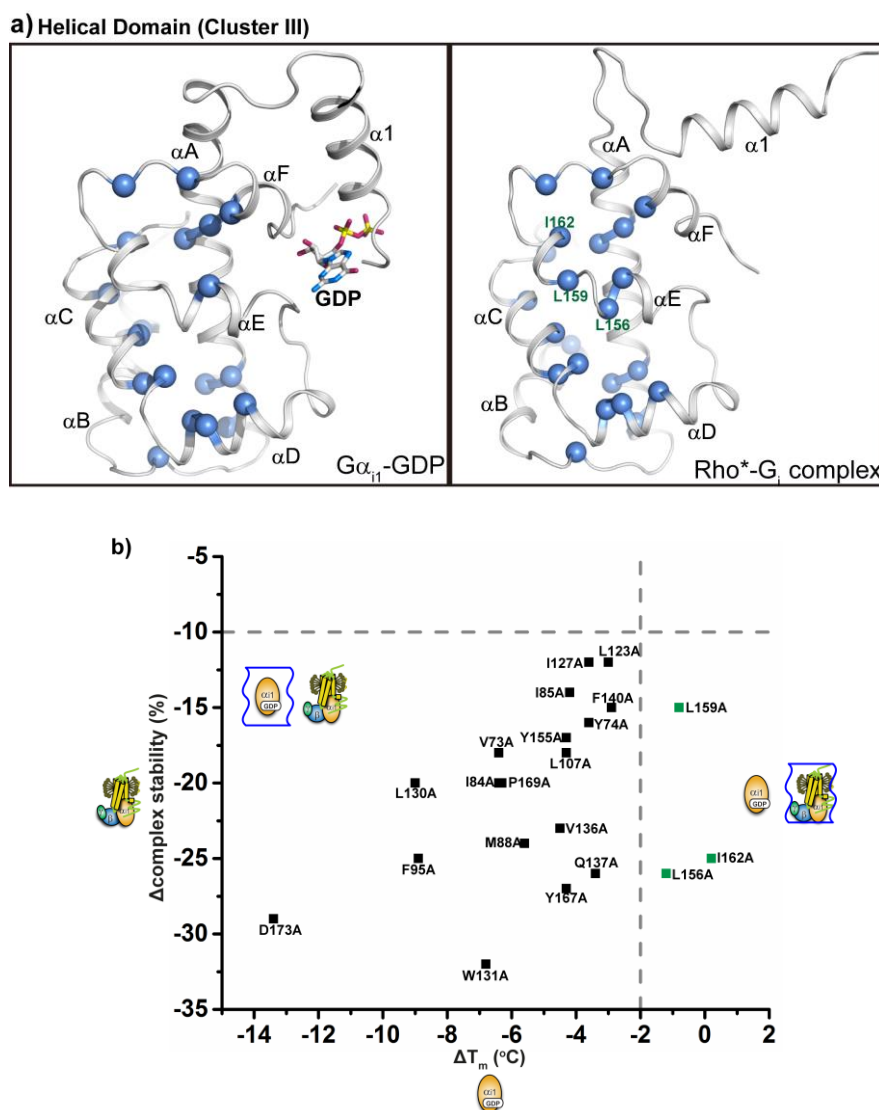


**Fig. 4.6. Stabilization clusters III in helical domain.** **a**, Close-up view of stabilization cluster III of helical domain in GDP-bound and receptor-bound states. **b**, Stability effect of alanine mutation of residues involved in stabilization cluster III on GDP-bound and receptor-bound state. The blue wavy box represents the destabilization effect on one of both states by alanine substitution.

#### 4.8 Perturbation of the inter-domain interface facilitates domain separation and GDP release

The inter-domain interface in  $G\alpha_{i1}$  is composed by the N-terminal part of helices  $\alpha A$ ,  $\alpha F$ ,  $\alpha 1$  and loop of  $\alpha F/\alpha 1$ . Mutation of the residues in this interface dramatically destabilizes the GDP-bound state (5-14 °C), but does not destabilize the Rho\*- $G_i$  complex. In fact, mutations K51A, K54A and I55A increase the relative stability of Rho\*- $G_i$  complex by 15-20% (Fig. 4.7a-b and Table. S1). A similar scenario is also observed for L175A and R176A, which increase complex stability by 9% and 17%, respectively (Fig. 4.7a-b and Table. S1). The sequence alignment shows that the residues located in the inter-domain interface of  $G\alpha_{i1}$  are highly conserved in all  $G\alpha$  subfamilies (Fig. 2.2; *see also* Flock et al[121]). My data suggest that subtle conformational perturbations in the inter-domain interface of GDP-bound state can facilitate the domain separation and the release of GDP, and support previous observations that the helical domain dissociates from the GTPase domain upon binding to the receptor [48, 54, 124].

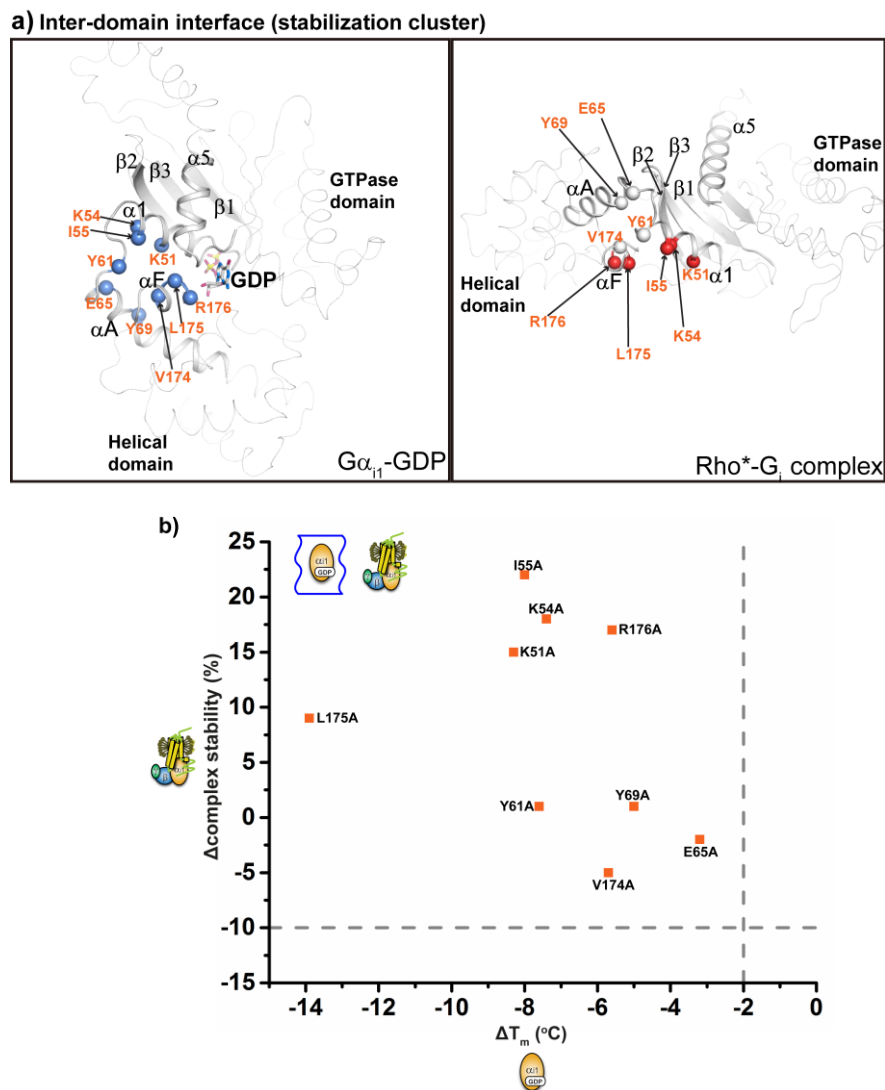


**Fig. 4.7. Stabilization cluster in the inter-domain interface.** **a**, Close-up view of stabilization cluster of the inter-domain interface in GDP-bound and receptor-bound states. **b**, Stability effect of alanine mutation of residues involved in the inter-domain interface on GDP-bound and receptor-bound state. The blue wavy box represents the destabilization effect on one or both states by alanine substitution.

The importance of weakening the inter-domain interface for G protein activation is further supported by the structure of the  $G\alpha_{i1}$  subunit from *Arabidopsis thaliana* (AtGPA1) [125, 126]. This protein shows a very similar structure with  $G\alpha_{i1}$  (RMSD of 1.8Å between backbone atoms). However, due to the absence of classical GPCRs in plants, AtGPA1 exchanges nucleotides by a self-activation mechanism attributed to the marginally stable helical domain, which shows a tendency to dissociate from the GTPases domain and unfold. Comparison between the  $G\alpha_{i1}$ -GDP and AtGPA1 structures shows that they contain similar residues at the inter-domain interface, whereas the cross-interface hydrogen bonds in AtGPA1 are weaker compared to those in  $G\alpha_{i1}$ -GDP (Fig. 4.8).

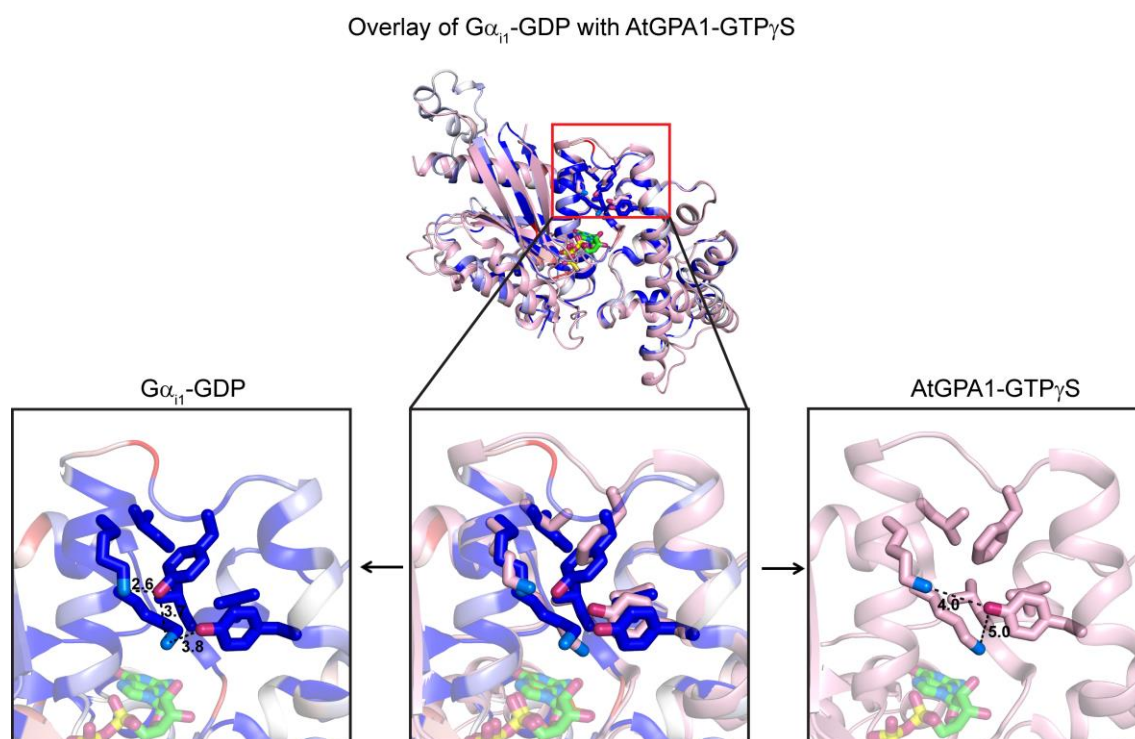


**Fig. 4.8. Structural overlay of  $G\alpha_{i1}$ -GDP with G protein  $\alpha$  subunit from the plant *Arabidopsis thaliana* (AtGPA1).** The crystal structure of GDP bound  $G\alpha_{i1}$ -GDP (PDB 1GDD) was mapped with the derived  $\Delta T_m$  of each residue as spectrum ranging from blue to white to red. The structure of AtGPA1-GTP $\gamma$ S (PDB 2XTZ) was coloured in light pink. The enlarged inter-domain interface shows that the inter-domain interaction in the AtGPA1-GTP $\gamma$ S state is much weaker compared to the  $G\alpha_{i1}$ -GDP state.

#### 4.9 Differences between GDP and GTP states

The GTP $\gamma$ S-bound state of  $G\alpha_{i1}$  is significantly more stable than the GDP bound state. The apparent melting temperatures were, 70 °C and 63 °C, respectively, at saturating concentrations of the corresponding nucleotides (Fig. 3.17e-f). In addition, GTP $\gamma$ S has a much higher affinity for  $G\alpha_{i1}$  compared to GDP, as judged by a significantly steeper concentration dependence of the stabilizing effect (Fig. 3.17a-d). I have observed that most mutations destabilize both GDP and GTP $\gamma$ S states, consistent with the relatively minor differences between the GDP- and GTP $\gamma$ S-bound crystallographic

structures of  $G\alpha_{i1}$  [127]. One interesting observation is that the  $GTP\gamma S$  bound state is on average two-fold less sensitive to mutations (Fig. 4.9a), again suggesting that this is a more stable state. Also, several mutations concentrated around the third phosphate group and at the  $G\beta\gamma$  interface have a disproportionately large effect on the  $GTP\gamma S$ -bound state (Fig. 4.9b).

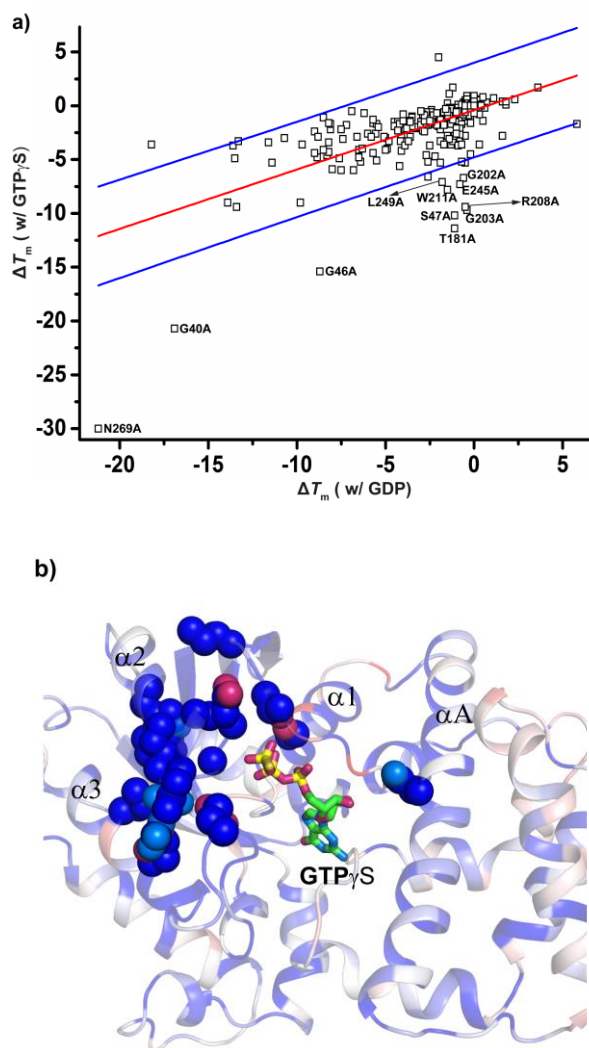


**Fig. 4.9. Mutations that affect GTP bound state cluster around the gamma phosphate of the  $GTP\gamma S$ .** Changes are plotted on pdb structure 1AS0. **a**, Correlation of the destabilization upon mutation. Red line shows linear correlation, blue lines indicate 95% confidence interval. The mutations that specifically affect GTP-bound state deviate from the correlation. The most destabilization residue is N269A involved in the nucleotide binding. **b**, A number of mutations are located near the gamma phosphate. In addition, the mutations in helix  $\alpha 2$  also specifically affect the GTP bound state, consistent with the conformational changes leading to the dissociation of the  $G\beta\gamma$  subunit.

#### 4.10 Nucleotide exchange in the $G\alpha_{i1}$ subunit mediated by the stabilization clusters

Based on observations, I provide one rational receptor-mediated nucleotide exchange in the  $G\alpha_{i1}$  subunit regulated by the observed stabilization clusters (Fig. 4.10). In the inactive state, the GDP-bound  $G\alpha_{i1}$  is stabilized by the observed stabilization clusters. Upon binding with the activated receptor,  $\alpha 5$ -helix in  $G\alpha$  subunit undergoes the movement of rotation and translation, which causes

the conformational changes of stabilization cluster I in GTPase domain, resulting in the disruption of interactions between  $\alpha 1$ -helix and GTPase domain and leading to an increase in the flexibility of the metastable  $\alpha 1$ -helix. As  $\alpha 1$ -helix has a central role in the inactive state in forming contacts to GDP and tethering the helical domain, the increase in flexibility of  $\alpha 1$ -helix causes the destabilization of the nucleotide binding pocket and facilitates the disruptions of the inter-domain interactions. The loss of integrity of the C-terminus of the  $\alpha 1$ -helix finally results in the release of GDP and opening of the helical domain. During the activation progress, the stabilization cluster II and III play the critical role in acting as structural scaffolds to maintain the integrity of GTPase and helical domains.

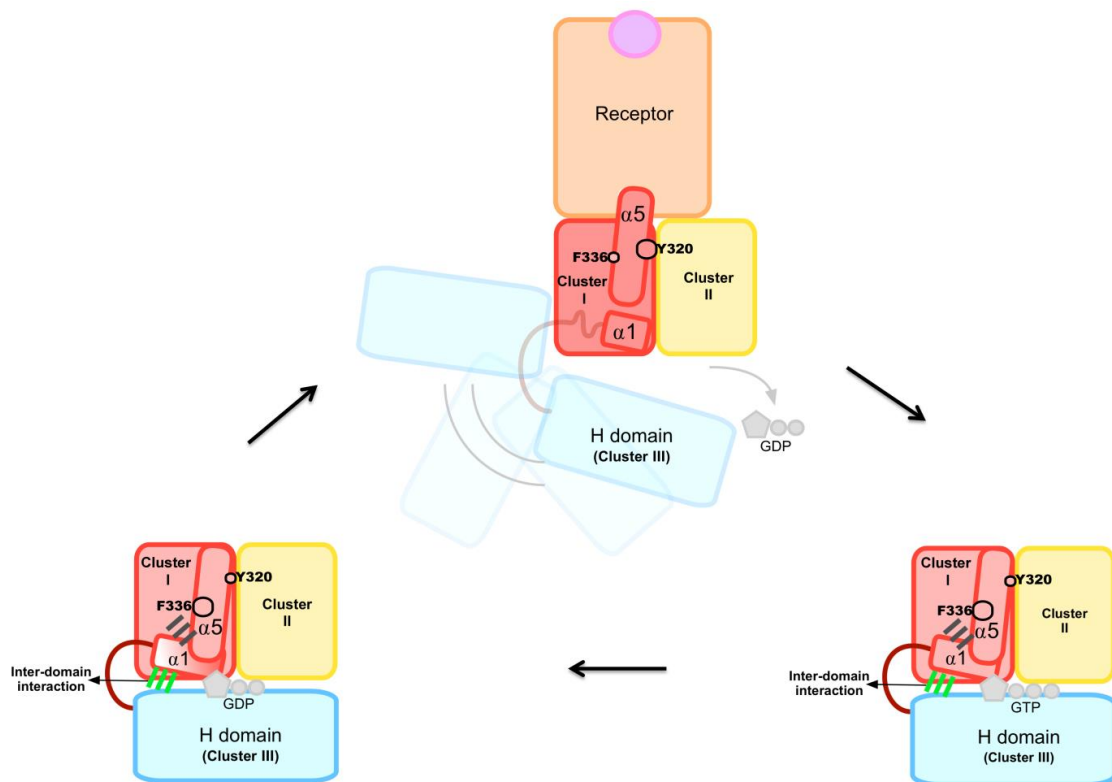


**Fig. 4.10. Nucleotide exchange in the  $G\alpha_1$  subunit mediated by the stabilization clusters.** Cluster I consists of helices  $\alpha 1$  and  $\alpha 5$  packed against strands  $\beta 1$ -3 in the nucleotide-bound states. In the receptor-bound state, these interactions are weakened and compensated by new interactions between helix  $\alpha 5$  and strands  $\beta 4$ -6. The most prominent examples of the residues involved in this rearrangement are Y320, which is crucial for the stabilization of the receptor bound state, and F336, important for the stability of the GDP and GTP bound states. Destabilization of helix  $\alpha 1$  results in weakening of the inter-domain

## Chapter 5 Conclusion and perspectives

To consolidate the existing knowledge and establish a detailed and comprehensive understanding of the G protein activation mechanism at the residue level, I have mutated each amino acid residue of  $G\alpha_{i1}$  to alanine or glycine and quantified efficiency of formation (relative abundance) and relative stability of the reconstituted rhodopsin- $G_i$  protein complex. In addition, I have studied the role of each amino acid of  $G\alpha_{i1}$  in the inactive GDP-bound state and the active GTP ( $GTP\gamma S$ )-bound state by measuring the thermal stability of each alanine mutant of  $G\alpha_{i1}$ . Comparison of the effect of each individual residue of  $G\alpha_{i1}$  on the receptor-bound complex and the GDP- and GTP-bound forms has allowed me to draw a functional map of the  $G\alpha_{i1}$  subunit stability and propose an activation mechanism at single amino acid resolution.

I have identified two clusters of residues that confer stability to the GTPase domain. Many mutations in cluster I preferentially affect either the nucleotide- or the receptor-bound state, and I have found several that stabilize the  $Rho^*-G_i$  complex. Cluster I consists of residues in helices  $\alpha 1$  and  $\alpha 5$  packed against residues in strands  $\beta 1-3$  in the nucleotide-bound states. In the receptor-bound state, the interactions between  $\alpha 5/\alpha 1$  and  $\beta 1-3$  are weakened and compensated by a new set of interactions between  $\alpha 5$  and strands  $\beta 4-6$ . The most prominent examples of residues involved in this rearrangement are Y320, which are crucial for the stabilization of the receptor-bound state but have no effect on the nucleotide bound state. Conversely, F336 is important for the stability of the GDP- and GTP-bound states, but plays little role in the stabilization of the  $Rho^*-G_i$  complex. Helix  $\alpha 1$  is likely to become mostly unstructured in the  $Rho^*-G_i$  complex, as judged by the absence of significant effect of mutations on complex stability. However, some mutations towards its C-terminus result in stabilization of the complex. The above-mentioned residues are just some of the most noticeable examples, but I have found a network of residues that contribute to the stabilization of these distinct conformational states. Cluster II includes residues in helices  $\alpha 3$ ,  $\alpha 4$  and  $\alpha G$  packed against residues in strands  $\beta 4$ ,  $\beta 5$  and  $\beta 6$ . The majority of mutations in this cluster similarly affect both states, and I conclude that this cluster provides a steady structural scaffold to the GTPase domain. As this cluster partially overlaps with cluster I, there were several mutations in strands  $\beta 4-6$ , such as I319, which preferentially affect the receptor-bound state.

A third cluster of residues maintains the structural integrity of the helical domain. Most mutations in this domain result in similar effects on the stability of the nucleotide-bound states or the  $Rho^*-G_i$  complex. Overall, these mutations were less detrimental to the stability than mutations in the GTPase domain. Several mutations, mostly located in helix  $\alpha H$ , destabilize the complex without affecting either the GDP- or the GTP-bound state. This suggests that the region of the helical domain around  $\alpha H$  undergoes some conformational changes. Mutations in the inter-domain interface between the



GTPase and the helical domains, consisting of  $\alpha A$ ,  $\alpha F$ ,  $\alpha 1$  and loop of  $\alpha F/\alpha 1$ , dramatically destabilize nucleotide-bound states but do not affect, and some even stabilize, the complex.

Overall, these data suggest that the most significant event in activation of  $G\alpha_{i1}$  is the destabilization of helix  $\alpha 1$  caused by a rearrangement on the stabilization cluster I. This leads to a perturbation and weakening of the inter-domain interface, dissociation of the helical domain from the GTPase domain in a rigid body movement, and release of the GDP.

How can binding of GTP trigger dissociation of the complex? It is likely that the answer may be found in the analysis of the relative stability of the GDP-, GTP- and receptor bound states. The GTP-bound state of  $G\alpha_{i1}$  is thermodynamically the most stable state of the protein, as reflected by the significantly higher thermal stability of the GTP $\gamma$ S-bound state. Due to GTP hydrolysis, the G protein is kinetically trapped in a less stable GDP-bound state. This is a meta-stable state because the nucleotide exchange rate is very low in the absence of the receptor, consistent with proposed role of the helical domain to protect the GDP from exchange with GTP[128] readily available in the cytoplasm. As the complex is formed and the nucleotide binding site becomes accessible, the additional stabilization by GTP overcomes the stability of the complex, leads to the stabilization of the helix  $\alpha 1$ , the inter-domain interface and re

verts the helix  $\alpha 5$  to its conformation in the nucleotide bound state.

It is still an open question to what extent my findings can be generalized to other GPCR-G protein combinations and which aspects are specific to the  $G\alpha_{i1}$  or the Rho\*- $G_i$  complex, although in the submitted manuscript by Flock et al.[121] we show that many of the residues identified here may play similar roles in all G proteins. Thus, more efforts are still required to provide additional constraints to refine and extend my observations made in rhodopsin- $G_i$  model system. The investigation of other GPCR-G protein systems by transferring my findings and developed HTP assay methods, as well as the elucidation of crystal structure of rhodopsin- $G_i$  and other GPCR- $G_i$  complex, will be the next research goal in my lab.



Mutants	G $\alpha_{11}$ -GDP				G $\alpha_{11}$ -GTP $\gamma$ S				Rho*-G $\gamma$ complex		Remarks
	T $_m$ (°C)	SD	$\Delta T_m$ (°C)	SD	T $_m$ (°C)	SD	$\Delta T_m$ (°C)	SD	Acomplex formation efficiency (%)	Acomplex stability (%)	
M1A	63.5	0.1	-0.2	0.5	70.2	0.1	-0.3	0.4	5	3	
G2A	63.4	0.1	-0.3	0.5	70.2	0.2	-0.3	0.5	1	1	
C3A	63.5	0	-0.2	0.4	70.3	0.2	-0.2	0.5	7	3	
T4A	63.5	0.1	-0.2	0.5	70.2	0.1	-0.3	0.4	1	3	
L5A	62.7	0.1	-1	0.5	69.4	0.1	-1.1	0.4	-23	-7	
S6A	63.5	0.1	-0.2	0.5	70.3	0.1	-0.2	0.4	-3	-4	
A7G	63.5	0	-0.2	0.4	70.4	0.1	-0.1	0.4	-4	-5	
E8A	63.4	0.1	-0.3	0.5	69.9	0.1	-0.6	0.4	1	-4	
D9A	63.3	0.1	-0.4	0.5	70	0.1	-0.5	0.4	-3	-5	
K10A	63.4	0.1	-0.3	0.5	70.2	0	-0.3	0.3	7	-7	
A11G	63.5	0	-0.2	0.4	70.2	0	-0.3	0.3	-5	-12	
A12G	64.1	0	0.4	0.4	70.8	0.1	0.3	0.4	-7	-14	
V13A	63.4	0.1	-0.3	0.5	70.3	0.1	-0.2	0.4	9	-2	
E14A	63.4	0	-0.3	0.4	70.3	0.1	-0.2	0.4	8	-16	
R15A	63.3	0.1	-0.4	0.5	70.2	0.1	-0.3	0.4	-8	-28	
S16A	63.2	0.1	-0.5	0.5	70.5	0.1	0	0.4	-37	-30	
K17A	63.3	0.1	-0.4	0.5	70.3	0.2	-0.2	0.5	-7	3	
M18A	63.4	0.1	-0.3	0.5	70.4	0.1	-0.1	0.4	-1	1	
I19A	63.3	0.2	-0.4	0.6	70.4	0.1	-0.1	0.4	-56	-34	
D20A	63.1	0.1	-0.6	0.5	70.8	0	0.3	0.3	-36	-36	
R21A	63.1	0.1	-0.6	0.5	70.4	0.1	-0.1	0.4	-17	2	
N22A	63.3	0.3	-0.4	0.7	70.4	0.1	-0.1	0.4	0	3	
L23A	63.5	0.3	-0.2	0.7	70.3	0.6	-0.2	0.9	-48	-35	
R24A	63.3	0.2	-0.4	0.6	70.1	0.1	-0.4	0.4	-7	9	
E25A	63.7	0.1	0	0.5	70.4	0.1	-0.1	0.4	4	-14	
D26A	63.6	0	-0.1	0.4	70.4	0.3	-0.1	0.6	-3	-7	
G27A	63.2	0.1	-0.5	0.5	70	0.1	-0.5	0.4	-9	0	
E28A	63.6	0.1	-0.1	0.5	70.3	0.2	-0.2	0.5	-3	-27	
K29A	62.9	0	-0.8	0.4	69.8	0.3	-0.7	0.6	-8	1	
A30G	63.3	0.1	-0.4	0.5	69.6	0.1	-0.9	0.4	-15	-14	
A31G	63.3	0.1	-0.4	0.5	70.4	0	-0.1	0.3	-11	-22	
R32A	62.8	0.1	-0.9	0.5	70	0.1	-0.5	0.4	-13	16	
E33A	62.2	0.1	-1.5	0.5	70.7	0.1	0.2	0.4	5	8	
V34A	61.1	0.1	-2.6	0.5	68.7	0.3	-1.8	0.6	-10	-12	
K35A	62.4	0.1	-1.3	0.5	66.9	0.1	-3.6	0.4	-15	3	
L36A	59.6	0.1	-4.1	0.5	67.8	0.2	-2.7	0.5	-24	-37	
L37A	62.5	0	-1.2	0.4	67.2	0.1	-3.3	0.4	-25	-37	
L38A	53	0.5	-10.7	0.9	67.5	0.3	-3	0.6	-15	8	
L39A	63.5	0	-0.2	0.4	66	0.1	-4.5	0.4	-11	4	
G40A	46.9	0.3	-16.8	0.7	49.8	0.4	-20.7	0.7	-45	-4	
A41G	61.8	0.1	-1.9	0.5	67.3	0	-3.2	0.3	-23	9	
G42A	66	0.1	2.3	0.5	71.1	0	0.6	0.3	-4	5	

E43A	62.7	0	-1	0.4	67.7	0.1	-2.8	0.4	-1	-18
S44A	63.7	0	0	0.4	70.6	0.3	0.1	0.6	0	-2
G45A	63.1	0.1	-0.6	0.5	70.8	0.1	0.3	0.4	-56	-19
K46A	55	0	-8.7	0.4	55.2	0.1	-15.3	0.4	-2	6
S47A	62.6	0	-1.1	0.4	60.3	0.1	-10.2	0.4	5	6
T48A	53.9	0.2	-9.8	0.6	61.6	0.1	-8.9	0.4	3	-1
I49A	45.5	0.1	-18.2	0.5	66.9	0.1	-3.6	0.4	-7	-1
V50A	62.5	0	-1.2	0.4	72.2	0.1	1.7	0.4	-9	-7
K51A	55.4	0	-8.3	0.4	66	0.1	-4.5	0.4	-17	15
Q52A	60.3	0	-3.4	0.4	69.5	0.2	-1	0.5	6	-7
M53A	55.5	0.2	-8.2	0.6	67.1	0.1	-3.4	0.4	-13	3
K54A	56.3	0.1	-7.4	0.5	67.4	0.2	-3.1	0.5	-16	18
I55A	55.7	0.1	-8	0.5	64.6	0.1	-5.9	0.4	-13	22
I56A	54	0.1	-9.7	0.5	66.9	0.1	-3.6	0.4	-12	18
H57A	63.2	0.1	-0.5	0.5	71	0.2	0.5	0.5	-7	19
E58A	64.4	0.1	0.7	0.5	70.8	0.1	0.3	0.4	8	-10
A59G	67.3	0.1	3.6	0.5	72.2	0.1	1.7	0.4	2	-10
G60A	61.4	0.1	-2.3	0.5	69.5	0.2	-1	0.5	-2	9
Y61A	56.1	0.1	-7.6	0.5	65.6	0.1	-4.9	0.4	1	1
S62A	61.8	0.1	-1.9	0.5	69.7	0.1	-0.8	0.4	8	-2
E63A	62.7	0.1	-1	0.5	70.1	0	-0.4	0.3	7	-4
E64A	62.9	0.1	-0.8	0.5	69.9	0.1	-0.6	0.4	8	-8
E65A	60.5	0.1	-3.2	0.5	68.4	0.1	-2.1	0.4	12	-2
C66A	60.5	0	-3.2	0.4	68.5	0.2	-2	0.5	5	-9
K67A	62.8	0.1	-0.9	0.5	70.2	0.1	-0.3	0.4	-14	-6
Q68A	63.7	0.1	0	0.5	70.7	0.1	0.2	0.4	1	-3
Y69A	58.7	0.1	-5	0.5	67.5	0.2	-3	0.5	5	1
K70A	62.3	0.1	-1.4	0.5	69.6	0.2	-0.9	0.5	6	-8
A71G	63.4	0.1	-0.3	0.5	70.2	0.1	-0.3	0.4	4	1
V72A	64	0.1	0.3	0.5	66.9	0	-3.6	0.3	5	-5
V73A	57.3	0.1	-6.4	0.5	65.3	0.1	-5.2	0.4	0	-18
Y74A	60.1	0.1	-3.6	0.5	67.6	0.1	-2.9	0.4	-7	-16
S75A	63.6	0.1	-0.1	0.5	70.5	0.1	0	0.4	0	4
N76A	61.1	0	-2.6	0.4	63.9	0.1	-6.6	0.4	0	4
T77A	62.2	0.1	-1.5	0.5	69.4	0.1	-1.1	0.4	-1	-3
I78A	61.1	0.1	-2.6	0.5	69.1	0.2	-1.4	0.5	-20	-5
Q79A	62.8	0	-0.9	0.4	69.1	0.1	-1.4	0.4	2	-2
S80A	63	0.1	-0.7	0.5	70	0.1	-0.5	0.4	3	-2
I81A	61.1	0.1	-2.6	0.5	68.7	0.1	-1.8	0.4	5	-8
I82A	62.6	0	-1.1	0.4	69.6	0.1	-0.9	0.4	-4	1
A83G	61.7	0.1	-2	0.5	68.6	0	-1.9	0.3	3	1
I84A	57.3	0	-6.4	0.4	66.4	0	-4.1	0.3	6	-20
I85A	59.5	0.1	-4.2	0.5	69	0.1	-1.5	0.4	4	-14
R86A	62.4	0	-1.3	0.4	70	0.2	-0.5	0.5	2	-4
A87G	61.5	0.1	-2.2	0.5	68.8	0.1	-1.7	0.4	0	-10
M88A	58.1	0	-5.6	0.4	68	0.1	-2.5	0.4	6	-24

G89A	63.3	0	-0.4	0.4		70.4	0.1	-0.1	0.4		8		-3
R90A	61.8	0.1	-1.9	0.5		69.2	0.2	-1.3	0.5		-3		1
L91A	59.5	0.2	-4.2	0.6		67.3	0.2	-3.2	0.5		2		6
K92A	62.6	0.1	-1.1	0.5		69.8	0.2	-0.7	0.5		2		2
I93A	58.6	0	-5.1	0.4		67.6	0.2	-2.9	0.5		2		-10
D94A	63.3	0.1	-0.4	0.5		70.1	0.1	-0.4	0.4		4		2
F95A	54.8	0.1	-8.9	0.5		65.7	0.1	-4.8	0.4		-2		-25
G96A	63.1	0	-0.6	0.4		69.6	0.6	-0.9	0.9		4		-1
D97A	62.4	0	-1.3	0.4		70.3	0.1	-0.2	0.4		-8		-5
S98A	64.1	0	0.4	0.4		71.1	0.1	0.6	0.4		-1		3
A99G	63.3	0.1	-0.4	0.5		70.6	0.1	0.1	0.4		-2		2
R100A	62.8	0.1	-0.9	0.5		70.1	0.1	-0.4	0.4		-9		2
A101G	63.3	0	-0.4	0.4		70.7	0.1	0.2	0.4		-3		-1
D102A	63.9	0.1	0.2	0.5		70.9	0.1	0.4	0.4		-1		0
D103A	57.7	0.1	-6	0.5		67.9	0.1	-2.6	0.4		-12		-21
A104G	61.3	0.1	-2.4	0.5		70.1	0.1	-0.4	0.4		-3		-7
R105A	63.7	0.1	0	0.5		70.7	0.1	0.2	0.4		-10		1
Q106A	63.7	0.1	0	0.5		70.8	0.2	0.3	0.5		-15		0
L107A	59.4	0	-4.3	0.4		69	0	-1.5	0.3		-7		-18
F108A	62.5	0	-1.2	0.4		69.6	0.2	-0.9	0.5		-2		-9
V109A	64.1	0	0.4	0.4		71	0.3	0.5	0.6		-4		-2
L110A	62.8	0.1	-0.9	0.5		69.9	0.1	-0.6	0.4		-5		-3
A111G	62.9	0.1	-0.8	0.5		70.2	0.1	-0.3	0.4		0		-6
G112A	63.7	0.1	0	0.5		70.8	0.1	0.3	0.4		-13		4
A113G	63.8	0.1	0.1	0.5		70.9	0.1	0.4	0.4		1		5
A114G	63.9	0.1	0.2	0.5		71	0.1	0.5	0.4		-2		3
E115A	63.3	0.1	-0.4	0.5		70.7	0.1	0.2	0.4		5		-2
E116A	63.8	0.1	0.1	0.5		71.4	0.1	0.9	0.4		-3		2
G117A	63.3	0	-0.4	0.4		70.8	0.3	0.3	0.6		-5		3
F118A	63.5	0	-0.2	0.4		70.9	0.1	0.4	0.4		-4		6
M119A	59.4	0.1	-4.3	0.5		68.3	0.2	-2.2	0.5		-3		-7
T120A	62.5	0	-1.2	0.4		70	0.1	-0.5	0.4		2		5
A121G	62.9	0	-0.8	0.4		70.2	0.1	-0.3	0.4		8		-1
E122A	62.6	0.1	-1.1	0.5		70.1	0.1	-0.4	0.4		9		-4
L123A	60.7	0.1	-3	0.5		69	0.1	-1.5	0.4		8		-12
A124G	61.8	0	-1.9	0.4		69.6	0.2	-0.9	0.5		7		-3
G125A	63.5	0	-0.2	0.4		71.2	0.1	0.7	0.4		1		-2
V126A	62.8	0	-0.9	0.4		70.3	0.1	-0.2	0.4		1		-7
I127A	60.1	0	-3.6	0.4		68.9	0.1	-1.6	0.4		7		-12
K128A	62.5	0.1	-1.2	0.5		70.3	0.1	-0.2	0.4		8		-8
R129A	61.3	0.1	-2.4	0.5		69.7	0.1	-0.8	0.4		6		-17
L130A	54.7	0.1	-9	0.5		66.1	0.1	-4.4	0.4		5		-20
W131A	56.9	0.1	-6.8	0.5		64.5	0.1	-6	0.4		1		-32
K132A	63.5	0.1	-0.2	0.5		70.9	0.1	0.4	0.4		0		-1
D133A	55.5	0	-8.2	0.4		66.2	0	-4.3	0.3		9		-19
S134A	63.3	0.1	-0.4	0.5		70.8	0.1	0.3	0.4		4		-22

G135A	60.2	0.1	-3.5	0.5		68.6	0.2	-1.9	0.5		4		-14	
V136A	59.2	0.1	-4.5	0.5		69	0.1	-1.5	0.4		4		-23	
Q137A	60.3	0	-3.4	0.4		69.4	0.1	-1.1	0.4		5		-26	
A138G	61.3	0	-2.4	0.4		69.4	0.1	-1.1	0.4		5		-23	
C139A	62.9	0	-0.8	0.4		70.2	0	-0.3	0.3		3		-12	
F140A	60.8	0	-2.9	0.4		68.8	0	-1.7	0.3		2		-15	
N141A	63.5	0.1	-0.2	0.5		70.8	0.1	0.3	0.4		0		-6	
R142A														NM
S143A	63.3	0	-0.4	0.4		70.1	0.1	-0.4	0.4		8		-6	
R144A	61.3	0.1	-2.4	0.5		69	0.1	-1.5	0.4		-5		6	
E145A	62.4	0	-1.3	0.4		70.3	0.1	-0.2	0.4		-3		-6	
Y146A	64.1	0	0.4	0.4		71.1	0.1	0.6	0.4		1		-6	
Q147A	63.3	0.1	-0.4	0.5		70.6	0.1	0.1	0.4		-3		1	
L148A	62.8	0.1	-0.9	0.5		70.1	0.1	-0.4	0.4		-1		-11	
N149A	63.3	0	-0.4	0.4		70.7	0.1	0.2	0.4		0		-2	
D150A	63.9	0.1	0.2	0.5		70.9	0.1	0.4	0.4		-3		7	
S151A	57.7	0.1	-6	0.5		67.9	0.1	-2.6	0.4		-1		-3	
A152G	61.3	0.1	-2.4	0.5		70.1	0.1	-0.4	0.4		-1		-5	
A153G	63.7	0.1	0	0.5		70.7	0.1	0.2	0.4		-7		-6	
Y154A	63.7	0.1	0	0.5		70.8	0.2	0.3	0.5		-7		-4	
Y155A	59.4	0	-4.3	0.4		69	0	-1.5	0.3		-9		-17	
L156A	62.5	0	-1.2	0.4		69.6	0.2	-0.9	0.5		-3		-26	
N157A	64.1	0	0.4	0.4		71	0.3	0.5	0.6		0		-1	
D158A	62.8	0.1	-0.9	0.5		69.9	0.1	-0.6	0.4		2		2	
L159A	62.9	0.1	-0.8	0.5		70.2	0.1	-0.3	0.4		-1		-15	
D160A	63.7	0.1	0	0.5		70.8	0.1	0.3	0.4		1		-7	
R161A	63.8	0.1	0.1	0.5		70.9	0.1	0.4	0.4		1		-14	
I162A	63.9	0.1	0.2	0.5		71	0.1	0.5	0.4		7		-25	
A163G	63.3	0.1	-0.4	0.5		70.7	0.1	0.2	0.4		2		-7	
Q164A	63.8	0.1	0.1	0.5		71.4	0.1	0.9	0.4		-3		4	
P165A	63.3	0	-0.4	0.4		70.8	0.3	0.3	0.6		0		0	
N166A	63.5	0	-0.2	0.4		70.9	0.1	0.4	0.4		2		-7	
Y167A	59.4	0.1	-4.3	0.5		68.3	0.2	-2.2	0.5		7		-27	
I168A	62.5	0	-1.2	0.4		70	0.1	-0.5	0.4		5		-13	
P169A	57.4	0	-6.3	0.4		66.5	0.1	-4	0.4		-4		-20	
T170A	58.9	0	-4.8	0.4		67.3	0	-3.2	0.3		-2		-14	
Q171A	61.6	0.1	-2.1	0.5		69.5	0	-1	0.3		-6		5	
Q172A	63	0	-0.7	0.4		69.6	0.2	-0.9	0.5		0		2	
D173A	50.3	0.1	-13.4	0.5		61.1	0.1	-9.4	0.4		1		-29	
V174A	58	0	-5.7	0.4		66.1	0	-4.4	0.3		-3		-5	
L175A	49.8	0.1	-13.9	0.5		61.5	0.2	-9	0.5		-23		9	
R176A	58.1	0.1	-5.6	0.5		68.9	0.1	-1.6	0.4		-13		17	
T177A	65.5	0.1	1.8	0.5		70.6	0.1	0.1	0.4		-4		1	
R178A	61.7	0.1	-2	0.5		75	0.1	4.5	0.4		-11		6	
V179A	62.3	0	-1.4	0.4		67.8	0.1	-2.7	0.4		2		8	
K180A	62.3	0.1	-1.4	0.5		71.6	0.3	1.1	0.6		-9		4	

T181A	62.6	0	-1.1	0.4		59.1	0.1	-11.4	0.4		1		0
T182A	62.9	0.1	-0.8	0.5		67.5	0.1	-3	0.4		1		-3
G183A	61.8	0	-1.9	0.4		69.6	0.1	-0.9	0.4		2		0
I184A	61.1	0	-2.6	0.4		65.3	0.1	-5.2	0.4		-18		-32
V185A	61.8	0.1	-1.9	0.5		68.3	0.1	-2.2	0.4		0		-12
E186A	61.9	0.1	-1.8	0.5		68.7	0.1	-1.8	0.4		-9		-18
T187A	63	0.1	-0.7	0.5		68.9	0.1	-1.6	0.4		-8		-6
H188A	63.3	0.1	-0.4	0.5		69.5	0.1	-1	0.4		2		8
F189A	52.3	0.7	-11.4	1.1		65.2	0.1	-5.3	0.4		-14		-18
T190A	61.2	0.1	-2.5	0.5		69.6	0.1	-0.9	0.4		1		3
F191A	62.2	0.1	-1.5	0.5		70.2	0.1	-0.3	0.4		-5		-36
K192A	58.2	0.1	-5.5	0.5		68.8	0.1	-1.7	0.4		-12		-35
D193A	62.4	0	-1.3	0.4		70	0.1	-0.5	0.4		-15		-32
L194A	59.8	0.1	-3.9	0.5		68.3	0.1	-2.2	0.4		-7		-24
H195A	61.7	0.1	-2	0.5		69.5	0.3	-1	0.6		-15		-8
F196A	50.1	0.1	-13.6	0.5		66.8	0.2	-3.7	0.5		-30		-32
K197A	62.4	0	-1.3	0.4		69.6	0.1	-0.9	0.4		-4		-2
M198A	56.8	0.1	-6.9	0.5		70	0.1	-0.5	0.4		-3		-26
F199A	59.6	0	-4.1	0.4		66.3	0.1	-4.2	0.4		3		-2
D200A	69.5	0	5.8	0.4		68.8	0.1	-1.7	0.4		-13		-36
V201A	61.5	0.1	-2.2	0.5		65.8	0.3	-4.7	0.6		-5		-18
G202A	63.1	0	-0.6	0.4		63.8	0.1	-6.7	0.4		8		-7
G203A	63.3	0.1	-0.4	0.5		60.8	0.1	-9.7	0.4		-6		-12
Q204A	64.2	0.1	0.5	0.5		69.1	0.1	-1.4	0.4		-12		-25
R205A	63.3	0	-0.4	0.4		65.2	0.2	-5.3	0.5		-11		-28
S206A	63.3	0	-0.4	0.4		69.2	0.1	-1.3	0.4		-10		-9
E207A	63	0	-0.7	0.4		65.3	0.1	-5.2	0.4		-3		-3
R208A	63.2	0.1	-0.5	0.5		61.1	0.1	-9.4	0.4		-7		-32
K209A	63.5	0	-0.2	0.4		69.5	0.3	-1	0.6		-15		-26
K210A	63	0.1	-0.7	0.5		68.9	0.1	-1.6	0.4		-37		-40
W211A	62.2	0.1	-1.5	0.5		62.7	0.1	-7.8	0.4		-32		-41
I212A	62.8	0	-0.9	0.4		69.7	0.1	-0.8	0.4		-17		-33
H213A	63.4	0	-0.3	0.4		70.5	0.1	0	0.4		-5		-25
C214A	63	0.1	-0.7	0.5		69	0.1	-1.5	0.4		-4		-23
F215A	62.9	0	-0.8	0.4		66.8	0.1	-3.7	0.4		-7		-20
E216A	63.3	0.1	-0.4	0.5		69.1	0.3	-1.4	0.6		-12		-41
G217A	63	0	-0.7	0.4		70.2	0.1	-0.3	0.4		-20		-8
V218A	63.5	0	-0.2	0.4		70.3	0.1	-0.2	0.4		-16		-30
T219A	62.9	0	-0.8	0.4		68.4	0.2	-2.1	0.5		-20		-31
A220G	63.6	0	-0.1	0.4		69.8	0.1	-0.7	0.4		-24		-32
I221A	62.4	0	-1.3	0.4		68.8	0.1	-1.7	0.4		-25		-32
I222A	56.5	0	-7.2	0.4		68.7	0.1	-1.8	0.4		5		-19
F223A	59.5	0	-4.2	0.4		64.9	0.3	-5.6	0.6		-16		-32
C224A	60.1	0.1	-3.6	0.5		69.1	0.1	-1.4	0.4		0		-4
V225A	64.3	0	0.6	0.4		71.3	0.1	0.8	0.4		5		5
A226G	65.3	0	1.6	0.4		70.9	0.3	0.4	0.6		-3		-30

L227A	58.8	0.1	-4.9	0.5		66.5	0.2	-4	0.5		-14		-33	
S228A	61.3	0.1	-2.4	0.5		69.9	0	-0.6	0.3		-8		-25	
D229A	63.5	0.1	-0.2	0.5		69	0.2	-1.5	0.5		-24		-32	
Y230A														NM
D231A	56.2	0.2	-7.5	0.6		64.6	0.2	-5.9	0.5		-5		-31	
L232A	61.2	0.1	-2.5	0.5		66.8	0.1	-3.7	0.4		0		-4	
V233A	63.1	0	-0.6	0.4		69.7	0.1	-0.8	0.4		-2		-2	
L234A	63.2	0.1	-0.5	0.5		67.7	0.1	-2.8	0.4		7		9	
A235G	62.9	0	-0.8	0.4		67.8	0.1	-2.7	0.4		6		5	
E236A	61.8	0.1	-1.9	0.5		65.3	0	-5.2	0.3		9		-11	
D237A	62.3	0.1	-1.4	0.5		67.4	0	-3.1	0.3		-4		-14	
E238A	63	0	-0.7	0.4		69.1	0.1	-1.4	0.4		0		6	
E239A	63.4	0.1	-0.3	0.5		70.1	0.1	-0.4	0.4		7		2	
M240A	62.8	0	-0.9	0.4		68.5	0.1	-2	0.4		6		2	
N241A	61	0.1	-2.7	0.5		65.9	0.2	-4.6	0.5		-21		-32	
R242A	59.8	0.1	-3.9	0.5		66.8	0.2	-3.7	0.5		-5		8	
M243A	55.3	0	-8.4	0.4		66.4	0.3	-4.1	0.6		-12		-33	
H244A	60.8	0.1	-2.9	0.5		68.2	0.1	-2.3	0.4		-8		-26	
E245A	62.9	0.1	-0.8	0.5		63.2	0.1	-7.3	0.4		-6		12	
S246A	63.1	0.1	-0.6	0.5		69.4	0.1	-1.1	0.4		-12		3	
M247A	62	0.1	-1.7	0.5		69.8	0.3	-0.7	0.6		-18		-36	
K248A	63.4	0	-0.3	0.4		71.4	0.1	0.9	0.4		-17		-15	
L249A	61.9	0.1	-1.8	0.5		63.4	0.1	-7.1	0.4		-9		-7	
F250A	50.2	0.6	-13.5	1		65.6	1	-4.9	1.3		-56		-12	
D251A	62.5	0.1	-1.2	0.5		69.2	0.1	-1.3	0.4		-11		-25	
S252A	62.4	0	-1.3	0.4		70	0.1	-0.5	0.4		-7		-10	
I253A	63	0	-0.7	0.4		67	0.2	-3.5	0.5		-34		-34	
C254A	62.4	0.1	-1.3	0.5		70.2	0.1	-0.3	0.4		-27		-33	
N255A	61	0.1	-2.7	0.5		69.1	0.1	-1.4	0.4		-23		-40	
N256A	63.5	0.1	-0.2	0.5		70.7	0.1	0.2	0.4		-5		-23	
K257A	63.3	0.1	-0.4	0.5		70.2	0.1	-0.3	0.4		-20		-22	
W258A	64	0.1	0.3	0.5		69.8	0	-0.7	0.3		-32		-38	
F259A	62	0.1	-1.7	0.5		66.9	0.1	-3.6	0.4		-45		-36	
T260A	63.2	0.1	-0.5	0.5		69.6	0.1	-0.9	0.4		-4		0	
D261A	62.3	0.1	-1.4	0.5		69.7	0	-0.8	0.3		-11		-32	
T262A	63.4	0.2	-0.3	0.6		69.6	0.1	-0.9	0.4		-24		-38	
S263A	62.2	0.1	-1.5	0.5		69.6	0.2	-0.9	0.5		-9		-17	
I264A	60	0.1	-3.7	0.5		67.2	0.1	-3.3	0.4		-10		-18	
I265A	63.3	0.1	-0.4	0.5		71.1	0.1	0.6	0.4		-21		-35	
L266A	59.9	0.1	-3.8	0.5		68.4	0.1	-2.1	0.4		-22		-40	
F267A	57.5	0.1	-6.2	0.5		69.8	0.4	-0.7	0.7		-23		-38	
L268A	57.1	0.1	-6.6	0.5		67.6	0.4	-2.9	0.7		-24		-35	
N269A	42.5	0.4	-21.2	0.8		40.5	0.3	-30	0.6		-58		-3	
K270A														NM
K271A	59.2	0.1	-4.5	0.5		68.6	0.2	-1.9	0.5		-2		-5	
D272A														NM

L273A	58	0	-5.7	0.4		69.2	0.3	-1.3	0.6		-3		-15	
F274A	55.2	0.1	-8.5	0.5		69.4	0.4	-1.1	0.7		-20		-31	
E275A	63.5	0.2	-0.2	0.6		70.4	0.2	-0.1	0.5		-12		2	
E276A	63.2	0.1	-0.5	0.5		70.1	0.1	-0.4	0.4		6		-23	
K277A	58.8	0	-4.9	0.4		66.4	0.1	-4.1	0.4		-1		-36	
I278A	55.6	0.1	-8.1	0.5		68.3	0.2	-2.2	0.5		-5		-19	
K279A	62.8	0.1	-0.9	0.5		70.6	0.2	0.1	0.5		5		-21	
K280A	61.8	0.1	-1.9	0.5		69.3	0.1	-1.2	0.4		7		-16	
S281A	61.6	0	-2.1	0.4		68.7	0.1	-1.8	0.4		5		-6	
P282A	61.4	0.1	-2.3	0.5		69.6	0.1	-0.9	0.4		5		-36	
L283A	50.4	0.1	-13.3	0.5		67.2	0.4	-3.3	0.7		-10		-40	
T284A	61.8	0	-1.9	0.4		69.8	0.1	-0.7	0.4		3		-32	
I285A	61	0	-2.7	0.4		68.9	0	-1.6	0.3		1		-24	
C286A	61.9	0	-1.8	0.4		69.8	0.1	-0.7	0.4		0		-36	
Y287A	52.1	0.4	-11.6	0.8		67.1	0.6	-3.4	0.9		1		-40	
P288A	61	0.1	-2.7	0.5		69.9	0.2	-0.6	0.5		-8		-38	
E289A	63.2	0.1	-0.5	0.5		70.3	0.1	-0.2	0.4		-20		-11	
Y290A	54.7	0.1	-9	0.5		68.1	0.3	-2.4	0.6		-8		-33	
A291G	63.6	0	-0.1	0.4		70.7	0.1	0.2	0.4		-9		2	
G292A	60.8	0.1	-2.9	0.5		69.7	0.1	-0.8	0.4		-7		-32	
S293A	63.9	0	0.2	0.4		70.5	0.2	0	0.5		-1		8	
N294A	62.3	0.1	-1.4	0.5		70.2	0.1	-0.3	0.4		-4		-23	
T295A	62.4	0.1	-1.3	0.5		70.2	0.1	-0.3	0.4		-6		-17	
Y296A	60.9	0.1	-2.8	0.5		69.1	0.1	-1.4	0.4		0		10	
E297A	65.3	0.1	1.6	0.5		67.7	0	-2.8	0.3		-8		-8	
E298A	62.4	0	-1.3	0.4		70.2	0.2	-0.3	0.5		-4		-18	
A299G	63.2	0.1	-0.5	0.5		70.5	0.1	0	0.4		-6		-10	
A300G	64.9	0.1	1.2	0.5		71.2	0.1	0.7	0.4		-2		-3	
A301G	63.5	0.1	-0.2	0.5		70.6	0.1	0.1	0.4		-1		-6	
Y302A	55.6	0.1	-8.1	0.5		68.9	0.3	-1.6	0.6		-6		-33	
I303A	57.9	0.1	-5.8	0.5		67.6	0.1	-2.9	0.4		-11		-40	
Q304A	62.8	0.1	-0.9	0.5		70.2	0.1	-0.3	0.4		-1		0	
C305A	63.9	0	0.2	0.4		70.6	0.1	0.1	0.4		-11		7	
Q306A	62.8	0.1	-0.9	0.5		70.3	0.1	-0.2	0.4		-9		-15	
F307A	54.9	0.1	-8.8	0.5		67.6	0.7	-2.9	1		-36		-39	
E308A	62.2	0.1	-1.5	0.5		70	0.1	-0.5	0.4		-4		-3	
D309A	64	0	0.3	0.4		70.6	0.2	0.1	0.5		-6		10	
L310A	61.4	0	-2.3	0.4		69	0.2	-1.5	0.5		0		-34	
N311A	62.7	0.1	-1	0.5		67.9	0.1	-2.6	0.4		-6		-33	
K312A	63.6	0	-0.1	0.4		70.4	0.1	-0.1	0.4		-6		-10	
R313A	64.3	0.1	0.6	0.5		70.4	0	-0.1	0.3		-1		3	
K314A	63.1	0	-0.6	0.4		69.8	0.2	-0.7	0.5		-5		-22	
D315A	64	0	0.3	0.4		70.5	0.1	0	0.4		-1		-8	
T316A	63.8	0.1	0.1	0.5		70.3	0.2	-0.2	0.5		-2		-6	
K317A	62	0	-1.7	0.4		68.7	0.1	-1.8	0.4		-11		-43	
E318A	63.8	0.1	0.1	0.5		70	0	-0.5	0.3		-14		-41	

I319A	59.5	0	-4.2	0.4		68.8	0.1	-1.7	0.4			-35		-40	
Y320A	62	0.1	-1.7	0.5		69.9	0.1	-0.6	0.4			-81		-44	
T321A	63.2	0.1	-0.5	0.5		69.9	0.3	-0.6	0.6			-5		-29	
H322A	62.7	0.1	-1	0.5		69.9	0.1	-0.6	0.4			-23		-19	
F323A	60.1	0.1	-3.6	0.5		69	0.2	-1.5	0.5			5		3	
T324A	59.7	0.1	-4	0.5		69.1	0.1	-1.4	0.4			-6		-36	
C325A	59.8	0	-3.9	0.4		69.7	0.2	-0.8	0.5			-2		-21	
A326G	59.4	0.1	-4.3	0.5		68.2	0.3	-2.3	0.6			-6		-1	
T327A	57.3	0	-6.4	0.4		65.7	0.2	-4.8	0.5			0		12	
D328A	56.3	0	-7.4	0.4		68.3	0.2	-2.2	0.5			-2		6	
T329A	58.2	0.1	-5.5	0.5		65.4	0.3	-5.1	0.6			-8		-7	
K330A	63.9	0	0.2	0.4		70.6	0.2	0.1	0.5			-29		-15	
N331A	60.9	0.1	-2.8	0.5		68.1	0.5	-2.4	0.8			-3		28	
V332A	55.5	0	-8.2	0.4		69	0.4	-1.5	0.7			-6		20	
Q333A	62.8	0.1	-0.9	0.5		70	0.1	-0.5	0.4			-1		-32	
F334A	65.5	0	1.8	0.4		70.9	0.1	0.4	0.4			-32		-43	
V335A	64.1	0.1	0.4	0.5		70.5	0.3	0	0.6			-6		-43	
F336A												-18		-12	
D337A	62.9	0.1	-0.8	0.5		70	0.2	-0.5	0.5			-11		-4	
A338G	60.9	0.1	-2.8	0.5		69.6	0.1	-0.9	0.4			-20		-39	
V339A	60.7	0.1	-3	0.5		70	0.2	-0.5	0.5			-5		-36	
T340A	63.8	0	0.1	0.4		69.8	0.1	-0.7	0.4			-6		-25	
D341A	61.6	0.1	-2.1	0.5		69.8	0.1	-0.7	0.4			-41		-46	
V342A	61.2	0.1	-2.5	0.5		69.1	0.1	-1.4	0.4			-38		-45	
I343A	58.3	0.1	-5.4	0.5		68.5	0	-2	0.3			-15		-30	
I344A	63.3	0	-0.4	0.4		70.7	0.1	0.2	0.4			-39		-29	
K345A	63	0.1	-0.7	0.5		70.6	0.2	0.1	0.5			-37		-43	
N346A	62.2	0.1	-1.5	0.5		69.9	0.2	-0.6	0.5			-7		-16	
N347A	62.1	0.1	-1.6	0.5		70.2	0.1	-0.3	0.4			-10		-2	
L348A	62.8	0.1	-0.9	0.5		70	0.1	-0.5	0.4			-87		-44	
K349A	62.7	0.1	-1	0.5		69.9	0.3	-0.6	0.6			-11		-31	
D350A	63.2	0.1	-0.5	0.5		70.5	0.1	0	0.4			-4		13	
C351A	63.5	0	-0.2	0.4		70.3	0.1	-0.2	0.4			-37		-49	
G352A	63.5	0.1	-0.2	0.5		70.5	0.4	0	0.7			-81		-44	
L353A	63.7	0.1	0	0.5		70.9	0.1	0.4	0.4			-94		-44	
F354A	63.7	0.1	0	0.5		70.5	0.1	0	0.4			-18		-48	

**SD:** Standard deviation

**NM:** Not measurable



## Reference:

1. Pierce, K.L., R.T. Premont, and R.J. Lefkowitz, *Seven-transmembrane receptors*. Nat Rev Mol Cell Biol, 2002. **3**(9): p. 639-50.
2. Oldham, W.M. and H.E. Hamm, *Structural basis of function in heterotrimeric G proteins*. Q Rev Biophys, 2006. **39**(2): p. 117-66.
3. Rosenbaum, D.M., S.G. Rasmussen, and B.K. Kobilka, *The structure and function of G-protein-coupled receptors*. Nature, 2009. **459**(7245): p. 356-63.
4. Hopkins, A.L. and C.R. Groom, *The druggable genome*. Nat Rev Drug Discov, 2002. **1**(9): p. 727-30.
5. Fredriksson, R., et al., *The G-protein-coupled receptors in the human genome form five main families. Phylogenetic analysis, paralogon groups, and fingerprints*. Mol Pharmacol, 2003. **63**(6): p. 1256-72.
6. Kristiansen, K., *Molecular mechanisms of ligand binding, signaling, and regulation within the superfamily of G-protein-coupled receptors: molecular modeling and mutagenesis approaches to receptor structure and function*. Pharmacol Ther, 2004. **103**(1): p. 21-80.
7. Katritch, V., V. Cherezov, and R.C. Stevens, *Structure-function of the G protein-coupled receptor superfamily*. Annu Rev Pharmacol Toxicol, 2013. **53**: p. 531-56.
8. Palczewski, K., et al., *Crystal structure of rhodopsin: A G protein-coupled receptor*. Science, 2000. **289**(5480): p. 739-45.
9. Ballesteros, J.A., L. Shi, and J.A. Javitch, *Structural mimicry in G protein-coupled receptors: implications of the high-resolution structure of rhodopsin for structure-function analysis of rhodopsin-like receptors*. Mol Pharmacol, 2001. **60**(1): p. 1-19.
10. Downes, G.B. and N. Gautam, *The G protein subunit gene families*. Genomics, 1999. **62**(3): p. 544-52.
11. Cabrera-Vera, T.M., et al., *Insights into G protein structure, function, and regulation*. Endocr Rev, 2003. **24**(6): p. 765-81.
12. Sah, V.P., et al., *The role of Rho in G protein-coupled receptor signal transduction*. Annu Rev Pharmacol Toxicol, 2000. **40**: p. 459-89.
13. Chen, C.A. and D.R. Manning, *Regulation of G proteins by covalent modification*. Oncogene, 2001. **20**(13): p. 1643-52.
14. Smotryś, J.E. and M.E. Linder, *Palmitoylation of intracellular signaling proteins: regulation and function*. Annu Rev Biochem, 2004. **73**: p. 559-87.

15. Schmidt, C.J., et al., *Specificity of G protein beta and gamma subunit interactions*. J Biol Chem, 1992. **267**(20): p. 13807-10.
16. Higgins, J.B. and P.J. Casey, *In vitro processing of recombinant G protein gamma subunits. Requirements for assembly of an active beta gamma complex*. J Biol Chem, 1994. **269**(12): p. 9067-73.
17. Zhang, F.L. and P.J. Casey, *Protein prenylation: molecular mechanisms and functional consequences*. Annu Rev Biochem, 1996. **65**: p. 241-69.
18. Clapham, D.E. and E.J. Neer, *G protein beta gamma subunits*. Annu Rev Pharmacol Toxicol, 1997. **37**: p. 167-203.
19. Coleman, D.E., et al., *Structures of active conformations of Gi alpha 1 and the mechanism of GTP hydrolysis*. Science, 1994. **265**(5177): p. 1405-12.
20. Sondek, J., et al., *GTPase mechanism of Gproteins from the 1.7-A crystal structure of transducin alpha-GDP-AIF-4*. Nature, 1994. **372**(6503): p. 276-9.
21. Wall, M.A., et al., *The structure of the G protein heterotrimer Gi alpha 1 beta 1 gamma 2*. Cell, 1995. **83**(6): p. 1047-58.
22. Tesmer, J.J., et al., *Structure of RGS4 bound to AIF4--activated G(i alpha1): stabilization of the transition state for GTP hydrolysis*. Cell, 1997. **89**(2): p. 251-61.
23. Sunahara, R.K., et al., *Crystal structure of the adenylyl cyclase activator Galpha*. Science, 1997. **278**(5345): p. 1943-7.
24. Tesmer, J.J., et al., *Structure of human G protein-coupled receptor kinase 2 in complex with the kinase inhibitor balanol*. J Med Chem, 2010. **53**(4): p. 1867-70.
25. Waldo, G.L., et al., *Kinetic scaffolding mediated by a phospholipase C-beta and Gq signaling complex*. Science, 2010. **330**(6006): p. 974-80.
26. Sprang, S.R., *G protein mechanisms: insights from structural analysis*. Annu Rev Biochem, 1997. **66**: p. 639-78.
27. Dohlman, H.G. and J.C. Jones, *Signal activation and inactivation by the Galpha helical domain: a long-neglected partner in G protein signaling*. Sci Signal, 2012. **5**(226): p. re2.
28. Lambright, D.G., et al., *Structural determinants for activation of the alpha-subunit of a heterotrimeric G protein*. Nature, 1994. **369**(6482): p. 621-8.
29. Mixon, M.B., et al., *Tertiary and quaternary structural changes in Gi alpha 1 induced by GTP hydrolysis*. Science, 1995. **270**(5238): p. 954-60.
30. Baltoumas, F.A., M.C. Theodoropoulou, and S.J. Hamodrakas, *Interactions of the alpha-subunits of heterotrimeric G-proteins with GPCRs, effectors and RGS proteins: a critical*

*review and analysis of interacting surfaces, conformational shifts, structural diversity and electrostatic potentials.* J Struct Biol, 2013. **182**(3): p. 209-18.

31. Sondek, J., et al., *Crystal structure of a G-protein beta gamma dimer at 2.1A resolution.* Nature, 1996. **379**(6563): p. 369-74.
32. Neer, E.J., *Heterotrimeric G proteins: organizers of transmembrane signals.* Cell, 1995. **80**(2): p. 249-57.
33. Osawa, S. and E.R. Weiss, *The effect of carboxyl-terminal mutagenesis of Gt alpha on rhodopsin and guanine nucleotide binding.* J Biol Chem, 1995. **270**(52): p. 31052-8.
34. Onrust, R., et al., *Receptor and betagamma binding sites in the alpha subunit of the retinal G protein transducin.* Science, 1997. **275**(5298): p. 381-4.
35. Bae, H., et al., *Two amino acids within the alpha4 helix of Galphai1 mediate coupling with 5-hydroxytryptamine1B receptors.* J Biol Chem, 1999. **274**(21): p. 14963-71.
36. Bae, H., et al., *Molecular determinants of selectivity in 5-hydroxytryptamine1B receptor-G protein interactions.* J Biol Chem, 1997. **272**(51): p. 32071-7.
37. Cai, K., Y. Itoh, and H.G. Khorana, *Mapping of contact sites in complex formation between transducin and light-activated rhodopsin by covalent crosslinking: use of a photoactivatable reagent.* Proc Natl Acad Sci U S A, 2001. **98**(9): p. 4877-82.
38. Mazzoni, M.R. and H.E. Hamm, *Interaction of transducin with light-activated rhodopsin protects it from proteolytic digestion by trypsin.* J Biol Chem, 1996. **271**(47): p. 30034-40.
39. Dratz, E.A., et al., *NMR structure of a receptor-bound G-protein peptide.* Nature, 1993. **363**(6426): p. 276-81.
40. Standfuss, J., et al., *The structural basis of agonist-induced activation in constitutively active rhodopsin.* Nature, 2011. **471**(7340): p. 656-60.
41. Grishina, G. and C.H. Berlot, *A surface-exposed region of G(salpha) in which substitutions decrease receptor-mediated activation and increase receptor affinity.* Mol Pharmacol, 2000. **57**(6): p. 1081-92.
42. Hu, J., et al., *Structural basis of G protein-coupled receptor-G protein interactions.* Nat Chem Biol, 2010.
43. Wess, J., *Molecular basis of receptor/G-protein-coupling selectivity.* Pharmacol Ther, 1998. **80**(3): p. 231-64.
44. Oldham, W.M., et al., *Mechanism of the receptor-catalyzed activation of heterotrimeric G proteins.* Nature structural & molecular biology, 2006. **13**(9): p. 772-7.

45. Van Eps, N., et al., *Structural and dynamical changes in an alpha-subunit of a heterotrimeric G protein along the activation pathway*. Proceedings of the National Academy of Sciences of the United States of America, 2006. **103**(44): p. 16194-9.
46. Preininger, A.M., J. Meiler, and H.E. Hamm, *Conformational flexibility and structural dynamics in GPCR-mediated G protein activation: a perspective*. Journal of Molecular Biology, 2013. **425**(13): p. 2288-98.
47. Oldham, W.M. and H.E. Hamm, *Heterotrimeric G protein activation by G-protein-coupled receptors*. Nat Rev Mol Cell Biol, 2007.
48. Rasmussen, S.G., et al., *Crystal structure of the beta2 adrenergic receptor-Gs protein complex*. Nature, 2011. **477**(7366): p. 549-55.
49. Taylor, J.M., et al., *Binding of an alpha 2 adrenergic receptor third intracellular loop peptide to G beta and the amino terminus of G alpha*. J Biol Chem, 1994. **269**(44): p. 27618-24.
50. Taylor, J.M., et al., *Receptor and membrane interaction sites on Gbeta. A receptor-derived peptide binds to the carboxyl terminus*. J Biol Chem, 1996. **271**(7): p. 3336-9.
51. Ford, C.E., et al., *Molecular basis for interactions of G protein betagamma subunits with effectors*. Science, 1998. **280**(5367): p. 1271-4.
52. Van Eps, N., et al., *Interaction of a G protein with an activated receptor opens the interdomain interface in the alpha subunit*. Proc Natl Acad Sci U S A, 2011. **108**(23): p. 9420-4.
53. Alexander, N.S., et al., *Energetic analysis of the rhodopsin-G-protein complex links the alpha5 helix to GDP release*. Nat Struct Mol Biol, 2014. **21**(1): p. 56-63.
54. Westfield, G.H., et al., *Structural flexibility of the G alpha s alpha-helical domain in the beta2-adrenoceptor Gs complex*. Proc Natl Acad Sci U S A, 2011. **108**(38): p. 16086-91.
55. Scheerer, P., et al., *Structural and kinetic modeling of an activating helix switch in the rhodopsin-transducin interface*. Proc Natl Acad Sci U S A, 2009. **106**(26): p. 10660-5.
56. Kapoor, N., et al., *Structural evidence for a sequential release mechanism for activation of heterotrimeric G proteins*. J Mol Biol, 2009. **393**(4): p. 882-97.
57. Marin, E.P., A.G. Krishna, and T.P. Sakmar, *Rapid activation of transducin by mutations distant from the nucleotide-binding site: evidence for a mechanistic model of receptor-catalyzed nucleotide exchange by G proteins*. J Biol Chem, 2001. **276**(29): p. 27400-5.
58. Marin, E.P., A.G. Krishna, and T.P. Sakmar, *Disruption of the alpha5 helix of transducin impairs rhodopsin-catalyzed nucleotide exchange*. Biochemistry, 2002. **41**(22): p. 6988-94.
59. Posner, B.A., et al., *The A326S mutant of Gialpha1 as an approximation of the receptor-bound state*. J Biol Chem, 1998. **273**(34): p. 21752-8.

60. Thomas, T.C., C.J. Schmidt, and E.J. Neer, *G-protein alpha o subunit: mutation of conserved cysteines identifies a subunit contact surface and alters GDP affinity*. Proc Natl Acad Sci U S A, 1993. **90**(21): p. 10295-9.
61. Natochin, M., M. Moussaif, and N.O. Artemyev, *Probing the mechanism of rhodopsin-catalyzed transducin activation*. J Neurochem, 2001. **77**(1): p. 202-10.
62. Oldham, W.M., et al., *Mechanism of the receptor-catalyzed activation of heterotrimeric G proteins*. Nat Struct Mol Biol, 2006. **13**(9): p. 772-7.
63. Iiri, T., Z. Farfel, and H.R. Bourne, *G-protein diseases furnish a model for the turn-on switch*. Nature, 1998. **394**(6688): p. 35-8.
64. Cherfils, J. and M. Chabre, *Activation of G-protein Galpha subunits by receptors through Galpha-Gbeta and Galpha-Ggamma interactions*. Trends Biochem Sci, 2003. **28**(1): p. 13-7.
65. Kisselev, O., et al., *Receptor-G protein coupling is established by a potential conformational switch in the beta gamma complex*. Proc Natl Acad Sci U S A, 1995. **92**(20): p. 9102-6.
66. Azpiazu, I. and N. Gautam, *G protein gamma subunit interaction with a receptor regulates receptor-stimulated nucleotide exchange*. J Biol Chem, 2001. **276**(45): p. 41742-7.
67. Grishina, G. and C.H. Berlot, *Mutations at the domain interface of GSalpha impair receptor-mediated activation by altering receptor and guanine nucleotide binding*. J Biol Chem, 1998. **273**(24): p. 15053-60.
68. Warner, D.R., et al., *A novel mutation in the switch 3 region of Gsalph in a patient with Albright hereditary osteodystrophy impairs GDP binding and receptor activation*. J Biol Chem, 1998. **273**(37): p. 23976-83.
69. Majumdar, S., S. Ramachandran, and R.A. Cerione, *Perturbing the linker regions of the alpha-subunit of transducin: a new class of constitutively active GTP-binding proteins*. J Biol Chem, 2004. **279**(38): p. 40137-45.
70. Ceruso, M.A., X. Periole, and H. Weinstein, *Molecular dynamics simulations of transducin: interdomain and front to back communication in activation and nucleotide exchange*. J Mol Biol, 2004. **338**(3): p. 469-81.
71. Kaya, A.I., et al., *A conserved phenylalanine as a relay between the alpha5 helix and the GDP binding region of heterotrimeric Gi protein alpha subunit*. The Journal of biological chemistry, 2014. **289**(35): p. 24475-87.
72. Maeda, S., et al., *Crystallization scale preparation of a stable GPCR signaling complex between constitutively active rhodopsin and G-protein*. PLoS One, 2014. **9**(6): p. e98714.
73. Iwata, S., *Methods and Results in Crystallization of Membrane Proteins*. 2002: International University Line.

74. Reeves, P.J., et al., *Structure and function in rhodopsin: high-level expression of rhodopsin with restricted and homogeneous N-glycosylation by a tetracycline-inducible N-acetylglucosaminyltransferase I-negative HEK293S stable mammalian cell line*. Proc Natl Acad Sci U S A, 2002. **99**(21): p. 13419-24.
75. Deupi, X., et al., *Stabilized G protein binding site in the structure of constitutively active metarhodopsin-II*. Proc Natl Acad Sci U S A, 2012. **109**(1): p. 119-24.
76. Xie, G., et al., *Preparation of an activated rhodopsin/transducin complex using a constitutively active mutant of rhodopsin*. Biochemistry, 2011. **50**(47): p. 10399-407.
77. Alexandrov, A.I., et al., *Microscale fluorescent thermal stability assay for membrane proteins*. Structure, 2008. **16**(3): p. 351-9.
78. Hattori, M., R.E. Hibbs, and E. Gouaux, *A fluorescence-detection size-exclusion chromatography-based thermostability assay for membrane protein precrystallization screening*. Structure, 2012. **20**(8): p. 1293-9.
79. Sun, D., et al., *AAscan, PCRdesign and MutantChecker: a suite of programs for primer design and sequence analysis for high-throughput scanning mutagenesis*. PLoS ONE, 2013. **8**(10): p. e78878.
80. Sievers, F., et al., *Fast, scalable generation of high-quality protein multiple sequence alignments using Clustal Omega*. Mol Syst Biol, 2011. **7**: p. 539.
81. Pettersen, E.F., et al., *UCSF Chimera--a visualization system for exploratory research and analysis*. J Comput Chem, 2004. **25**(13): p. 1605-12.
82. Eswar, N., et al., *Comparative protein structure modeling using Modeller*. Curr Protoc Bioinformatics, 2006. **Chapter 5**: p. Unit 5 6.
83. Liu, W., et al., *Structural basis for allosteric regulation of GPCRs by sodium ions*. Science, 2012. **337**(6091): p. 232-6.
84. Mahalingam, M., et al., *Two protonation switches control rhodopsin activation in membranes*. Proc Natl Acad Sci U S A, 2008. **105**(46): p. 17795-800.
85. Tajkhorshid, E., et al., *Molecular dynamics study of the nature and origin of retinal's twisted structure in bacteriorhodopsin*. Biophys J, 2000. **78**(2): p. 683-93.
86. Nina, M., B. Roux, and J.C. Smith, *Functional interactions in bacteriorhodopsin: a theoretical analysis of retinal hydrogen bonding with water*. Biophys J, 1995. **68**(1): p. 25-39.
87. Lower, R., et al., *Influence of additional methyl groups in the N-epsilon-amino position of lysine on the renal handling*. Pflugers Arch, 1974. **347**(2): p. 159-72.
88. Phillips, J.C., et al., *Scalable molecular dynamics with NAMD*. J Comput Chem, 2005. **26**(16): p. 1781-802.

89. MacKerell, A.D., et al., *All-atom empirical potential for molecular modeling and dynamics studies of proteins*. J Phys Chem B, 1998. **102**(18): p. 3586-616.
90. Waterhouse, A.M., et al., *Jalview Version 2--a multiple sequence alignment editor and analysis workbench*. Bioinformatics, 2009. **25**(9): p. 1189-91.
91. Brandt, T., et al., *Stability of p53 homologs*. PLoS One, 2012. **7**(10): p. e47889.
92. Smith, S.J. and K. Rittinger, *Preparation of GTPases for structural and biophysical analysis*. Methods Mol Biol, 2002. **189**: p. 13-24.
93. Faurobert, E., et al., *Tryptophan W207 in transducin T alpha is the fluorescence sensor of the G protein activation switch and is involved in the effector binding*. EMBO J, 1993. **12**(11): p. 4191-8.
94. Bigay, J., et al., *Fluoride complexes of aluminium or beryllium act on G-proteins as reversibly bound analogues of the gamma phosphate of GTP*. EMBO J, 1987. **6**(10): p. 2907-13.
95. Antonny, B., J. Bigay, and M. Chabre, *A novel magnesium-dependent mechanism for the activation of transducin by fluoride*. FEBS Lett, 1990. **268**(1): p. 277-80.
96. Antonny, B., et al., *GTP hydrolysis mechanisms in ras p21 and in the ras-GAP complex studied by fluorescence measurements on tryptophan mutants*. Biochemistry, 1991. **30**(34): p. 8287-95.
97. Higashijima, T. and K.M. Ferguson, *Tryptophan fluorescence of G proteins: analysis of guanine nucleotide binding and hydrolysis*. Methods Enzymol, 1991. **195**: p. 321-8.
98. Phillips, W.J. and R.A. Cerione, *The intrinsic fluorescence of the alpha subunit of transducin. Measurement of receptor-dependent guanine nucleotide exchange*. J Biol Chem, 1988. **263**(30): p. 15498-505.
99. Guy, P.M., J.G. Koland, and R.A. Cerione, *Rhodopsin-stimulated activation-deactivation cycle of transducin: kinetics of the intrinsic fluorescence response of the alpha subunit*. Biochemistry, 1990. **29**(30): p. 6954-64.
100. Ernst, O.P., et al., *Monomeric G protein-coupled receptor rhodopsin in solution activates its G protein transducin at the diffusion limit*. Proc Natl Acad Sci U S A, 2007. **104**(26): p. 10859-64.
101. Xie, G., A.K. Gross, and D.D. Oprian, *An opsin mutant with increased thermal stability*. Biochemistry, 2003. **42**(7): p. 1995-2001.
102. Standfuss, J., et al., *Crystal structure of a thermally stable rhodopsin mutant*. J Mol Biol, 2007. **372**(5): p. 1179-88.

103. Standfuss, J., et al., *Structural impact of the E113Q counterion mutation on the activation and deactivation pathways of the G protein-coupled receptor rhodopsin*. J Mol Biol, 2008. **380**(1): p. 145-57.
104. Han, M., S.O. Smith, and T.P. Sakmar, *Constitutive activation of opsin by mutation of methionine 257 on transmembrane helix 6*. Biochemistry, 1998. **37**(22): p. 8253-61.
105. Liu, H. and J.H. Naismith, *An efficient one-step site-directed deletion, insertion, single and multiple-site plasmid mutagenesis protocol*. BMC biotechnology, 2008. **8**: p. 91.
106. Bubeck, P., M. Winkler, and W. Bautsch, *Rapid cloning by homologous recombination in vivo*. Nucleic Acids Research, 1993. **21**(15): p. 3601-2.
107. Olieric, N., et al., *Automated seamless DNA co-transformation cloning with direct expression vectors applying positive or negative insert selection*. BMC Biotechnology, 2010. **10**: p. 56.
108. van den Ent, F. and J. Lowe, *RF cloning: a restriction-free method for inserting target genes into plasmids*. Journal of biochemical and biophysical methods, 2006. **67**(1): p. 67-74.
109. Liang, X., et al., *A method for multi-site-directed mutagenesis based on homologous recombination*. Analytical Biochemistry, 2012. **427**(1): p. 99-101.
110. Marmur, J. and P. Doty, *Determination of the base composition of deoxyribonucleic acid from its thermal denaturation temperature*. Journal of Molecular Biology, 1962. **5**: p. 109-18.
111. Canaves, J.M., A. Morse, and B. West, *PCR primer selection tool optimized for high-throughput proteomics and structural genomics*. Biotechniques, 2004. **36**(6): p. 1040-2.
112. Aslanidis, C., P.J. de Jong, and G. Schmitz, *Minimal length requirement of the single-stranded tails for ligation-independent cloning (LIC) of PCR products*. PCR methods and applications, 1994. **4**(3): p. 172-7.
113. Festa, F., et al., *High-throughput cloning and expression library creation for functional proteomics*. Proteomics, 2013. **13**(9): p. 1381-99.
114. Don, R.H., et al., *'Touchdown' PCR to circumvent spurious priming during gene amplification*. Nucleic Acids Res, 1991. **19**(14): p. 4008.
115. Fire, A. and S.Q. Xu, *Rolling replication of short DNA circles*. Proc Natl Acad Sci U S A, 1995. **92**(10): p. 4641-5.
116. Matouschek, A., et al., *Mapping the transition state and pathway of protein folding by protein engineering*. Nature, 1989. **340**(6229): p. 122-6.
117. Garcia, P.D., et al., *Transducin-alpha C-terminal mutations prevent activation by rhodopsin: a new assay using recombinant proteins expressed in cultured cells*. The EMBO journal, 1995. **14**(18): p. 4460-9.



118. Hamm, H.E., et al., *Site of G protein binding to rhodopsin mapped with synthetic peptides from the alpha subunit*. Science, 1988. **241**(4867): p. 832-5.
119. Chung, K.Y., et al., *Conformational changes in the G protein Gs induced by the beta2 adrenergic receptor*. Nature, 2011. **477**(7366): p. 611-5.
120. Alexander, N.S., et al., *Energetic analysis of the rhodopsin-G-protein complex links the alpha5 helix to GDP release*. Nature structural & molecular biology, 2014. **21**(1): p. 56-63.
121. Flock, T., et al., *A universal allosteric mechanism for Gα protein activation*. submitted, 2014.
122. Gales, C., et al., *Probing the activation-promoted structural rearrangements in preassembled receptor-G protein complexes*. Nature structural & molecular biology, 2006. **13**(9): p. 778-86.
123. Liu, W. and J.K. Northup, *The helical domain of a G protein alpha subunit is a regulator of its effector*. Proceedings of the National Academy of Sciences of the United States of America, 1998. **95**(22): p. 12878-83.
124. Van Eps, N., et al., *Interaction of a G protein with an activated receptor opens the interdomain interface in the alpha subunit*. Proc Natl Acad Sci U S A, 2011.
125. Jones, J.C., et al., *The crystal structure of a self-activating G protein alpha subunit reveals its distinct mechanism of signal initiation*. Sci Signal, 2011. **4**(159): p. ra8.
126. Urano, D., et al., *Heterotrimeric G protein signalling in the plant kingdom*. Open Biol, 2013. **3**(3): p. 120186.
127. Raw, A.S., et al., *Structural and biochemical characterization of the GTPgammaS-, GDP.Pi-, and GDP-bound forms of a GTPase-deficient Gly42 --> Val mutant of Gialpha1*. Biochemistry, 1997. **36**(50): p. 15660-9.
128. Noel, J.P., H.E. Hamm, and P.B. Sigler, *The 2.2 Å crystal structure of transducin-alpha complexed with GTP gamma S*. Nature, 1993. **366**(6456): p. 654-63.

# DAWEI SUN

## PERSONAL DATA:

**Date and place of birth:** 31. Aug.1980, Yanji (China)  
**Marital status:** Married  
**Nationality:** Chinese  
**Address:** OFLG 126, PSI, Villigen, 5232.

## EDUCATION:

**May.2011-Present:**

### **PhD student**

Dept. of Biology in Swiss Federal Institute of Technology Zürich (ETHZ) and Paul Scherrer Institut, Switzerland

**Thesis Title:** “*Probing  $G\alpha_{i1}$  protein activation at single amino acid resolution*”

**Advisor:** Prof. Gebhard Schertler and Dr. Dmitry Veprintsev

**Mar.2004-Feb.2006:**

### **Master Degree (M.S)**

Dept. of Chemistry, Korea Advanced Institute of Science and Technology (KAIST), Republic of Korea

**Graduation Thesis:** “*NMR studies on coiled-coil domain and RPA-ssDNA binding domain of ATR-interacting protein*”

**Advisor:** Prof. Byong-Seok Choi

**Sept.1998-June.2002:**

### **Bachelor Degree**

Dept. of Chemical Engineering, YanBian University, P. R. China

## WORK EXPERIENCE:

**Nov.2010-Feb.2011:**

### **Research Specialist**

Dept. of Pharmacology, University of Minnesota, USA

**May.2006-Oct.2010:**

### **Researcher**

Division of Magnetic Resonance, Korea Basic Science Institute (KBSI), Republic of Korea

**July.2002-Feb.2004:**

### **Research Assistant**

Dept. of Chemistry, YanBian University, P. R. China

## LANGUAGE:

- Chinese Mandarin: Mother tongue
- English: Fluent in reading/writing/speaking
- Korean: Intermediate level

## **AWARDS&SCHOLARSHIP:**

### **Honor:**

Mar.2011: Chinese Government Award for Outstanding Self-financed Students Abroad

### **Scholarship:**

Dec.2013: Conference Travel Grant, ETH ZURICH

Mar.2004-Feb. 2006: Korea Research Foundation (KRF)

## **POSTERS & TALKS:**

- 10<sup>th</sup> D-BIOL-Symposium ETH Zurich, Switzerland, June.2014. **(Poster)**
- GPCR Workshop, USA, Dec.2013. **(Poster)**
- Retreat of Biomolecular Structure and Mechanism, Switzerland, July.2013. **(Speaker)**
- 15<sup>th</sup> International Retinal Protein Meeting, Switzerland, Sept.2012. **(Poster)**
- 9<sup>th</sup> D-BIOL-Symposium ETH Zurich, Switzerland, June.2012. **(Poster)**
- 10<sup>th</sup> Conference of Asian Crystallographic Association, Republic of Korea, Oct.2010. **(Poster)**

## **PATENT:**

- Mutants stabilizing the active state of the G protein and screening methodology (European Patent, **in progress**)  
**Dawei Sun**, Gebhard Schertler, Dmitry Veprintsev

## **PUBLICATIONS:**

- ***Dawei Sun***, Andrea Prota, Dmitry B Veprintsev **(In Preparation)**  
Studies of a highly conserved valine provide insights into the mechanism of G protein activation.
- ***Dawei Sun***, Tilman Flock, Xavier Deupi, Shoji Maeda, Sandro Mendieta, Daniel Mayer, Roger Dawson, Gebhard Schertler, M. Madan Babu, Dmitry Veprintsev **(Under peer-review in Nature)**  
Probing G $\alpha_{i1}$  protein activation at a single amino acid resolution.
- Tilman Flock, ***Dawei Sun***, Charles Ravarani, A. Venkatakrishnan, Melis Kayikci, Chris Tate, Dmitry Veprintsev, M. Madan Babu **(Under peer-review in Nature)**  
Mechanism of a universal allosteric activation mechanism in G proteins decouples allostery from GPCR interaction specificity.
- Shoji Maeda, ***Dawei Sun***, Ankita Singhal, Marcello Foggetta, Joerg Standfuss, Michael Hennig, Roger J.P. Dawson, Dmitry Veprintsev, Gebhard Schertler. "Crystallization scale preparation of a stable GPCR signaling complex between constitutively active rhodopsin and G-protein", *PLOS ONE*, 9(6): e98714 (2014).
- ***Dawei Sun***, Martin Ostermaier, Franziska Heydenreich, Daniel Mayer, Joerg Standfuss, Rolf Jaussi and Dmitry B. Veprintsev. "AlaScan-automatic primer design for scanning mutagenesis", *PLOS ONE*, 10(8): e78878 (2013).

- Dinan Liu, Kyoung-Seok Ryu, Junsang Ko, **Dawei Sun**, Kyungeun Lim, Jie-Oh Lee, Jung me Hwang, Zee-won Lee and Byong-Seok Choi. “Insights into the regulation of human Rev1 for translesion synthesis polymerases revealed by the structural studies on its polymerase-interacting Domain” *Journal of Molecular Cell Biology*, 5(3): 204-206 (2013).
- Guiqing Peng, **Dawei Sun**, Kanagalaghatta Rajashankar, Zhaohui Qian, Kathryn Holmes, Fang Li. “Crystal structure of mouse coronavirus receptor-binding domain complexed with its receptor murine CEACAM1” *Proceedings of the National Academy of Sciences*, 108(26): 10696-10701(2011).
- **Dawei Sun**, Hye-Yeon Kim, Young Ho Jeon. “Purification, crystallization and preliminary X-ray crystallographic analysis of human ppGpp hydrolase, Mesh1”, *Journal of Analytical Science and Technology*, 1(2) :109-112 (2010)
- **Dawei Sun**, Gina Lee, Jun Hee Lee, Hye-Yeon Kim, Hyun-Woo Rhee, Seung-Yeol Park, Kyung-Jin Kim, Yongsung Kim, Bo Yeon Kim, Jong-In Hong, Chankyu Park, Hyon E Choy, Jung Hoe Kim, Young Ho Jeon & Jongkyeong Chung. “A metazoan ortholog of SpoT hydrolyzes ppGpp and functions in starvation responses”, *Nature Structural and Molecular Biology*, 17: 1188–1194 (2010).
- Sung-Hun Bae, Sang Hoon Yun, **Dawei Sun**, Heon M. Lim, and Byong-Seok Choi. “Structural and dynamic basis of a supercoiling-responsive DNA element”, *Nucleic Acid Research*, 34, 254–261 (2006).